UNIVERSITY OF AMSTERDAM

UvA-DARE (Digital Academic Repository)

Search for Higgs boson pair production in the two bottom quarks plus two photons final state in pp collisions at √s = 13 TeV with the ATLAS detector

Aad, G.; ATLAS Collaboration

DOI
10.1103/PhysRevD.106.052001

Publication date
2022

Document Version
Final published version

Published in
Physical Review D

License
CC BY

Link to publication

Citation for published version (APA):
Aad, G., & ATLAS Collaboration (2022). Search for Higgs boson pair production in the two bottom quarks plus two photons final state in *pp* collisions at $\sqrt{s}$ = 13 TeV with the ATLAS detector. *Physical Review D*, *106*(5), Article 052001. https://doi.org/10.1103/PhysRevD.106.052001

General rights
It is not permitted to download or to forward/distribute the text or part of it without the consent of the author(s) and/or copyright holder(s), other than for strictly personal, individual use, unless the work is under an open content license (like Creative Commons).

Disclaimer/Complaints regulations
If you believe that digital publication of certain material infringes any of your rights or (privacy) interests, please let the Library know, stating your reasons. In case of a legitimate complaint, the Library will make the material inaccessible and/or remove it from the website. Please Ask the Library: https://uba.uva.nl/en/contact, or a letter to: Library of the University of Amsterdam, Secretariat, P.O. Box 19185, 1000 GD Amsterdam, The Netherlands. You will be contacted as soon as possible.

UvA-DARE is a service provided by the library of the University of Amsterdam (https://dare.uva.nl)

Download date:13 Sept 2026

Search for Higgs boson pair production in the two bottom quarks plus two photons final state in pp collisions at $\sqrt{s} = 13$ TeV with the ATLAS detector

G. Aad *et al.*[*]
(ATLAS Collaboration)

(Received 23 December 2021; accepted 1 August 2022; published 6 September 2022)

Searches are performed for nonresonant and resonant di-Higgs boson production in the $b\bar{b}\gamma\gamma$ final state. The dataset used corresponds to an integrated luminosity of 139 fb^{-1} of proton–proton collisions at a center-of-mass energy of 13 TeV recorded by the ATLAS detector at the CERN Large Hadron Collider. No excess above the expected background is found and upper limits on the di-Higgs boson production cross sections are set. A 95% confidence-level upper limit of 4.2 times the cross section predicted by the Standard Model is set on $pp \to HH$ nonresonant production, where the expected limit is 5.7 times the Standard Model predicted value. The expected constraints are obtained for a background hypothesis excluding $pp \to HH$ production. The observed (expected) constraints on the Higgs boson trilinear coupling modifier κ_λ are determined to be $[-1.5, 6.7]$ ($[-2.4, 7.7]$) at 95% confidence level, where the expected constraints on κ_λ are obtained excluding $pp \to HH$ production from the background hypothesis. For resonant production of a new hypothetical scalar particle X ($X \to HH \to b\bar{b}\gamma\gamma$), limits on the cross section for $pp \to X \to HH$ are presented in the narrow-width approximation as a function of m_X in the range 251 GeV $\leq m_X \leq$ 1000 GeV. The observed (expected) limits on the cross section for $pp \to X \to HH$ range from 640 fb to 44 fb (391 fb to 46 fb) over the considered mass range.

DOI: 10.1103/PhysRevD.106.052001

I. INTRODUCTION

Since the discovery of the Higgs boson in 2012 [1,2], one of the priorities of the ATLAS and CMS Collaborations has been to better understand the properties of the Brout-Englert-Higgs mechanism [3–8]. The Higgs boson self-coupling provides information about the structure of the Higgs potential. It is possible to directly probe the self-coupling of the Higgs boson by studying Higgs boson pair (HH) production. Furthermore, any deviation of the Higgs boson pair production rate from the Standard Model (SM) prediction would point to new physics beyond the Standard Model (BSM) and may be within the sensitivity reach of the proton–proton (pp) collision data collected at $\sqrt{s} = 13$ TeV during Run 2 of the Large Hadron Collider (LHC) [9].

At leading order (LO), the production of Higgs boson pairs via gluon–gluon fusion (ggF) proceeds through the two diagrams shown in Fig. 1. These diagrams interfere destructively, leading to a small-production cross section [10–12]. For 13 TeV pp collisions and a Higgs boson mass $m_H = 125.09$ GeV [13], the ggF cross section, calculated at next-to-next-to-leading-order (NNLO) accuracy in the finite top-quark mass approximation (FTapprox), is $\sigma_{HH}(\text{ggF}) = 31.02^{+2.2\%}_{-5.0\%}(\text{Scale})^{+4\%}_{-18\%}(m_{\text{top}}) \pm 3.0\%(\alpha_s + \text{PDF})$ fb [14–17], where "Scale" represents the uncertainty due to the finite order of the quantum chromodynamics (QCD) calculation, "m_{top}" the uncertainty related to the top-quark mass scheme [17,18] which is added linearly to the Scale uncertainty, and "α_s + PDF" the effect of uncertainties in the strong coupling constant and parton distribution functions.

The di-Higgs vector-boson fusion (VBF) production cross section, calculated at next-to-next-to-next-to-leading order (N3LO) for $m_H = 125.09$ GeV, is $\sigma_{HH}(\text{VBF}) = 1.72^{+0.03\%}_{-0.04\%}(\text{Scale}) \pm 2.1\%(\alpha_s + \text{PDF})$ fb [14], which is one order of magnitude lower than the cross section of the ggF process. The VBF production mode provides the analysis with additional sensitivity to the Higgs trilinear coupling, as shown in Fig. 2. Both the ggF and VBF production modes of Higgs boson pairs are considered as signal modes in this paper. The other production modes have lower cross sections [19] and are neglected.

Nonresonant enhancements to the Higgs boson pair cross section can originate either from loop corrections involving new particles, such as light, colored scalars [20], or from non-SM couplings between the Higgs boson and other SM particles. The nonresonant production cross section can also be altered by the trilinear self-coupling, λ_{HHH}, being different from the SM prediction, as discussed

[*]Full author list given at the end of the article.

Published by the American Physical Society under the terms of the Creative Commons Attribution 4.0 International license. Further distribution of this work must maintain attribution to the author(s) and the published article's title, journal citation, and DOI. Funded by SCOAP[3].

 © 2022 CERN, for the ATLAS Collaboration

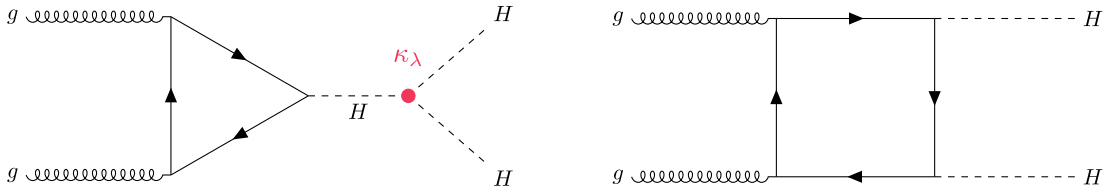

(a) Trilinear coupling (b) Box diagram

FIG. 1. The Feynman diagrams for the dominant gluon–gluon fusion production processes. In the Standard Model, the (a) trilinear coupling process, and (b) the box diagram, and the destructive interference between the two processes, contribute to the total cross section. In the figure, κ_λ represents the Higgs boson trilinear coupling modifier. The quark content in the diagram is dominated by the top-quark contribution due to the large top-quark Yukawa coupling to the Higgs boson.

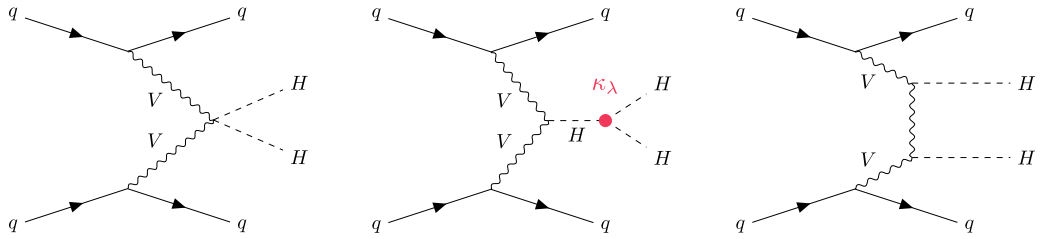

(a) $HHVV$ vertex (b) Trilinear coupling (c) VVH Production mode

FIG. 2. The VBF production of Higgs boson pairs via (a) the $HHVV$ vertex, (b) the trilinear coupling, and (c) the VVH production mode. In the figure, κ_λ denotes the Higgs boson trilinear coupling modifier.

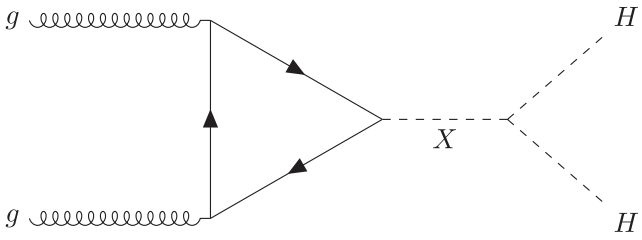

FIG. 3. Gluon–gluon fusion production of a heavy resonance decaying into a Higgs boson pair.

in Refs. [21,22]. Such an effect can be captured by a scale factor κ_λ defined as $\kappa_\lambda = \lambda_{HHH}/\lambda_{HHH}^{\mathrm{SM}}$, where $\lambda_{HHH}^{\mathrm{SM}}$ is the SM value of the parameter.

In addition to the nonresonant enhancements, searching for resonant production of Higgs boson pairs is well motivated. Figure 3 shows a ggF production diagram possible in BSM theories predicting the existence of heavy scalar particles that can decay into a pair of Higgs bosons. Such theories include models with two Higgs doublets [23], such as the minimal supersymmetric extension of the SM [24], twin Higgs models [25], and composite Higgs models [26], adding a second complex scalar doublet to the Higgs sector. Alternatively, the Randall-Sundrum model of warped extra dimensions [27] predicts spin-0 radions that could couple to a Higgs boson pair.

This paper presents a search for di-Higgs production in the $b\bar{b}\gamma\gamma$ final state, including dedicated assessments of nonresonant and resonant contributions. The analysis considers the full Run 2 dataset of 139 fb^{-1} at 13 TeV. For both the nonresonant and resonant HH searches, the analysis employs a multivariate method designed to reject background processes, and the statistical results are obtained from a fit of the diphoton invariant mass, $m_{\gamma\gamma}$. For the nonresonant search, data are divided into different categories based on the four-body invariant mass to target different κ_λ ranges. The resonant search focuses on probing the existence of a narrow-width scalar particle X in the mass range $251 < m_X < 1000$ GeV decaying into a pair of Higgs bosons. The selection criteria depend on the mass of the probed scalar particle. The main background processes are diphoton-plus-jets production and processes where a Higgs boson is produced and decays into a pair of photons. In the context of the resonant search, nonresonant HH production is considered as a background.

Previous results from the ATLAS Collaboration were obtained in this channel with an integrated luminosity of 36 fb^{-1} of data at 13 TeV collected during Run 2, and they were found to be consistent with SM expectations within uncertainties [28]. The search for nonresonant enhancements of Higgs boson pair production set an observed (expected) 95% confidence level (C.L.) upper limit on the HH cross section of 0.73 (0.93) pb, corresponding to 22

(28) times the SM prediction. The Higgs trilinear coupling was constrained to the range $-8.2 < \kappa_\lambda < 13.2$ at 95% C.L. ($-8.3 < \kappa_\lambda < 13.2$ expected). A previous combination of searches for HH pair production performed by the ATLAS Collaboration with up to 36 fb^{-1} of 13 TeV data provided constraints of $-5.0 < \kappa_\lambda < 12.0$ at 95% C.L. [29]. A search for enhancements due to the decay of a narrow-width scalar particle was performed in this channel as well, and results were given as a function of the resonance mass, m_X. The observed (expected) limits were between 1.1 pb and 0.12 pb over the range 260 GeV $< m_X <$ 1000 GeV. A combination of searches by the ATLAS Collaboration with up to 36 fb^{-1} of 13 TeV data for a narrow-width scalar resonance decaying into a HH pair was performed and provided upper limits between 851 fb and 4.6 fb over the range 260 GeV $< m_X <$ 3000 GeV [29]. The CMS Collaboration also set observed (expected) upper limits of 7.7 (5.2) times the SM prediction at 95% C.L. on nonresonant enhancements of Higgs boson pair production in the $b\bar{b}\gamma\gamma$ final state with 137 fb^{-1} of 13 TeV data [30]. In the same final state, the CMS Collaboration set 95% C.L. upper limits on the production cross section of a narrow-width scalar particle between 4.2 pb and 0.23 pb over the range 260 $< m_X <$ 900 GeV with 35.9 fb^{-1} of 13 TeV data [31].

II. THE ATLAS DETECTOR

The ATLAS detector [32] at the LHC covers nearly the entire solid angle around the collision point.[1] It consists of an inner tracking detector surrounded by a thin superconducting solenoid, electromagnetic and hadron calorimeters, and a muon spectrometer incorporating three large superconducting air-core toroidal magnets.

The inner-detector system (ID) is immersed in a 2 T axial magnetic field and provides charged-particle tracking in the range $|\eta| < 2.5$. The high-granularity silicon pixel detector covers the vertex region and typically provides four measurements per track, the first hit normally being in the insertable B-layer installed before Run 2 [33,34]. It is followed by the silicon microstrip tracker, which usually provides eight measurements per track. These silicon detectors are complemented by the transition radiation tracker (TRT), which enables radially extended track reconstruction up to $|\eta| = 2.0$. The TRT also provides electron identification information.

The calorimeter system covers the pseudorapidity range $|\eta| < 4.9$. Within the region $|\eta| < 3.2$, electromagnetic calorimetry is provided by barrel and end cap high-granularity lead/liquid-argon (LAr) calorimeters, with an additional thin LAr presampler covering $|\eta| < 1.8$ to correct for energy loss in material upstream of the calorimeters. Hadron calorimetry is provided by the steel/scintillator-tile calorimeter, segmented into three barrel structures within $|\eta| < 1.7$, and two copper/LAr hadron end cap calorimeters. The solid angle coverage is completed with forward copper/LAr and tungsten/LAr calorimeter modules optimized for electromagnetic and hadronic energy measurements respectively.

The muon spectrometer (MS) comprises separate trigger and high-precision tracking chambers measuring the deflection of muons in a magnetic field generated by the superconducting air-core toroidal magnets. The field integral of the toroids ranges between 2.0 Tm and 6.0 Tm across most of the detector. A set of precision chambers covers the region $|\eta| < 2.7$ with three layers of monitored drift tubes, complemented by cathode-strip chambers in the forward region, where the background is highest. The muon trigger system covers the range $|\eta| < 2.4$ with resistive-plate chambers in the barrel and thin-gap chambers in the end cap regions.

Interesting events are selected by the first-level trigger system implemented in custom hardware, followed by selections made by algorithms implemented in software in the high-level trigger [35]. The first-level trigger accepts events from the 40 MHz bunch crossings at a rate below 100 kHz, which the high-level trigger reduces in order to record events at rate of about 1 kHz. An extensive software suite [36] is used in the reconstruction and analysis of real and simulated data, in detector operations, and in the trigger and data acquisition systems of the experiment.

III. DATA AND SIMULATION SAMPLES

This analysis uses pp collision data collected by the ATLAS experiment from 2015 to 2018 with proton beams colliding at a center-of-mass energy of $\sqrt{s} = 13$ TeV. After data quality requirements [37] the full dataset represents an integrated luminosity of 139.0 ± 2.4 fb^{-1} [38,39]. The mean number of inelastic pp interactions per bunch crossing is 34.2 [40].

Monte Carlo (MC) simulations are available for the signal as well as most background processes as detailed in the rest of this section. The reducible backgrounds from final states with jets wrongly identified as photons (γ–jet and dijet backgrounds) are, however, estimated using a data-driven technique detailed in Sec. IV C.

Events from ggF nonresonant HH production were generated at next-to-leading-order accuracy in QCD with finite top-quark mass in both the real and virtual corrections (NLO FT) [11], using the POWHEG BOX v2 [41] generator in the finite top-quark mass approximation [42,43] with the

[1] ATLAS uses a right-handed coordinate system with its origin at the nominal interaction point (IP) in the center of the detector and the z-axis along the beam pipe. The x-axis points from the IP to the center of the LHC ring, and the y-axis points upwards. Cylindrical coordinates (r, ϕ) are used in the transverse plane, ϕ being the azimuthal angle around the z-axis. The pseudorapidity is defined in terms of the polar angle θ as $\eta = -\ln\tan(\theta/2)$. The rapidity y is defined in terms of the energy, the momentum and the polar angle θ: $y = \frac{1}{2}\ln(\frac{E+p\cdot\cos\theta}{E-p\cdot\cos\theta})$. The angular distance is measured in units of $\Delta R \equiv \sqrt{(\Delta\eta)^2 + (\Delta\phi)^2}$.

PDF4LHC 15 parton distribution function (PDF) set [44]. The PYTHIA 8.244 generator was used for parton showering, hadronization and underlying-event simulation. HERWIG 7.1.6 was used as an alternative generator to calculate the theory uncertainty from the parton shower. Samples were generated for coupling modifier values $\kappa_\lambda = 1$ and 10.

For ggF nonresonant HH production, a reweighting method based on the di-Higgs invariant mass m_{HH} is used to provide predictions on the cross section at different κ_λ values, starting from the existing $\kappa_\lambda = 1$ sample. The reweighting method derives the scale factors as a function of κ_λ in bins of m_{HH} by performing a linear combination of samples generated at different κ_λ values [45]. Histograms of the truth m_{HH} distribution are produced for each κ_λ sample and the distributions of the other relevant kinematic variables are obtained applying an event-per-event weight based on the ratio between the binned m_{HH} distribution for the targeted κ_λ by the binned m_{HH} distribution for the SM ($\kappa_\lambda = 1$) sample.

This method was validated by comparing the event yields and the distributions of the relevant Higgs boson kinematic variables, including the $m_{\gamma\gamma}$ variable, of the sample generated with $\kappa_\lambda = 10$ to the sample generated with $\kappa_\lambda = 1$ and reweighted to $\kappa_\lambda = 10$. Good agreement is obtained in all categories. A systematic uncertainty in the range of 3%–4% is associated with the reweighting process, based on the maximum differences of signal yields observed in this validation. For each κ_λ value, the inclusive cross section is normalized according to Ref. [46]. A fit with a second order polynomial to the MC prediction is performed in each analysis category, in order to parametrize the event yields as a function of κ_λ.

For VBF nonresonant HH production, MadGraph5_aMC@NLO 2.6.0 [47] was used to generate events at LO [47,48]. The NNPDF3.0NLO PDF set [49] was used in the matrix element, interfaced to PYTHIA 8.244. The cross section of the VBF HH process is evaluated at N3LO in QCD [50–52], as outlined in Sec. I. Since samples were generated at LO for four values of the coupling modifier, $\kappa_\lambda = 0$, 1, 2 and 10, the N3LO-to-LO cross section ratio at the SM value is calculated and this factor is applied to the VBF HH cross section. These samples are used to derive a parametrization of the signal yields in the signal region as a function of κ_λ by fitting a second-order polynomial to the MC predictions in each analysis category, as described in Sec. IV B 2.

The production of a heavy spin-0 resonance X via ggF and its decay into a pair of Higgs bosons, $pp \to X \to HH$, was simulated using MadGraph5_aMC@NLO 2.6.1 [47] at LO accuracy with the NNPDF2.3LO PDF set. The event generator was interfaced with HERWIG7.1.3 [53,54] to model the parton shower, hadronization, and underlying event. No specific theoretical model for the phenomenology of the new particle is assumed in the process generation. The mass of X was varied between 251 GeV and 1000 GeV in the simulation, while its width was set to 10 MeV. In total 25 m_X mass hypotheses have been generated, corresponding to $m_X = 251$, 260, 270, 280, 290, 300, 312.5, 325, 337.5, 350, 375, 400, 425, 450, 475, 500, 550, 600, 650, 700, 750, 800, 850, 900, 1000 GeV. The interference with nonresonant Higgs boson pair production was neglected.

Production of single Higgs bosons via ggF, VBF, WH, ZH ($qq \to ZH$ and $gg \to ZH$), $t\bar{t}H$, tH (tHq and tHW), and bbH was modeled using the same set of MC samples as described in Ref. [55]. For single Higgs boson production, as well as both nonresonant and resonant di-Higgs production, a Higgs boson mass of 125.09 GeV was assumed [13]. The analysis assumes a branching ratio of 0.227% for the Higgs boson decay into two photons and a branching ratio of 58.2% for the Higgs boson decay into two b-quarks [56,57]. The inclusive cross sections of these processes are normalized to the most precise available theoretical values [56].

The $\gamma\gamma$ + jets process was simulated with the SHERPA 2.2.4 [58] generator. QCD NLO-accurate matrix elements for up to one parton, and LO-accurate matrix elements for up to three partons, were calculated with the Comix [59] and OPENLOOPS [60–62] libraries. These were calculated in the five-flavor scheme including b-quarks in the massless approximation and merged with the SHERPA parton shower [63] using the MEPS@NLO prescription [64,65] with a dynamic merging cut [66] of 10 GeV. Within the parton shower, b-quarks were then treated as being massive. Finally, events from $t\bar{t}\gamma\gamma$ processes were produced with MadGraph5_aMC@NLO in the four-flavor scheme [47]. The simulation samples used in the analysis are listed in Table I.

Different pileup conditions from additional interactions the same and neighboring bunch crossings were simulated by overlaying the hard-scattering event with inelastic pp events generated by PYTHIA8.186 using the NNPDF2.3LO PDF set and the A3 tune [85]. Differences between the simulated and observed distributions of the number of interactions per bunch crossing are corrected for by applying pileup scale factors to simulated events. A full simulation of the ATLAS detector [86] based on GEANT4 [87] was used to reproduce the detector response to single-Higgs-boson processes. The continuum background and signal samples were processed by AtlFastII [88], a fast simulation of the ATLAS detector response which was shown to be able to accurately simulate diphoton events.

IV. OBJECT AND EVENT SELECTIONS

A. Object selection

Photons are reconstructed from topologically connected clusters [89] of energy deposits in the electromagnetic calorimeter in the region $|\eta| < 2.37$. The transition region between the barrel and end cap electromagnetic calorimeters, $1.37 < |\eta| < 1.52$, is excluded. Photon candidates matched to conversion vertices or tracks that are consistent with originating from photon conversions are classified as

TABLE I. Summary of nominal Higgs boson pair signal samples and single-Higgs-boson background samples, split by production mode, and continuum background samples. The generator used in the simulation, the PDF set, and set of tuned parameters (tune) are also provided.

Process	Generator	PDF set	Showering	Tune
Nonresonant ggF HH	POWHEG BOXv2+FT [41,42,43]	PDFLHC [44]	PYTHIA8.2 [67]	A14 [68]
Nonresonant VBF HH	MadGraph5_aMC@NLO [47]	NNPDF3.0NLO [69]	PYTHIA8.2	A14
Resonant ggF HH	MadGraph5_aMC@NLO	NNPDF2.3LO	HERWIG7.1.3 [53,54]	H7.1—Default [70]
ggF H	NNLOPS [71–73] [74,75]	PDFLHC	PYTHIA8.2	AZNLO [76]
VBF H	POWHEG BOXv2 [41,72,77–83]	PDFLHC	PYTHIA8.2	AZNLO
WH	POWHEG BOXv2	PDFLHC	PYTHIA8.2	AZNLO
$qq \to ZH$	POWHEG BOXv2	PDFLHC	PYTHIA8.2	AZNLO
$gg \to ZH$	POWHEG BOXv2	PDFLHC	PYTHIA8.2	AZNLO
$t\bar{t}H$	POWHEG BOXv2 [78–80,83,84]	NNPDF3.0NLO	PYTHIA8.2	A14
bbH	POWHEG BOXv2	NNPDF3.0NLO	PYTHIA8.2	A14
tHq	MadGraph5_aMC@NLO	NNPDF3.0NLO	PYTHIA8.2	A14
tHW	MadGraph5_aMC@NLO	NNPDF3.0NLO	PYTHIA8.2	A14
$\gamma\gamma$ + jets	SHERPA 2.2.4 [58]	NNPDF3.0NNLO	SHERPA 2.2.4	⋯
$t\bar{t}\gamma\gamma$	MadGraph5_aMC@NLO	NNPDF2.3LO	PYTHIA8.2	⋯

converted photons. Those without a matched conversion vertex or track are classified as unconverted photons.

The calibration of the photon energy is based on a multivariate regression algorithm trained with MC samples, where the input variables are corrected with data-driven techniques. The calibrated energy is finally corrected by applying scale factors derived from $Z \to e^+e^-$ events [90]. The photon direction is reconstructed using the longitudinal (i.e., shower-depth) segmentation of the calorimeters and constrained to be compatible with the luminous region of the proton-beam collisions. Additionally, information about the position of the conversion vertex and about the tracks associated with the conversion vertex is considered in the case of converted photons.

Events are required to have at least one reconstructed collision vertex, defined as a vertex associated with at least two tracks with transverse momentum (p_{T}) larger than 0.5 GeV. The primary vertex is selected from the reconstructed collision vertices using a neural-network algorithm [91] based on the extrapolated photon trajectories and the tracks associated with each candidate vertex.

Photon identification is based on the lateral shower profile of the energy deposits in the first and second electromagnetic calorimeter layers and on the energy leakage fraction in the hadronic calorimeter. It reduces the misidentification of hadronic jets containing large neutral components, primarily π^0 particles, which decay into a pair of highly collimated photons. "Tight" identification criteria, which are tuned for converted and unconverted photons separately, are applied [90].

To further improve the rejection of misidentified photons, two isolation variables are defined to quantify the activity around a photon. Calorimeter-based isolation $E_{\mathrm{T}}^{\mathrm{iso}}$ is defined as the sum of the transverse energy of topological clusters within a cone of size $\Delta R = 0.2$ around the photon, correcting for the energy of the photon candidate itself as well as for an average expected pileup contribution. Track-based isolation $p_{\mathrm{T}}^{\mathrm{iso}}$ is defined as the scalar sum of the transverse momenta of all tracks with $p_{\mathrm{T}} > 1$ GeV that originate from the primary vertex and are within a cone of $\Delta R = 0.2$ around the photon. Isolated photons must have $E_{\mathrm{T}}^{\mathrm{iso}} < 0.065 \cdot E_{\mathrm{T}}$ and $p_{\mathrm{T}}^{\mathrm{iso}} < 0.05 \cdot E_{\mathrm{T}}$ (the "loose" working point [90]), where E_{T} is the transverse energy of the photon. For isolated photons with transverse momenta between 30 GeV and 250 GeV, the identification efficiency for unconverted and converted photons ranges from 84% to 98% [90].

Electrons are reconstructed from energy deposits measured in the electromagnetic calorimeter which are matched to ID tracks [90]. They are required to satisfy $|\eta| < 2.47$, excluding the calorimeter transition region $1.37 < |\eta| < 1.52$, and have a transverse momentum $p_{\mathrm{T}} > 10$ GeV. Electrons are required to satisfy a "medium" identification criterion based on the use of shower shape, track-cluster matching and TRT parameters in a likelihood-based algorithm [90]. Muons are reconstructed from high-quality tracks found in the MS [92]. A matching of these tracks to ID tracks is required in the region $|\eta| < 2.5$. Muons are required to have $|\eta| < 2.7$ and $p_{\mathrm{T}} > 10$ GeV, and to satisfy a "medium" identification criterion [93]. Both the electrons and muons are matched to the primary vertex via requirements on the tracks' longitudinal and transverse impact parameters, $|z_0|$ and $|d_0|$, respectively. These requirements are $|z_0| \sin\theta < 0.5$ mm (where θ is the polar angle of the track) for electrons and muons and $|d_0|/\sigma_{d_0} < 5(3)$ for electrons (muons).

Reconstructed jets are based on particle-flow objects built from noise-suppressed positive-energy topological clusters in the calorimeter and reconstructed tracks [94]. The anti-k_t algorithm [95,96] with a radius parameter of $R = 0.4$ is used. They are required to have rapidity $|y| < 4.4$ and

$p_T > 25$ GeV. To further suppress jets produced in concurrent pp interactions, each jet within the tracking acceptance of $|\eta| < 2.4$, and with $p_T < 60$ GeV, is required to satisfy the "tight" jet-vertex tagger [97] criteria used to identify the jet as originating from the selected primary vertex of the event.

The flavor of jets is determined using a deep-learning neural network, DL1r. The DL1r b-tagging is based on distinctive features of b-hadron decays in terms of the impact parameters of the tracks and the displaced vertices reconstructed in the inner detector [98]. The inputs of the DL1r network also include discriminating variables constructed by a recurrent neural network (RNNIP) [99], which exploits the spatial and kinematic correlations between tracks originating from the same b-hadron. For high-p_T jets, this approach is found to give better performance [100] than a previously used multivariate technique [101]. Operating points are defined by a single selection value on the discriminant output distribution and are chosen to provide a specific b-jet efficiency for an inclusive $t\bar{t}$ MC sample. The b-tagging requirements result in an efficiency of 77% for jets containing b-hadrons (b-tagged jets), and the misidentification rate is 1/130 (1/4.9) for light-flavor (charm) jets [98]. Scale factors are applied to the simulated events to correct for differences in b-tagging efficiency between data and simulation. These scale factors are measured as a function of jet p_T using a likelihood-based method in a sample highly enriched in $t\bar{t}$ events [98]. Only jets with $|\eta| < 2.5$ are considered for flavor-tagging.

The energy of b-tagged jets is corrected for the possible contribution of muons from semileptonic b-hadron decays. In addition, the undetected energy of the neutrinos and out-of-cone effects are corrected for with scale factors derived as a function of the b-jet p_T from a $t\bar{t}$ MC sample. The two corrections together improve the resolution of the invariant mass of the two jets with the highest b-tagging score ($m_{b\bar{b}}$) by about 20%. The procedure closely follows the one used in Ref. [102].

An overlap removal procedure is applied to avoid multiple usage of the same detector signals in the same event. Photons are prioritized in this analysis, requiring the removal of electrons, muons and jets within $\Delta R = 0.4$ of a selected photon. Next, jets within $\Delta R = 0.2$ of electrons are removed. In the last step, electrons and muons within $\Delta R = 0.4$ of any jet are removed.

The missing transverse momentum E_T^{miss} in an event is calculated as the magnitude of the negative vectorial sum of the transverse momenta of all selected and calibrated physics objects that can be matched to the primary vertex. A component called the "soft term" is calculated from the residual tracks that originate from the primary vertex but are not associated with any other object and is added to the E_T^{miss} calculation [103].

B. Event selection

Both the nonresonant and resonant HH searches employ multivariate analysis techniques to select events. Events are selected if they satisfy a common set of preselection requirements; they are then required to fulfill different requirements for the nonresonant search and the resonant search. Both analyses employ a fit of the diphoton invariant mass distribution to extract the HH signal contribution.

1. Common preselection

For both the nonresonant and resonant analyses, events are selected using diphoton triggers requiring two reconstructed photon candidates with minimum transverse energies of 35 GeV for the leading photon and 25 GeV for the subleading photon, where leading (subleading) refers to the photon candidate with the highest (second-highest) transverse energy [104]. The triggers used in 2015 and 2016 required both photons to satisfy a Loose photon identification criterion, while the Medium criterion [90] was adopted in 2017–2018 to cope with the increased pp interaction rate. Once the full diphoton event selection described in this section is applied, the average trigger efficiency for $H \to \gamma\gamma$ events is found to be greater than 99% for the 2015–2016 data-taking period, and greater than 98% for the 2017–2018 data-taking period.

On top of the trigger requirements, events are selected if:

(i) At least two photons satisfy the object selection criteria detailed in Sec. IV A.
(ii) The diphoton invariant mass, built with the two leading photons, satisfies 105 GeV $< m_{\gamma\gamma} <$ 160 GeV.
(iii) The leading (subleading) photon p_T is larger than 35% (25%) of the mass of the diphoton system.
(iv) Exactly two b-tagged jets are present. In order to remain statistically independent of the ATLAS search for $HH \to b\bar{b}b\bar{b}$ [105], any event with more than two b-jets passing the 77% efficient working point is rejected.
(v) No electrons or muons are present.
(vi) Fewer than six central ($|\eta| < 2.5$) jets are present. This helps to reject $t\bar{t}H$ events where the top quarks decay hadronically.

The acceptance times efficiency of the common preselection for the SM ggF HH simulation sample is 14% and it is 8.5% (14%) for a resonant scalar particle with $m_X =$ 300 GeV ($m_X = 500$ GeV). Multivariate techniques are then used to target the nonresonant ggF production mode or the resonant production mode of Higgs boson pairs. For both the nonresonant and resonant analyses, the resulting categories, each based on a boosted decision tree (BDT), must have at least nine continuum background events in the data sideband region. This guarantees that the final selection on the data sideband retains enough events to perform a

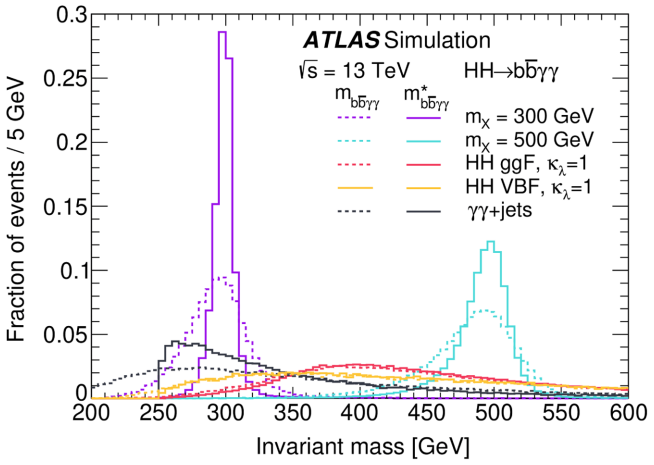

FIG. 4. Reconstructed four-body mass for $m_X = 300$ GeV and $m_X = 500$ GeV resonant signal benchmarks, for the SM HH production processes and for the $\gamma\gamma$ + jets background. Dashed lines represent the distribution of $m_{bb\gamma\gamma}$ while solid lines represent the distribution of $m^*_{bb\gamma\gamma}$, defined in Sec. IV B 1. Distributions are normalized to unit area.

fit to the distribution of the diphoton invariant mass, $m_{\gamma\gamma}$. The data sideband region is defined as the range 105 GeV $< m_{\gamma\gamma} <$ 160 GeV, excluding 120 GeV $< m_{\gamma\gamma} <$ 130 GeV.

The invariant mass of the diphoton plus b-tagged jets system, $m^*_{bb\gamma\gamma}$, is defined as $m^*_{bb\gamma\gamma} = m_{bb\gamma\gamma} - m_{bb} - m_{\gamma\gamma} +$ 250 GeV (where 250 GeV is about twice the Higgs boson mass value and m_{bb} is the invariant mass of the two jets with the highest b-tagging score). It is used to implement selection criteria for both the nonresonant and resonant analyses. Figure 4 shows that, compared with $m_{bb\gamma\gamma}$, the $m^*_{bb\gamma\gamma}$ variable improves the four-object mass resolution, particularly for resonant signal particles decaying into a pair of Higgs bosons, due to detector resolution effects canceling out.

2. Nonresonant selection

Following the preselection, events are divided into two regions using the value of the $m^*_{bb\gamma\gamma}$ variable. A high-mass region, with $m^*_{bb\gamma\gamma} > 350$ GeV, targets the SM signal ($\kappa_\lambda = 1$), while a low-mass region, with $m^*_{bb\gamma\gamma} < 350$ GeV, is used to retain sensitivity for BSM signals ($\kappa_\lambda = 10$). The dependence of $m^*_{bb\gamma\gamma}$ on κ_λ can be seen in Fig. 5.

In each mass region, a dedicated BDT is trained using XGBoost [106] to discriminate between a benchmark HH signal and a combination of $\gamma\gamma$, $t\bar{t}H$, ggH, and ZH simulated backgrounds. In the high-mass region, the SM HH sample is used as signal, while in the low-mass region, the $\kappa_\lambda = 10$ sample is used as signal.

The BDT input variables are summarized in Table II. Identical variable sets are used for high-mass and low-mass categories. The BDT combines several input variables that exploit the different kinematic properties of signal and background events, as well as the b-tagging information. Observables based on the kinematic properties of the reconstructed photons, such as the leading and subleading photon's angular information, and the transverse momentum of the diphoton system divided by its invariant mass, are combined with jet-based information. The "single topness" variable (χ_{Wt}) is also used. It is defined as

$$\chi_{Wt} = \min \sqrt{\left(\frac{m_{j_1 j_2} - m_W}{m_W}\right)^2 + \left(\frac{m_{j_1 j_2 j_3} - m_t}{m_t}\right)^2}, \quad (1)$$

where the minimum is taken over all combinations of three jets in the event (with no requirements on b-tagging status), $m_W = 80$ GeV, and $m_t = 173$ GeV. Among the input variables in Table II, m_{bb} and H_T show the highest discriminating power against the $\gamma\gamma$ + jets continuum background. Particular care was taken to ensure that the BDT event selection does not lead to biases in the $m_{\gamma\gamma}$ background distribution. Variables which have a strong

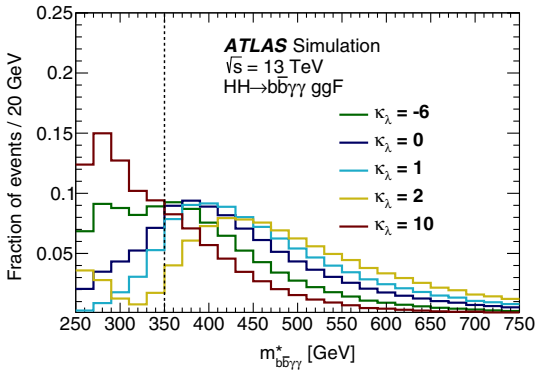

(a) ggF HH production mode

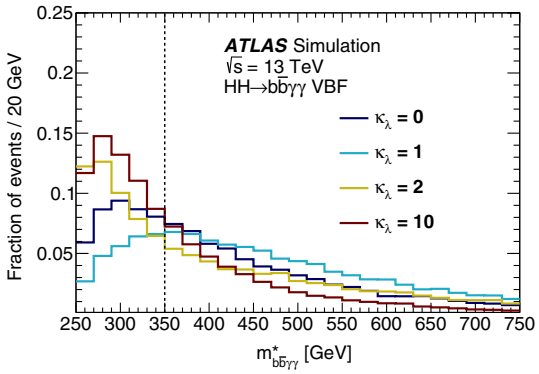

(b) VBF HH production mode

FIG. 5. The $m^*_{bb\gamma\gamma}$ distributions after the common preselection for (a) nonresonant ggF HH and (b) VBF HH signals with several κ_λ values. The value of $m^*_{bb\gamma\gamma} = 350$ GeV is chosen as the boundary between categories targeting the SM and BSM κ_λ signals.

TABLE II. Variables used in the BDT for the nonresonant analysis. All vectors in the event are rotated so that the leading photon ϕ is equal to zero, while their relative azimuthal angular differences are kept unchanged.

Variable	Definition
Photon-related kinematic variables	
$p_T/m_{\gamma\gamma}$	Transverse momentum of each of the two photons divided by the diphoton invariant mass $m_{\gamma\gamma}$
η and ϕ	Pseudorapidity and azimuthal angle of the leading and subleading photon
Jet-related kinematic variables	
b-tag status	Tightest fixed b-tag working point (60%, 70%, or 77%) that the jet passes
p_T, η and ϕ	Transverse momentum, pseudorapidity and azimuthal angle of the two jets with the highest b-tagging score
$p_T{}^{b\bar{b}}$, $\eta_{b\bar{b}}$ and $\phi_{b\bar{b}}$	Transverse momentum, pseudorapidity and azimuthal angle of the b-tagged jets system
$m_{b\bar{b}}$	Invariant mass of the two jets with the highest b-tagging score
H_T	Scalar sum of the p_T of the jets in the event
Single topness	For the definition, see Eq. (1)
Missing transverse momentum variables	
E_T^{miss} and ϕ^{miss}	Missing transverse momentum and its azimuthal angle

correlation with the diphoton invariant mass are avoided in the training in order to prevent the BDT event selection from biasing the $m_{\gamma\gamma}$ background distribution. To this end, the transverse momentum values of the photons are divided by $m_{\gamma\gamma}$ before being used as BDT input variables. A check for potential biases in the $m_{\gamma\gamma}$ background distribution is described in Sec. V B. The BDT score distributions in the low-mass and high-mass regions are shown in Fig. 6 for events passing the common preselection. In each mass region, two categories based on the BDT score are defined. The boundaries of the categories are chosen by maximizing the combined number-counting significance [107] using signal and background yields in the mass window $120\ \text{GeV} < m_{\gamma\gamma} < 130\ \text{GeV}$ in the chosen categories. The four resulting BDT categories are defined in Table III.

3. Resonant selection

The resonant search uses a multivariate analysis based on a BDT technique. A potential limitation of a BDT-based selection is the low number of background events for higher resonance masses. To overcome this limitation, BDTs are trained jointly for all resonance masses hypotheses and background. The signal events corresponding to the different mass hypotheses are combined. The signal events are reweighted event-by-event to match the $m^*_{b\bar{b}\gamma\gamma}$ distribution of the background events, such that the training is independent of the resonant signal mass hypothesis, but it still retains information of the correlation with the rest of the event variables. The procedure allows to reduce the fluctuations of the BDT performance between nearby mass points. It was checked that the procedure provides similar or better performance than employing separated BDT trainings for each individual signal mass hypothesis.

Using the TMVA toolkit [108], two BDTs are trained to better separate the signal from backgrounds of different nature; the $\gamma\gamma$ and $t\bar{t}\gamma\gamma$ backgrounds ($\text{BDT}_{\gamma\gamma}$) and the single-Higgs-boson background ($\text{BDT}_{\text{Single}H}$), where the ZH and $t\bar{t}H$ processes produce the dominant resonant backgrounds.

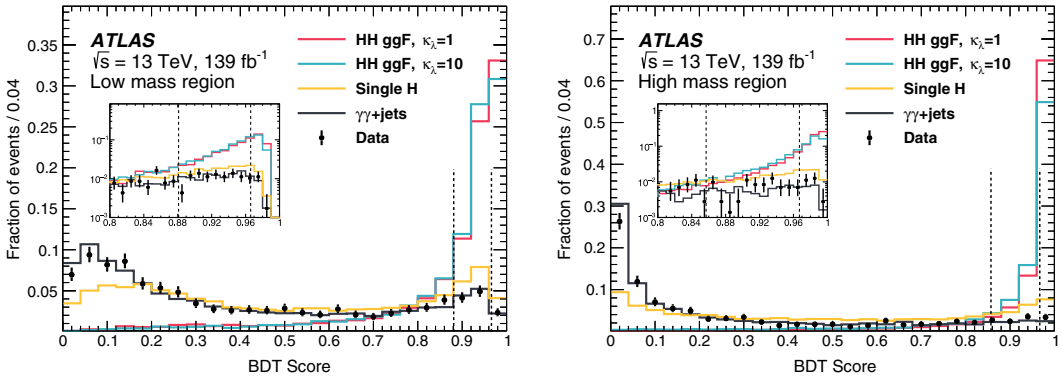

(a) Low mass region (b) High mass region

FIG. 6. The BDT distribution of the di-Higgs ggF signal for two different values of k_λ and the main backgrounds in the (a) low-mass region and (b) high-mass region. Distributions are normalized to unit area. The dashed lines denote the category boundaries. Events with a BDT score below 0.881 in the low-mass region or below 0.857 in the high-mass region are discarded.

TABLE III. Definition of the categories used in the HH nonresonant search. Before entering the BDT-based categories, events are required to satisfy the common preselection.

Category	Selection criteria
High mass BDT tight	$m^*_{b\bar{b}\gamma\gamma} \geq 350$ GeV, BDT score $\in [0.967, 1]$
High mass BDT loose	$m^*_{b\bar{b}\gamma\gamma} \geq 350$ GeV, BDT score $\in [0.857, 0.967]$
Low mass BDT tight	$m^*_{b\bar{b}\gamma\gamma} < 350$ GeV, BDT score $\in [0.966, 1]$
Low mass BDT loose	$m^*_{b\bar{b}\gamma\gamma} < 350$ GeV, BDT score $\in [0.881, 0.966]$

The nonresonant HH process is not included in the training of the BDTs. A complete list of the variables used for the BDT training is given in Table IV. The $E_{\mathrm{T}}^{\mathrm{miss}}$ information is used in the training because it is useful in rejecting the single-Higgs-boson background ($t\bar{t}H$ in particular) and the $t\bar{t}\gamma\gamma$ background.

The combined BDT score of an event is obtained by combining the two BDT scores in quadrature, as shown in Eq. (2),

$$\mathrm{BDT}_{\mathrm{tot}} = \frac{1}{\sqrt{C_1^2 + C_2^2}} \times \sqrt{C_1^2 \left(\frac{\mathrm{BDT}_{\gamma\gamma} + 1}{2}\right)^2 + C_2^2 \left(\frac{\mathrm{BDT}_{\mathrm{Single}H} + 1}{2}\right)^2}. \tag{2}$$

The two coefficients C_1 and C_2 ($C_2 = 1 - C_1$) and $\mathrm{BDT}_{\mathrm{tot}}$ take values in the range [0, 1]. Only events passing a minimum requirement on the value of $\mathrm{BDT}_{\mathrm{tot}}$ are considered in the analysis. To reduce the effect of limited statistics of the Monte Carlo samples in the determination the minimum value required for $\mathrm{BDT}_{\mathrm{tot}}$, and of the C_1 and C_2 coefficients, a two-stage procedure is used. The values of the C_1 and C_2 as well as the BDT cut value are scanned twice in order to maximize the significance. This two-stage optimization procedure first finds the maximum significance that can be achieved for each resonance mass point independently, leading to different coefficient values and $\mathrm{BDT}_{\mathrm{tot}}$ requirement values for the various mass points. A second scan is done to select all coefficients providing a significance within 5% of the maximum value, for each of the resonance mass values. From those possible combinations a common C_1 coefficient is sought (resulting in $C_1 = 0.65$) across all the resonances so that the selection will have common coefficients for all resonance mass points, but different $\mathrm{BDT}_{\mathrm{tot}}$ values. For each of the resonance mass hypotheses, a requirement is set on the $m^*_{b\bar{b}\gamma\gamma}$ value to select events within $\pm 2\sigma$ of the expected mean value for signal events (where σ is the standard deviation parameter of the Crystal Ball function that best fits the $m^*_{b\bar{b}\gamma\gamma}$ distribution). In the case of the 900 GeV and 1000 GeV mass hypotheses, the requirement is relaxed to $\pm 4\sigma$ to increase the number of events used for the signal extraction. The $\mathrm{BDT}_{\mathrm{tot}}$ distributions are shown in Fig. 7 for two signal hypotheses ($m_X = 300$ GeV and 500 GeV).

TABLE IV. Variables used in the BDT for the resonant analysis. For variables depending on b-tagged jets, only jets b-tagged using the 77% working point are considered as described in Sec. IV A.

Variable	Definition
Photon-related kinematic variables	
$p_{\mathrm{T}}^{\gamma\gamma}$, $y^{\gamma\gamma}$	Transverse momentum and rapidity of the diphoton system
$\Delta\phi_{\gamma\gamma}$ and $\Delta R_{\gamma\gamma}$	Azimuthal angle and ΔR between the two photons
Jet-related kinematic variables	
$m_{b\bar{b}}$, $p_{\mathrm{T}}^{b\bar{b}}$ and $y_{b\bar{b}}$	Invariant mass, transverse momentum and rapidity of the b-tagged jets system
$\Delta\phi_{b\bar{b}}$ and $\Delta R_{b\bar{b}}$	Azimuthal angle and ΔR between the two b-tagged jets
N_{jets} and $N_{b\text{-jets}}$	Number of jets and number of b-tagged jets
H_{T}	Scalar sum of the p_{T} of the jets in the event
Diphoton + dijet-related kinematic variables	
$m^*_{b\bar{b}\gamma\gamma}$	Invariant mass of the diphoton plus b-tagged jets system
$\Delta y_{\gamma\gamma,b\bar{b}}$, $\Delta\phi_{\gamma\gamma,b\bar{b}}$ and $\Delta R_{\gamma\gamma,b\bar{b}}$	Distance in rapidity, azimuthal angle and ΔR between the diphoton and the b-tagged jets system
Missing transverse momentum variables	
$E_{\mathrm{T}}^{\mathrm{miss}}$	Missing transverse momentum

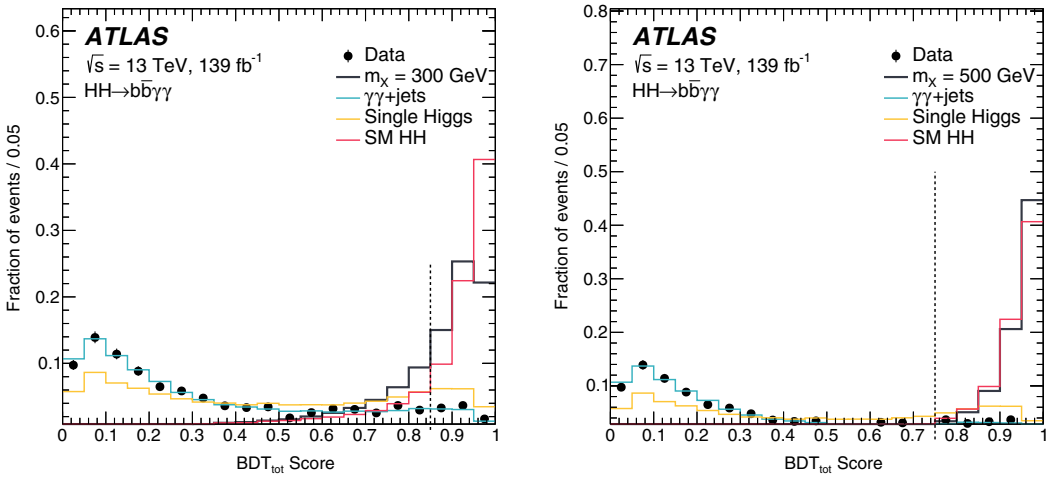

FIG. 7. The $\mathrm{BDT_{tot}}$ score for the benchmark signals ((a) $m_X = 300$ GeV and (b) $m_X = 500$ GeV) and for the main backgrounds. Distributions are normalized to unit area. The dashed lines denote the event selection thresholds. Events with a $\mathrm{BDT_{tot}}$ score below 0.85 for $m_X = 300$ GeV or below 0.75 for $m_X = 500$ GeV are discarded.

C. Comparison of data and predictions

The analysis selection described in Sec. IV B requires two "tight" photons and this region is mainly composed of $\gamma\gamma$, γ–jet, and dijet events, where either one or two jets are misidentified as photons. The fractional contribution of each component can be estimated using a data-driven approach [109] based on the photon identification and isolation distributions from genuine and misidentified photons. After the common preselection, $(85 \pm 3)\%$ of sideband events are genuine diphoton events, with the remaining $(15 \pm 4)\%$ consisting of γ–jet events and a negligible number of dijet events. The uncertainties in the above fractions include both the statistical and systematic uncertainties, where the systematic uncertainty is estimated by using different photon identification criteria. In the BDT-based categories, the proportion of genuine diphoton events increases but the method suffers from a low event count for both the nonresonant and resonant cases.

Figure 8 shows the level of agreement between data and the background prediction for the $m_{\gamma\gamma}$ and $m^*_{b\bar{b}\gamma\gamma}$ distributions, after the common preselection. The continuum background is scaled by the $\gamma\gamma$, γ–jet, and dijet fractions and normalized to the data sideband. The $\gamma\gamma + \text{jets}$ continuum background is further divided according to the flavors of the two jets (for example $b\bar{b}$ or other jets). This decomposition is taken directly from the proportions predicted by the SHERPA event generator, as described in Sec. III, and it is shown for illustration. Figures 9 and 10 show the $m_{\gamma\gamma}$ distribution after the nonresonant and resonant BDT categorization and for two benchmark mass points $m_X = 300$ GeV and $m_X = 500$ GeV. The figures illustrate the signal and background composition. The background distributions shown in these figures are not directly used to model the background processes in the analysis workflow explained in Sec. V.

V. SIGNAL AND BACKGROUND PARAMETRIZATION

The signal and backgrounds are extracted by fitting analytic functions to the diphoton invariant mass distribution in the range $105 < m_{\gamma\gamma} < 160$ GeV in both the resonant and nonresonant HH searches.

A. $H \to \gamma\gamma$ parametrization

For the di-Higgs signal and single-Higgs-boson background distributions, the parameterized forms are determined through fits to simulated samples and the expected normalizations are obtained from their theoretical cross sections multiplied by the product of the acceptance times efficiency from the simulation. The diphoton invariant mass distribution shapes are modeled with a double-sided Crystal Ball function [91,110], which is characterized by a Gaussian core and asymmetric power-law tails. This function allows the modeling of event distributions in which non-Gaussian tails can arise from experimental effects, such as photon-energy mismeasurements.

The shape parameters are determined by fitting the diphoton mass distribution in simulation for each category. The width of the fitted function is largely insensitive to the specific signal processes considered in the analysis, with maximum variations of approximately 10%. For the nonresonant search, the parameterized form of $m_{\gamma\gamma}$ is obtained from the simulation of the ggF and VBF HH processes with $\kappa_\lambda = 1$, described in Sec. III. No significant dependence of the functional form on κ_λ was found. For the resonant search, the functional form is obtained from the simulation of the heavy-resonance signals. Table V shows

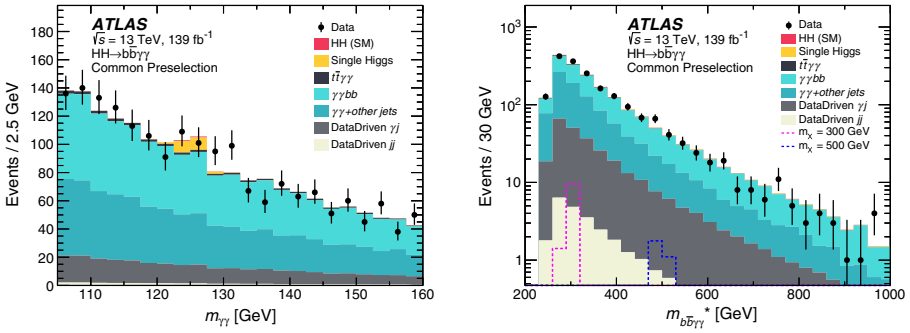

FIG. 8. Distributions of (a) $m_{\gamma\gamma}$ and (b) $m^{*}_{b\bar{b}\gamma\gamma}$ for events satisfying the common preselection criteria. The data-derived fractions of nonresonant $\gamma\gamma$, γ–jet or jet–γ, and dijet background are applied and the total background is normalized to the data sideband. The scalar resonance signal is scaled to a total production cross section $\sigma(pp \to X \to HH) = 370$ fb for $m_X = 300$ GeV or $\sigma(pp \to X \to HH) = 67$ fb for $m_X = 500$ GeV, corresponding to the expected exclusion limits presented in Sec. VII C.

the resolution parameter of the double-sided Crystal Ball functional form fit to the $m_{\gamma\gamma}$ distribution for simulated Higgs boson pair events in the nonresonant categories and for two different mass hypotheses for a heavy resonant signal. For both searches, the chosen functional forms are found to model both the single Higgs and di-Higgs boson events well. As no statistically significant bias is observed in injection tests between the input and fitted signals, the same parametrized functions are used for both the single Higgs and di-Higgs boson processes.

B. Background parametrization

The continuum diphoton background is modeled using a functional form chosen by fitting a highly populated MC

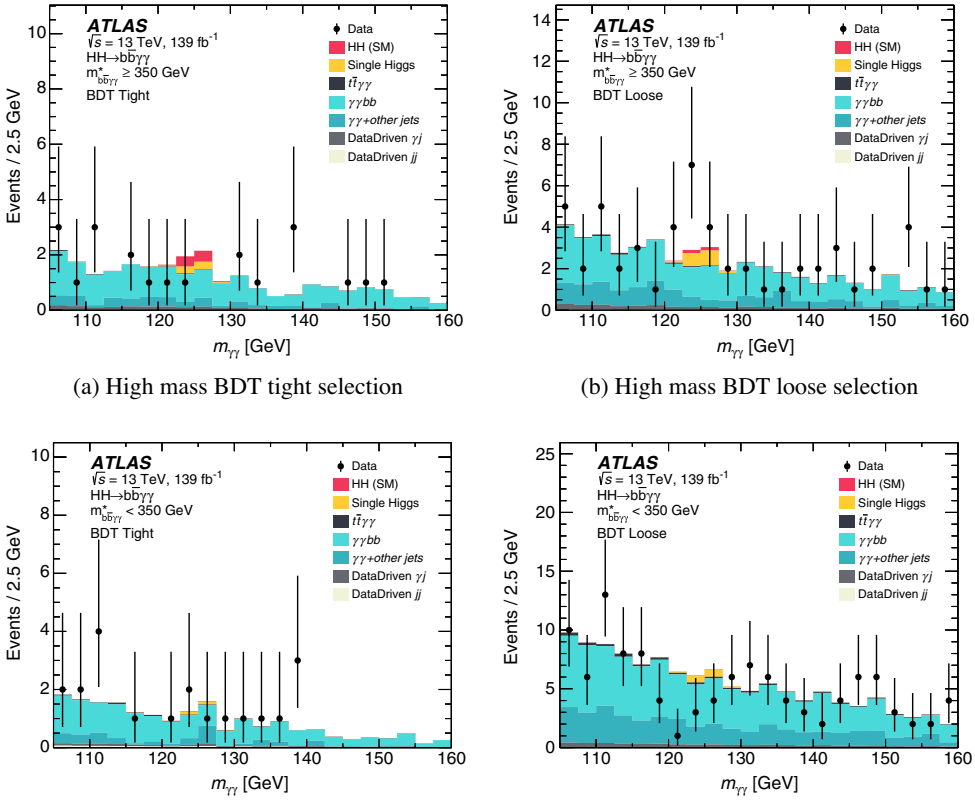

FIG. 9. Distributions of $m_{\gamma\gamma}$ in all signal categories for the nonresonant HH search: (a) high mass BDT tight, (b) high mass BDT loose, (c) low mass BDT tight, (d) low mass BDT loose. The data-derived fractions of nonresonant $\gamma\gamma$, γ–jet or jet–γ, and dijet background are applied and the total background is normalized to the data sideband.

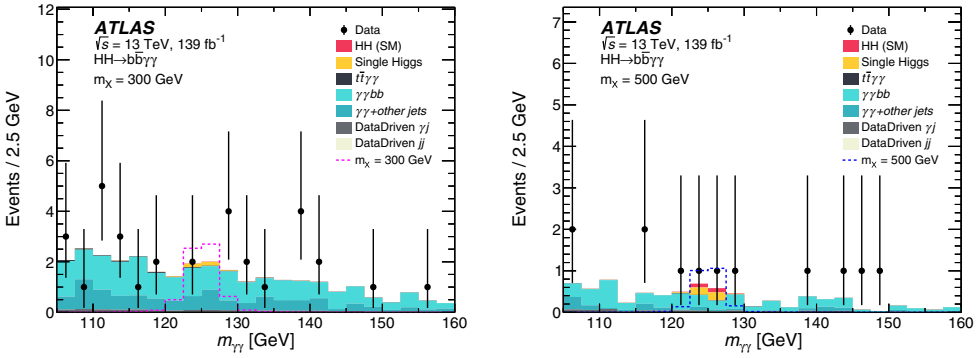

FIG. 10. Distributions of $m_{\gamma\gamma}$ for the selections used for the resonance mass points (a) $m_X = 300$ GeV and (b) $m_X = 500$ GeV for the resonant search. The data-derived fractions of nonresonant $\gamma\gamma$, γ–jet or jet–γ, and dijet background are applied and the total background is normalized to the data sideband. The scalar resonance signal is scaled to a total production cross section $\sigma(pp \to X \to HH) = 370$ fb for $m_X = 300$ GeV or $\sigma(pp \to X \to HH) = 67$ fb for $m_X = 500$ GeV, corresponding to the expected exclusion limits presented in Sec. VII C.

background template. Given the high $\gamma\gamma$ purity quoted in Sec. IV C, the background template is constructed in each category from the $\gamma\gamma$ + jets simulation which is normalized to the data sideband in the mass windows of 105 GeV–120 GeV and 130 GeV–160 GeV in the $m_{\gamma\gamma}$ spectrum.

The potential bias associated with the choice of a specific analytic function to model the continuum background is estimated for each category as prescribed in Refs. [91,111]. It is obtained as the signal event yield extracted from a signal-plus-background fit to the background-only diphoton invariant mass distribution in the range 105 GeV $< m_{\gamma\gamma} <$ 160 GeV. This bias is also called the "spurious signal". The number of fitted signal events is computed for Higgs boson masses in intervals of 1 GeV from 121 GeV to 129 GeV. The bias is taken as the largest number of fitted spurious signal events in this 8 GeV mass window. Of the different analytic functions that are tested, the one with the smallest number of parameters is chosen from the functions with a spurious signal smaller than 20% of the data's statistical uncertainty plus two times the MC statistical uncertainty.

TABLE V. The resolution parameter of the double-sided Crystal Ball functional form and the corresponding statistical uncertainty are obtained from the fit to the $m_{\gamma\gamma}$ distribution for simulated Higgs boson pair events for the nonresonant categories and for two different mass hypotheses for a heavy-resonance signal.

Category	σ_{DSCB} [GeV]
High mass BDT tight	1.33 ± 0.01
High mass BDT loose	1.47 ± 0.02
Low mass BDT tight	1.50 ± 0.06
Low mass BDT loose	1.64 ± 0.03
Resonant $m_X = 300$ GeV	1.78 ± 0.02
Resonant $m_X = 500$ GeV	1.46 ± 0.01

In each category of the nonresonant search and in all the analysis regions defined in the resonant HH search, an exponential function $\exp(a \cdot m_{\gamma\gamma})$ is found to be the best choice since it has the smallest number of degrees of freedom and yields a consistently small bias. Wald tests [112] on data show that the data do not prefer a higher-degree functional form to the exponential form. The bias is found to be at most 40% (60%) of the expected error on the fitted signal yield originating from the data statistics for the nonresonant (resonant) search. The difference in shape between the simulated events and the exponential form measured in the sidebands is found to have a negligible impact on the spurious signal. To study the impact on the spurious signal from the difference in shape between the MC background template and the data sideband, the MC template is reweighted to data using a linear function of $m_{\gamma\gamma}$ derived from the MC-data difference. The spurious signal value evaluated from the reweighted MC template is found to be compatible with the nominal one used as the systematic uncertainty.

VI. SYSTEMATIC UNCERTAINTIES

The sensitivity of the analysis is limited by the statistical precision. The assessment of the systematic uncertainties is described below and their impact on the results is discussed in Sec. VII D. The uncertainty in the integrated luminosity of the full Run 2 dataset is 1.7% [39], obtained using the LUCID-2 detector [38] for the primary luminosity measurements.

The continuum background processes of the analysis are estimated from data and are subject to uncertainties related to the potential bias arising from the chosen background model, as described in Sec. V B. The background functional form bias is assessed as an additional uncertainty in the total number of signal events in each category. For the single

Higgs boson and di-Higgs boson production processes, both of which are estimated using simulation, experimental and theoretical systematic uncertainties are propagated through the full analysis procedure, as described in the following.

The efficiency of the diphoton trigger used to select events is evaluated in simulation and data using a bootstrap method and radiative Z decays [113]. The difference between data and MC is taken as a systematic uncertainty. In the diphoton invariant mass range of $105 < m_{\gamma\gamma} < 160$ GeV, the trigger efficiency uncertainty affects the acceptance by 1% in each category. The uncertainty in the vertex selection efficiency is assessed by comparing the efficiency of finding photon-pointing vertices in $Z \to e^+e^-$ events in data with that in simulation [114]. The resulting uncertainty is found to have a negligible effect on the signal selection efficiency.

The systematic uncertainties from the photon identification and isolation efficiencies are estimated following the prescriptions in Ref. [90]. They are evaluated by varying the correction factors for photon selection efficiencies in simulation by the corresponding uncertainties and affect the diphoton selection efficiency. The experimental uncertainties in the photon-energy scale and resolution are obtained from Ref. [90].

The jet-energy scale and resolution uncertainties [115] affect the $m_{b\bar{b}}$ distribution, while flavor-tagging uncertainties affect the acceptance of the analysis categories. The experimental uncertainties in jet energy scale and resolution are propagated to the $E_{\mathrm{T}}^{\mathrm{miss}}$ calculation. In addition, the uncertainties in the scale and resolution of the $E_{\mathrm{T}}^{\mathrm{miss}}$ soft term are evaluated by using the method described in Ref. [103]. The flavor-tagging uncertainties for b- and c-jets are estimated in $t\bar{t}$ events [98,116], while the misidentification uncertainty of light-flavor jets is determined using dijet events [117]. Additional uncertainties from the b-jet momentum correction accounting for the presence of muons and neutrinos are found to be negligible.

For single Higgs boson and SM HH production, the effects of theoretical scale uncertainties due to missing higher-order corrections on the production rates are estimated by varying the factorization and renormalization scales up and down from their nominal values by a factor of two, recalculating the cross section in each case, and taking the largest deviation from the nominal cross section as the uncertainty. The uncertainties in SM HH ggF production arising from the choice of renormalization scheme and scale of the top-quark mass and their combination with those from factorization and renormalization scale variations are based on Ref. [17]. The uncertainties in the cross sections, including effects of PDF + α_{s} uncertainties, and the uncertainties in the $H \to \gamma\gamma$ and $H \to b\bar{b}$ branching fractions, are taken from Refs. [14,56]. The uncertainty in the value of the Higgs boson mass is considered [13]. An additional 100% uncertainty is assigned to the single-Higgs-boson ggF and VBF production modes and to Higgs boson production in association with a W boson. This is motivated by studies of heavy-flavor production in association with top-quark pairs [118,119] and of W boson production in association with b-jets [120]. No additional heavy-flavor uncertainty is assigned to the single-Higgs-boson $t\bar{t}H$ and ZH production modes, where the dominant heavy-flavor production is already accounted for in the LO process. For all samples, the uncertainty related to the choice of parton showering model is evaluated by comparing the predictions of the nominal MC samples and alternative samples using a different parton showering model. In addition, for the nonresonant HH production processes, a systematic uncertainty is assigned to the κ_λ reweighting, as discussed in Sec. III.

In the resonant search, the systematic uncertainty sources considered are the same as for the nonresonant case, except that uncertainties due to the finite order of the QCD calculations are not assigned to the resonant signal cross section. In this search the SM HH production processes are considered as background.

VII. RESULTS

The statistical framework used to derive the results for both the nonresonant and resonant searches is described in the following.

A. Statistical framework

For both the nonresonant and resonant searches, the results of the analysis are obtained from a maximum-likelihood fit of the $m_{\gamma\gamma}$ distribution in the range $105\ \mathrm{GeV} < m_{\gamma\gamma} < 160\ \mathrm{GeV}$, performed simultaneously over all relevant categories described in Sec. IV B. The likelihood function is defined in Eq. (3),

$$\mathcal{L} = \prod_c \left(\mathrm{Pois}(n_c | N_c(\boldsymbol{\theta})) \cdot \prod_{i=1}^{n_c} f_c(m_{\gamma\gamma}^i, \boldsymbol{\theta}) \cdot G(\boldsymbol{\theta}) \right), \quad (3)$$

where for each event i in a category c, n_c is the observed number of events, N_c is the expected number of events, f_c is the value of the probability density function, $\boldsymbol{\theta}$ are nuisance parameters, and $G(\boldsymbol{\theta})$ are constraint pdfs for the nuisance parameters.

The expected number of events N_c, defined in Eq. (4), is the sum of the expected yields from di-Higgs boson production processes, single Higgs boson production, the nonresonant background, as well as the spurious-signal uncertainty,

$$N_c(\boldsymbol{\theta}) = \mu \cdot N_{HH,\mathrm{c}}(\boldsymbol{\theta}_{HH}^{\mathrm{yield}}) + N_{\mathrm{bkg,c}}^{\mathrm{res}}(\boldsymbol{\theta}_{\mathrm{res}}^{\mathrm{yield}}) + N_{\mathrm{SS,c}} \cdot \boldsymbol{\theta}^{\mathrm{SS,c}} + N_{\mathrm{bkg,c}}^{\mathrm{nonres}}, \quad (4)$$

where μ is the signal strength, $\boldsymbol{\theta}^{\mathrm{SS,c}}$ represent the nuisance parameters associated with the background function bias and $\boldsymbol{\theta}^{\mathrm{yield}}$ represent the nuisance parameters affecting the event yield, as detailed in Sec. VI. Correlation of the nuisance parameters across different signal and background components, as well as categories, is taken into account. In the case of the nonresonant search, $N^{\mathrm{res}}_{\mathrm{bkg,c}} = N_{H,\mathrm{c}}$, while in the case of the resonant analysis $N^{\mathrm{res}}_{\mathrm{bkg,c}} = N_{H,\mathrm{c}} + N_{\mathrm{SM}HH,\mathrm{c}}$.

The probability density function f_c represents the shape information. The sum of the double-sided Crystal Ball functions modeling the HH production processes, single Higgs boson production, and the spurious signal, and of the analytic function modeling the nonresonant background as described in Sec. V B, is shown in Eq. (5),

$$\begin{aligned} f_c(m_{\gamma\gamma},\boldsymbol{\theta}) = [&\mu \cdot N_{HH,\mathrm{c}}(\boldsymbol{\theta}^{\mathrm{yield}}_{HH}) \cdot f_{HH,\mathrm{c}}(m_{\gamma\gamma},\boldsymbol{\theta}^{\mathrm{shape}}_{HH}) \\ &+ N^{\mathrm{res}}_{\mathrm{bkg,c}}(\boldsymbol{\theta}^{\mathrm{yield}}_{\mathrm{res}}) \cdot f^{\mathrm{res}}_{\mathrm{bkg,c}}(m_{\gamma\gamma},\boldsymbol{\theta}^{\mathrm{shape}}_{\mathrm{res}}) \\ &+ N_{\mathrm{SS,c}} \cdot \boldsymbol{\theta}^{\mathrm{SS,c}}_{HH} \cdot f_{HH,\mathrm{c}}(m_{\gamma\gamma},\boldsymbol{\theta}^{\mathrm{shape}}_{HH}) \\ &+ N^{\mathrm{nonres}}_{\mathrm{bkg,c}} \cdot f^{\mathrm{nonres}}_{\mathrm{bkg,c}}(m_{\gamma\gamma},\boldsymbol{\theta}^{\mathrm{shape}}_{\mathrm{nonres}})]/N_c(\boldsymbol{\theta}^{\mathrm{yield}}_{\mathrm{nonres}}), \end{aligned} \tag{5}$$

where $\boldsymbol{\theta}^{\mathrm{shape}}$ represent nuisance parameters related to the shape variations of the functional forms. When a nuisance parameter is related to shape and yield variations at the same time, the two effects are correlated.

The nominal yields of the resonant background processes are initially set to values from simulation. The likelihood function includes all the nuisance parameters that describe the systematic uncertainties. The signal strength is a free parameter in the fit. The measurement of the parameter of interest is carried out using a statistical test based on the profile likelihood ratio [107], as shown in Eq. (6),

$$\Lambda(\mu) = \frac{\mathcal{L}(\mu,\hat{\hat{\boldsymbol{\theta}}}(\mu))}{\mathcal{L}(\hat{\mu},\hat{\boldsymbol{\theta}})}, \tag{6}$$

where μ and $\boldsymbol{\theta}$ are respectively the parameter of interest and the nuisance parameters. In the numerator, the nuisance parameters are set to their profiled values $\hat{\hat{\boldsymbol{\theta}}}(\mu)$, which maximize the likelihood function for a fixed value of the parameter of interest μ. In the denominator, the parameter of interest and the nuisance parameters are set to the values $\hat{\mu}$ and $\hat{\boldsymbol{\theta}}$, respectively, which jointly maximize the likelihood.

In the absence of signal, exclusion limits are set on Higgs boson pair production in the $b\bar{b}\gamma\gamma$ final state. The limits for both nonresonant and resonant production are calculated

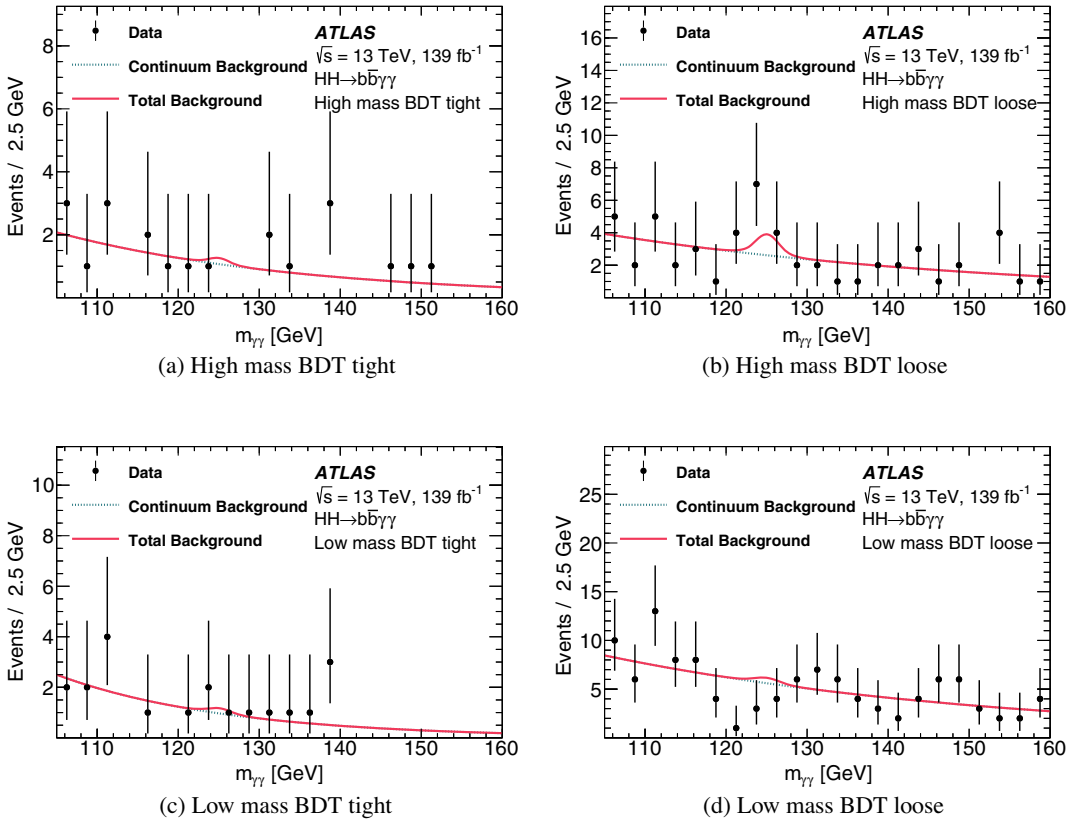

(a) High mass BDT tight (b) High mass BDT loose

(c) Low mass BDT tight (d) Low mass BDT loose

FIG. 11. Data are compared with the background-only fit for the four categories of the nonresonant search: (a) high mass BDT tight, (b) high mass BDT loose, (c) low mass BDT tight, and (d) low mass BDT loose. Both the continuum background and the background from single Higgs boson production are considered. The data points in the Figure are the same as shown in Fig. 9.

TABLE VI. The number of data events observed in the 120 GeV $< m_{\gamma\gamma} <$ 130 GeV window, the number of HH signal events expected for $\kappa_\lambda = 1$ and for $\kappa_\lambda = 10$, and events expected for single Higgs boson production (estimated using MC simulation), as well as for continuum background. For the single Higgs boson, "Rest" includes the following production modes: VBF, WH, tHq, and tHW. The values are obtained from a fit of the Asimov dataset [107] generated under the SM signal-plus-background hypothesis, $\kappa_\lambda = 1$. The continuum background component of the Asimov dataset is obtained from the fit of the data sideband. The uncertainties in HH signals and single Higgs boson background include the systematic uncertainties discussed in Sec. VI. The uncertainty in the continuum background is given by the sum in quadrature of the statistical uncertainty from the fit to the data and the spurious-signal uncertainty.

	High mass BDT tight	High mass BDT loose	Low mass BDT tight	Low mass BDT loose
Continuum background	$4.9^{+1.1}_{-1.3}$	$9.5^{+1.5}_{-1.7}$	$3.7^{+0.9}_{-1.1}$	$24.9^{+2.3}_{-2.5}$
Single Higgs boson background	$0.67^{+0.29}_{-0.13}$	$1.6^{+0.6}_{-0.2}$	$0.23^{+0.09}_{-0.03}$	$1.40^{+0.33}_{-0.16}$
ggF + bbH	$0.26^{+0.28}_{-0.16}$	$0.4^{+0.5}_{-0.2}$	$0.07^{+0.08}_{-0.04}$	$0.27^{+0.27}_{-0.16}$
$t\bar{t}H$	$0.19^{+0.03}_{-0.03}$	$0.49^{+0.09}_{-0.07}$	$0.107^{+0.022}_{-0.017}$	$0.75^{+0.13}_{-0.11}$
ZH	$0.142^{+0.035}_{-0.025}$	$0.48^{+0.09}_{-0.07}$	$0.040^{+0.020}_{-0.014}$	$0.27^{+0.06}_{-0.04}$
Rest	$0.074^{+0.032}_{-0.014}$	$0.16^{+0.07}_{-0.03}$	$0.012^{+0.008}_{-0.004}$	$0.111^{+0.030}_{-0.012}$
SM $HH(\kappa_\lambda = 1)$ signal	$0.87^{+0.10}_{-0.18}$	$0.37^{+0.04}_{-0.07}$	$0.049^{+0.006}_{-0.010}$	$0.078^{+0.008}_{-0.015}$
ggF	$0.86^{+0.10}_{-0.18}$	$0.35^{+0.04}_{-0.07}$	$0.046^{+0.006}_{-0.010}$	$0.072^{+0.008}_{-0.015}$
VBF	$(12.6^{+1.3}_{-1.2}) \times 10^{-3}$	$(16.1^{+1.4}_{-1.2}) \times 10^{-3}$	$(3.2^{+0.4}_{-0.4}) \times 10^{-3}$	$(6.9^{+0.5}_{-0.6}) \times 10^{-3}$
Alternative $HH(\kappa_\lambda = 10)$ signal	$6.5^{+1.0}_{-0.8}$	$3.6^{+0.6}_{-0.4}$	$4.5^{+0.7}_{-0.6}$	$8.5^{+1.3}_{-1.0}$
Data	2	17	5	14

using the CL_S method [121], with the profile-likelihood-ratio-based test statistic $\tilde{q}_\mu$, defined in Eq. (7) [107],

$$\tilde{q}_\mu = \begin{cases} -2\ln\frac{\Lambda(\mu,\hat{\hat{\boldsymbol{\theta}}}(\mu))}{\Lambda(0,\hat{\hat{\boldsymbol{\theta}}}(0))} & \hat{\mu} < 0, \\ -2\ln\frac{\Lambda(\mu,\hat{\hat{\boldsymbol{\theta}}}(\mu))}{\Lambda(\hat{\mu},\hat{\boldsymbol{\theta}}(\mu))} & 0 \le \hat{\mu} \le \mu, \\ 0 & \hat{\mu} > \mu. \end{cases} \tag{7}$$

The asymptotic approximation [107] is used for the test-statistic distribution. The inaccuracy of the asymptotic approximation is checked with pseudoexperiment studies for the key results reported in this paper.

B. Nonresonant search results

Figure 11 shows the background fits to the data. No significant excess over the SM background expectations is found, as summarized in Table VI. The statistical analysis sets a 95% C.L. upper limit on the nonresonant HH production cross section at 130 fb, while 180 fb is expected. An observed (expected) upper limit at 95% C.L. on the signal strength of 4.2 (5.7) times the SM prediction is obtained. The expected constraints are obtained for a background hypothesis excluding $pp \to HH$ production. For the upper limits on the cross section, all theoretical uncertainties are included, except those related to the signal cross section itself, while constraints on the signal strength are computed including uncertainties in the predicted signal cross section. A check of the results that quantifies the upper limits by using pseudoexperiments is performed and the increase of the limit value relative to the asymptotic approximation is found to be less than 8% for both the observed and expected upper limits. A check of the expected upper limits using prefit values for the nuisance parameters associated with the systematic uncertainties is

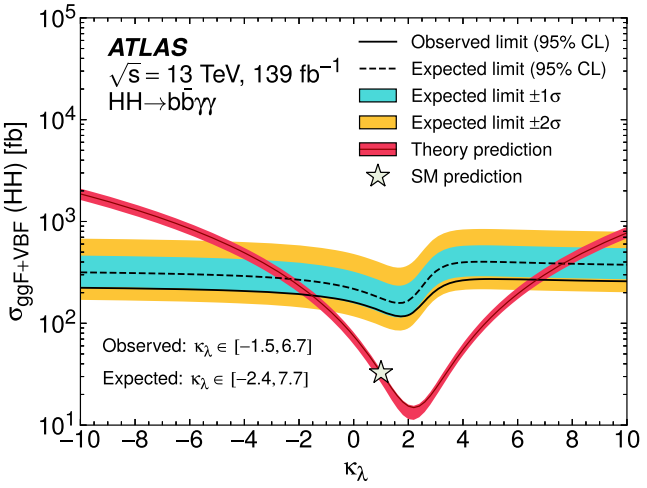

FIG. 12. Observed and expected limits at 95% C.L. on the cross section of nonresonant Higgs boson pair production as a function of the Higgs boson self-coupling modifier $\kappa_\lambda = \lambda_{HHH}/\lambda^{\mathrm{SM}}_{HHH}$. The expected constraints on κ_λ are obtained with a background hypothesis excluding $pp \to HH$ production. The $\pm 1\sigma$ and $\pm 2\sigma$ variations about the expected limit due to statistical and systematic uncertainties are also shown. The theory prediction curve represents the scenario where all parameters and couplings are set to their SM values except for κ_λ. The uncertainty band of the theory prediction curve shows the cross section uncertainty.

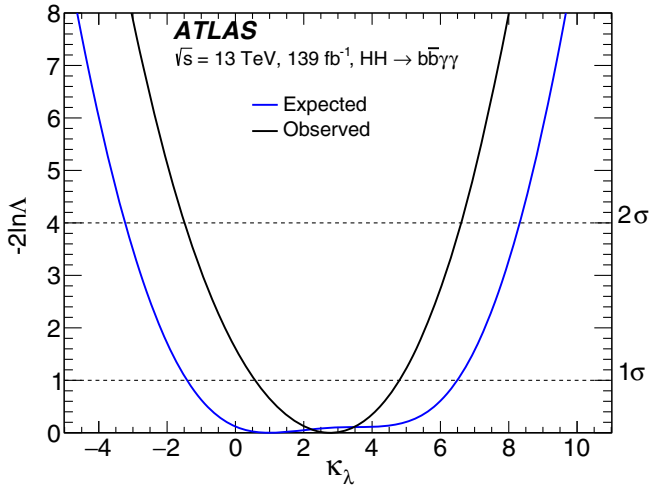

FIG. 13. Values of the negative log-profile-likelihood ratio $(-2\ln\Lambda)$ as a function of κ_λ evaluated for the combination of all the categories of the nonresonant search. The coupling of the Higgs boson to fermions and gauge bosons is set to SM values in the profile likelihood calculation. The expected result corresponds to a Asimov dataset [107] generated under the SM signal-plus-background hypothesis, $\kappa_\lambda = 1$. All systematic uncertainties, including the theoretical uncertainties in the di-Higgs boson production cross section, are included. The intersections of the solid curves and the horizontal dashed lines indicate the 1σ and 2σ confidence level intervals.

performed and an increase of 4% relative to the nominal result is found. The difference is dominated by the contribution from the spurious signal.

Upper limits on the HH production cross section are also computed as a function of κ_λ, as shown in Fig. 12. For this purpose, single-Higgs-boson production cross sections and Higgs boson decay branching ratios are assumed to have SM values, and the coupling strength between the Higgs boson and other particles are also set to their SM values [55]. The theory uncertainties related to the signal cross section are not included.

TABLE VII. The number of events observed in the $120 < m_{\gamma\gamma} < 130$ GeV window in data, the number of events expected for scalar resonance signals of masses $m_X = 300$ GeV and $m_X = 500$ GeV assuming a total production cross section $\sigma(pp \to X \to HH)$ equal to the observed exclusion limits of Fig. 15, and events expected for SM HH and single Higgs boson production (estimated using MC simulation), as well as for continuum background. The values are obtained from a fit of the Asimov dataset [107] generated under the signal-plus-background hypothesis. The continuum background component of the Asimov dataset is obtained from the fit of the data sideband. The uncertainties in the resonant signals and the SM HH and single-Higgs-boson backgrounds include the systematic uncertainties discussed in Sec. VI. The uncertainty in the continuum background is given by the sum in quadrature of the statistical uncertainty from the fit to the data and the spurious-signal uncertainty.

	$m_X = 300$ GeV	$m_X = 500$ GeV
Continuum background	$5.5^{+1.3}_{-1.5}$	$1.6^{+0.6}_{-0.9}$
Single Higgs boson background	$0.34^{+0.14}_{-0.07}$	$0.40^{+0.18}_{-0.08}$
SM HH background	$0.021^{+0.005}_{-0.009}$	$0.20^{+0.09}_{-0.09}$
$X \to HH$ signal	$6.1^{+0.9}_{-0.8}$	$6.1^{+0.8}_{-0.6}$
Data	6	4

The expected constraints on κ_λ at 95% C.L., as obtained with a background hypothesis excluding $pp \to HH$ production, are $[-2.4, 7.7]$, whereas the observed constraints are $[-1.5, 6.7]$ at 95% C.L. The inclusion of the VBF HH production mode tightens the constraints by about 5% relative to an alternative fit considering only the ggF production mode.

An alternative statistical analysis consists in determining the best-fit value of the κ_λ coupling modifier. The best-fit value of κ_λ and its uncertainty are obtained by means of a negative log-likelihood scan. The coupling strengths of the Higgs boson to fermions and gauge bosons are set to their SM values. The values of the negative log-likelihood ratio,

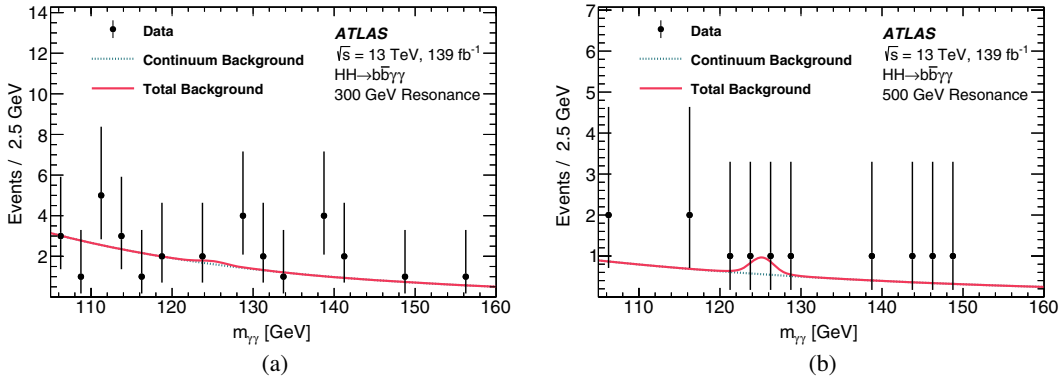

FIG. 14. Data are compared with the background-only fit for the resonant search for the (a) $m_X = 300$ GeV and (b) $m_X = 500$ GeV mass hypotheses. The continuum background, as well as the background from single Higgs boson production and from SM HH production, is considered. The data points in the Figure are the same as shown in Fig. 10.

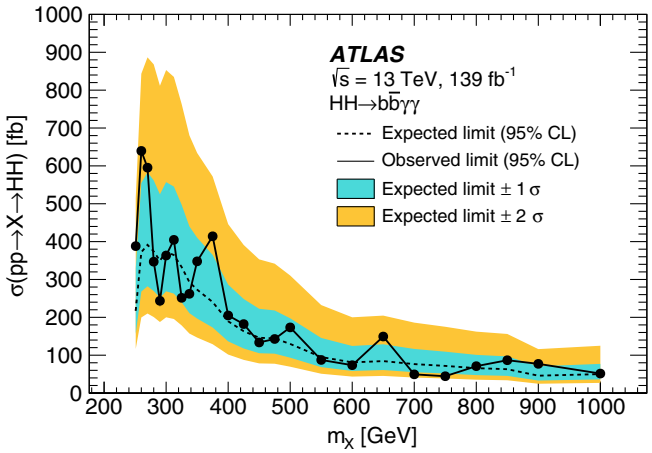

FIG. 15. Observed and expected limits at 95% C.L. on the production cross section of a narrow-width scalar resonance X as a function of the mass m_X of the hypothetical scalar particle. The black solid line represents the observed upper limits. The dashed line represents the expected upper limits. The $\pm 1\sigma$ and $\pm 2\sigma$ variations about the expected limit due to statistical and systematic uncertainties are also shown.

$-2\ln\Lambda(\mu)$, as a function of κ_λ are shown in Fig. 13. The Asimov dataset [107] is generated under the SM signal-plus-background hypothesis, $\kappa_\lambda = 1$. All systematic uncertainties, including those of the theoretical prediction of the HH production cross section, are included. The best-fit value corresponds to $\kappa_\lambda = 2.8^{+2.0}_{-2.2}$ $(^{+3.8}_{-4.3})$ for the 1σ (2σ) confidence interval. The expected value corresponds to $\kappa_\lambda = 1.0^{+5.5}_{-2.4}$ $(^{+7.3}_{-4.2})$ for the 1σ (2σ) confidence interval. The second minimum in the expected likelihood scan curve corresponds to a similar fitted signal yield with respect to the κ_λ point at the first minimum, which is a consequence of a higher cross section, but lower acceptance and worse signal-to-background separation. The m_{HH} distribution has a different shape at each of the two minima, as shown in Fig. 5.

C. Resonant search results

Figure 14 shows the fit to the data of the resonant search for two benchmark values of the mass m_X of a hypothetical scalar particle. No significant excess over the SM background expectations is found, as shown in Table VII. Figure 15 shows the observed and expected upper limits at 95% C.L. on the production cross section of a narrow-width scalar resonance. The observed (expected) upper limits vary between 640–44 fb (391–46 fb) in the range 251 GeV $\leq m_X \leq$ 1000 GeV. A check on the upper limits using pseudoexperiments is performed. For the expected limits, the results based on the pseudo-experiments are found to be up to 10% higher compared with those derived based on the asymptotic approximation. As for the observed limits, the pseudoexperiments yield typically 10% higher results compared with the asymptotic approximation in most of the m_X range explored, and the difference increases to 15% for the $m_X = 700$ GeV signal hypothesis.

D. Impact of systematic uncertainties

The dominant systematic uncertainties are listed in Table VIII for both the nonresonant and resonant searches. The main uncertainties are related to the choice of functional form for the continuum background (spurious signal), to the parton showering model, and to the photon energy resolution.

TABLE VIII. Breakdown of the dominant systematic uncertainties. The impact of the uncertainties corresponds to the relative variation of the expected upper limit on the cross section when reevaluating the profile likelihood ratio after fixing the nuisance parameter in question to its best-fit value, while all remaining nuisance parameters remain free to float. The impact is shown in %. Only systematic uncertainties with an impact of at least 0.2% are shown. Uncertainties of the "Norm + Shape" type affect both the normalization and the parameters of the functional form. The rest of the uncertainties affect only the yields.

		Relative impact of the systematic uncertainties [%]	
Source	Type	Nonresonant analysis HH	Resonant analysis $m_X = 300$ GeV
Experimental			
Photon energy resolution	Norm. + Shape	0.4	0.6
Jet energy scale and resolution	Normalization	<0.2	0.3
Flavor tagging	Normalization	<0.2	0.2
Theoretical			
Factorization and renormalization scale	Normalization	0.3	<0.2
Parton showering model	Norm. + Shape	0.6	2.6
Heavy-flavor content	Normalization	0.3	<0.2
$\mathcal{B}(H \to \gamma\gamma, b\bar{b})$	Normalization	0.2	<0.2
Spurious signal	Normalization	3.0	3.3

VIII. CONCLUSIONS

Searches for nonresonant and resonant Higgs boson pair production are performed in the $b\bar{b}\gamma\gamma$ final state using 139 fb^{-1} of 13 TeV pp collision data collected with the ATLAS detector at the LHC. No significant excess above the Standard Model background expectation is observed. A 95% C.L. upper limit of 130 fb is set on the $pp \to HH$ nonresonant production cross section, where the expected limit is 180 fb. The observed (expected) limit corresponds to 4.2 (5.7) times the cross section predicted by the Standard Model. Constraints on the Higgs boson self-coupling are also derived and limits of $-1.5 < \kappa_\lambda < 6.7$ are obtained, where $-2.4 < \kappa_\lambda < 7.7$ is expected. The expected constraints on the HH nonresonant production cross section and on κ_λ are obtained with a background hypothesis excluding $pp \to HH$ production. For resonant production of a scalar particle $X \to HH \to b\bar{b}\gamma\gamma$, upper limits on the production cross section are obtained for the narrow-width hypothesis as a function of m_X. The observed (expected) upper limits are in the range 640–44 fb (391–46 fb) for $251\,\text{GeV} \leq m_X \leq 1000\,\text{GeV}$. Compared to the previous ATLAS result based on 36 fb^{-1} of 13 TeV pp collisions, the present analysis uses a dataset about four times larger, incorporates a categorization based on $m^*_{b\bar{b}\gamma\gamma}$ and multivariate event selections, and expands the analyzed mass range of the resonance search to lower values. The results improve upon the previous ATLAS limits on the $HH \to b\bar{b}\gamma\gamma$ production cross section by up to a factor of five, and the allowed κ_λ range shrinks by about a factor of two. For the resonant search, the expected limit on the cross section improves by a factor of two to three depending on the m_X value. Of those improvements, a factor of two arises from the increase in integrated luminosity, while the additional improvement can be attributed to the use of multivariate techniques, more precise object reconstruction and calibration and, for the nonresonant search, the categorization based on $m^*_{b\bar{b}\gamma\gamma}$. The present analysis also sets constraints that are tighter than those from a combination of ATLAS searches for HH production in up to 36 fb^{-1} of 13 TeV data.

ACKNOWLEDGMENTS

We thank CERN for the very successful operation of the LHC, as well as the support staff from our institutions without whom ATLAS could not be operated efficiently. We acknowledge the support of ANPCyT, Argentina; YerPhI, Armenia; ARC, Australia; BMWFW and FWF, Austria; ANAS, Azerbaijan; SSTC, Belarus; CNPq and FAPESP, Brazil; NSERC, NRC and CFI, Canada; CERN; ANID, Chile; CAS, MOST and NSFC, China; Minciencias, Colombia; MEYS CR, Czech Republic; DNRF and DNSRC, Denmark; IN2P3-CNRS and CEA-DRF/IRFU, France; SRNSFG, Georgia; BMBF, HGF and MPG, Germany; GSRI, Greece; RGC and Hong Kong SAR, China; ISF and Benoziyo Center, Israel; INFN, Italy; MEXT and JSPS, Japan; CNRST, Morocco; NWO, Netherlands; RCN, Norway; MEiN, Poland; FCT, Portugal; MNE/IFA, Romania; JINR; MES of Russia and NRC KI, Russian Federation; MESTD, Serbia; MSSR, Slovakia; ARRS and MIZŠ, Slovenia; DSI/NRF, South Africa; MICINN, Spain; SRC and Wallenberg Foundation, Sweden; SERI, SNSF and Cantons of Bern and Geneva, Switzerland; MOST, Taiwan; TAEK, Turkey; STFC, United Kingdom; DOE and NSF, USA. In addition, individual groups and members have received support from BCKDF, CANARIE, Compute Canada and CRC, Canada; COST, ERC, ERDF, Horizon 2020 and Marie Skłodowska-Curie Actions, European Union; Investissements d'Avenir Labex, Investissements d'Avenir Idex and ANR, France; DFG and AvH Foundation, Germany; Herakleitos, Thales and Aristeia programmes co-financed by EU-ESF and the Greek NSRF, Greece; BSF-NSF and GIF, Israel; Norwegian Financial Mechanism 2014-2021, Norway; NCN and NAWA, Poland; La Caixa Banking Foundation, CERCA Programme Generalitat de Catalunya and PROMETEO and GenT Programmes Generalitat Valenciana, Spain; Göran Gustafssons Stiftelse, Sweden; The Royal Society and Leverhulme Trust, United Kingdom. The crucial computing support from all WLCG partners is acknowledged gratefully, in particular from CERN, the ATLAS Tier-1 facilities at TRIUMF (Canada), NDGF (Denmark, Norway, Sweden), CC-IN2P3 (France), KIT/GridKA (Germany), INFN-CNAF (Italy), NL-T1 (Netherlands), PIC (Spain), ASGC (Taiwan), RAL (UK) and BNL (USA), the Tier-2 facilities worldwide and large non-WLCG resource providers. Major contributors of computing resources are listed in Ref. [122].

[1] ATLAS Collaboration, Observation of a new particle in the search for the Standard Model Higgs boson with the ATLAS detector at the LHC, Phys. Lett. B **716**, 1 (2012).
[2] CMS Collaboration, Observation of a new boson at a mass of 125 GeV with the CMS experiment at the LHC, Phys. Lett. B **716**, 30 (2012).
[3] F. Englert and R. Brout, Broken Symmetry and the Mass of Gauge Vector Mesons, Phys. Rev. Lett. **13**, 321 (1964).
[4] P. W. Higgs, Broken symmetries, massless particles and gauge fields, Phys. Lett. **12**, 132 (1964).
[5] P. W. Higgs, Broken Symmetries and the Masses of Gauge Bosons, Phys. Rev. Lett. **13**, 508 (1964).

[6] G. S. Guralnik, C. R. Hagen, and T. W. B. Kibble, Global Conservation Laws and Massless Particles, Phys. Rev. Lett. **13**, 585 (1964).

[7] P. W. Higgs, Spontaneous symmetry breakdown without massless bosons, Phys. Rev. **145**, 1156 (1966).

[8] T. W. B. Kibble, Symmetry breaking in non-abelian gauge theories, Phys. Rev. **155**, 1554 (1967).

[9] P. Huang, A. J. Long, and L.-T. Wang, Probing the electroweak phase transition with Higgs factories and gravitational waves, Phys. Rev. D **94**, 075008 (2016).

[10] S. Dawson, S. Dittmaier, and M. Spira, Neutral Higgs-boson pair production at hadron colliders: QCD corrections, Phys. Rev. D **58**, 115012 (1998).

[11] S. Borowka, N. Greiner, G. Heinrich, S. P. Jones, M. Kerner, J. Schlenk, U. Schubert, and T. Zirke, Higgs Boson Pair Production in Gluon Fusion at Next-to-Leading Order with Full Top-Quark Mass Dependence, Phys. Rev. Lett. **117**, 012001 (2016); Erratum, Phys. Rev. Lett. **117**, 079901 (2016).

[12] D. de Florian and J. Mazzitelli, Higgs Boson Pair Production at Next-to-Next-to-Leading Order in QCD, Phys. Rev. Lett. **111**, 201801 (2013).

[13] ATLAS and CMS Collaborations, Combined Measurement of the Higgs Boson Mass in pp Collisions at $\sqrt{s} = 7$ and 8 TeV with the ATLAS and CMS Experiments, Phys. Rev. Lett. **114**, 191803 (2015).

[14] J. Alison, M. Gouzevitch, J. Mazzitelli, and C. Vernieri, Higgs boson potential at colliders: Status and perspectives, Rev. Phys. **5**, 100045 (2020).

[15] D. Y. Shao, C. S. Li, H. T. Li, and J. Wang, Threshold resummation effects in Higgs boson pair production at the LHC, J. High Energy Phys. 07 (2013) 169.

[16] D. de Florian and J. Mazzitelli, Higgs pair production at next-to-next-to-leading logarithmic accuracy at the LHC, J. High Energy Phys. 09 (2015) 053.

[17] J. Baglio, F. Campanario, S. Glaus, M. Mühlleitner, J. Ronca, and M. Spira, $gg \to HH$: Combined uncertainties, Phys. Rev. D **103**, 056002 (2021).

[18] M. Grazzini, G. Heinrich, S. Jones, S. Kallweit, M. Kerner, J. M. Lindert, and J. Mazzitelli, Higgs boson pair production at NNLO with top quark mass effects, J. High Energy Phys. 05 (2018) 059.

[19] R. Frederix, S. Frixione, V. Hirschi, F. Maltoni, O. Mattelaer, P. Torrielli, E. Vryonidou, and M. Zaro, Higgs pair production at the LHC with NLO and parton-shower effects, Phys. Lett. B **732**, 142 (2014).

[20] G. D. Kribs and A. Martin, Enhanced di-Higgs production through light colored scalars, Phys. Rev. D **86**, 095023 (2012).

[21] L. Di Luzio, R. Gröber, and M. Spannowsky, Maxi-sizing the trilinear Higgs self-coupling: How large could it be?, Eur. Phys. J. C **77**, 788 (2017).

[22] G. D. Kribs, A. Maier, H. Rzehak, M. Spannowsky, and P. Waite, Electroweak oblique parameters as a probe of the trilinear Higgs boson self-interaction, Phys. Rev. D **95**, 093004 (2017).

[23] T. D. Lee, A theory of spontaneous T violation, Phys. Rev. D **8**, 1226 (1973).

[24] S. Dimopoulos and H. Georgi, Softly broken supersymmetry and SU(5), Nucl. Phys. **B193**, 150 (1981).

[25] Z. Chacko, Y. Nomura, M. Papucci, and G. Perez, Natural little hierarchy from a partially goldstone twin Higgs, J. High Energy Phys. 01 (2006) 126.

[26] J. Mrazek, A. Pomarol, R. Rattazzi, M. Redi, J. Serra, and A. Wulzer, The other natural two Higgs doublet model, Nucl. Phys. **B853**, 1 (2011).

[27] L. Randall and R. Sundrum, Large Mass Hierarchy from a Small Extra Dimension, Phys. Rev. Lett. **83**, 3370 (1999).

[28] ATLAS Collaboration, Search for Higgs boson pair production in the $\gamma\gamma b\bar{b}$ final state with 13 TeV pp collision data collected by the ATLAS experiment, J. High Energy Phys. 11 (2018) 040.

[29] ATLAS Collaboration, Combination of searches for Higgs boson pairs in pp collisions at $\sqrt{s} = 13$ TeV with the ATLAS detector, Phys. Lett. B **800**, 135103 (2020).

[30] CMS Collaboration, Search for nonresonant Higgs boson pair production in final states with two bottom quarks and two photons in proton–proton collisions at $\sqrt{s} = 13$ TeV, J. High Energy Phys. 03 (2021) 257.

[31] CMS Collaboration, Search for Higgs boson pair production in the $\gamma\gamma b\bar{b}$ final state in pp collisions at $\sqrt{s} = 13$ TeV, Phys. Lett. B **788**, 7 (2019).

[32] ATLAS Collaboration, The ATLAS experiment at the CERN Large Hadron Collider, J. Instrum. **3**, S08003 (2008).

[33] ATLAS Collaboration, ATLAS insertable B-layer: Technical design report, Reports No. ATLAS-TDR-19, No. CERN-LHCC-2010-013, 2010, https://cds.cern.ch/record/1291633; Addendum, Reports No. ATLAS-TDR-19-ADD-1, No. CERN-LHCC-2012-009, 2012, https://cds.cern.ch/record/1451888.

[34] B. Abbott *et al.*, Production and integration of the ATLAS Insertable B-Layer, J. Instrum. **13**, T05008 (2018).

[35] ATLAS Collaboration, Performance of the ATLAS trigger system in 2015, Eur. Phys. J. C **77**, 317 (2017).

[36] ATLAS Collaboration, The ATLAS Collaboration software and firmware, Report No. ATL-SOFT-PUB-2021-001, 2021, https://cds.cern.ch/record/2767187.

[37] ATLAS Collaboration, ATLAS data quality operations and performance for 2015–2018 data-taking, J. Instrum. **15**, P04003 (2020).

[38] G. Avoni *et al.*, The new LUCID-2 detector for luminosity measurement and monitoring in ATLAS, J. Instrum. **13**, P07017 (2018).

[39] ATLAS Collaboration, Luminosity determination in pp collisions at $\sqrt{s} = 13$ TeV using the ATLAS detector at the LHC, Report No. ATLAS-CONF-2019-021, 2019, https://cds.cern.ch/record/2677054.

[40] ATLAS Collaboration, Emulating the impact of additional proton-proton interactions in the ATLAS simulation by pre-sampling sets of inelastic Monte Carlo events, Comput. Softw. Big Sci. **6**, 3 (2022).

[41] P. Nason and C. Oleari, NLO Higgs boson production via vector-boson fusion matched with shower in POWHEG, J. High Energy Phys. 02 (**2010**) 037.

[42] G. Heinrich, S. P. Jones, M. Kerner, G. Luisoni, and E. Vryonidou, NLO predictions for Higgs boson pair production with full top quark mass dependence matched to parton showers, J. High Energy Phys. 08 (2017) 088.

[43] G. Heinrich, S. Jones, M. Kerner, G. Luisoni, and L. Scyboz, Probing the trilinear Higgs boson coupling in di-

Higgs production at NLO QCD including parton shower effects, J. High Energy Phys. 06 (2019) 066.
[44] J. Butterworth *et al.*, PDF4LHC recommendations for LHC Run II, J. Phys. G **43**, 023001 (2016).
[45] ATLAS Collaboration, Validation of signal Monte Carlo event generation in searches for Higgs boson pairs with the ATLAS detector, Report No. ATL-PHYS-PUB-2019-007, 2019, https://cds.cern.ch/record/2665057.
[46] S. Amoroso *et al.*, Les Houches 2019: Physics at TeV Colliders: Standard Model Working Group Report, Proceedings of the 11th Les Houches Workshop on Physics at TeV Colliders: PhysTeV Les Houches, 2020, arXiv:2003.01700.
[47] J. Alwall, S. Frixione, V. Hirschi, F. Maltoni, O. Mattelaer, H.-S. Shao, T. Stelzer, P. Torrielli, and M. Zaro *et al.*, The automated computation of tree-level and next-to-leading order differential cross sections, and their matching to parton shower simulations, J. High Energy Phys. 07 (2014) 079.
[48] F. Bishara, R. Contino, and J. Rojo, Higgs pair production in vector-boson fusion at the LHC and beyond, Eur. Phys. J. C **77**, 481 (2017).
[49] R. D. Ball *et al.*, Parton distributions with LHC data, Nucl. Phys. **B867**, 244 (2013).
[50] L.-S. Ling , R.-Y. Zhang, W.-G. Ma, L. Guo, W.-H. Li, and X.-Z. Li *et al.*, NNLO QCD corrections to Higgs pair production via vector boson fusion at hadron colliders, Phys. Rev. D **89**, 073001 (2014).
[51] F. A. Dreyer and A. Karlberg, Vector-boson fusion Higgs pair production at N3LO, Phys. Rev. D **98**, 114016 (2018).
[52] F. A. Dreyer and A. Karlberg, Fully differential vector-boson fusion Higgs pair production at next-to-next-to-leading order, Phys. Rev. D **99**, 074028 (2019).
[53] M. Bähr *et al.*, HERWIG++ physics and manual, Eur. Phys. J. C **58**, 639 (2008).
[54] J. Bellm *et al.*, HERWIG 7.0/HERWIG++ 3.0 release note, Eur. Phys. J. C **76**, 196 (2016).
[55] ATLAS Collaboration, Combined measurements of Higgs boson production and decay using up to 80 fb^{-1} of proton–proton collision data at $\sqrt{s} = 13$ TeV collected with the ATLAS experiment, Phys. Rev. D **101**, 012002 (2020).
[56] D. de Florian *et al.*, Handbook of LHC Higgs cross sections: 4. Deciphering the nature of the Higgs sector, arXiv:1610.07922.
[57] A. Djouadi, J. Kalinowski, and M. Spira, HDECAY: A program for Higgs boson decays in the standard model and its supersymmetric extension, Comput. Phys. Commun. **108**, 56 (1998).
[58] E. Bothmann *et al.*, Event generation with SHERPA 2.2, SciPost Phys. **7**, 034 (2019).
[59] T. Gleisberg and S. Höche, Comix, a new matrix element generator, J. High Energy Phys. 12 (2008) 039.
[60] F. Buccioni, J.-N. Lang, J. M. Lindert, P. Maierhöfer, S. Pozzorini, H. Zhang, and M. F. Zoller *et al.*, OPENLOOPS2, Eur. Phys. J. C **79**, 866 (2019).
[61] F. Cascioli, P. Maierhöfer, and S. Pozzorini, Scattering Amplitudes with Open Loops, Phys. Rev. Lett. **108**, 111601 (2012).
[62] A. Denner, S. Dittmaier, and L. Hofer, Collier: A fortran-based complex one-loop library in extended regularizations, Comput. Phys. Commun. **212**, 220 (2017).
[63] S. Schumann and F. Krauss, A parton shower algorithm based on Catani–Seymour dipole factorisation, J. High Energy Phys. 03 (2008) 038.
[64] S. Höche, F. Krauss, M. Schönherr, and F. Siegert, A critical appraisal of NLO + PS matching methods, J. High Energy Phys. 09 (2012) 049.
[65] S. Höche, F. Krauss, M. Schönherr, and F. Siegert, QCD matrix elements + parton showers. The NLO case, J. High Energy Phys. 04 (2013) 027.
[66] F. Siegert, A practical guide to event generation for prompt photon production with SHERPA, J. Phys. G **44**, 044007 (2017).
[67] T. Sjöstrand, S. Ask, J. R. Christiansen, R. Corke, N. Desai, P. Ilten, S. Mrenna, S. Prestel, C. O. Rasmussen, and P. Z. Skands, An introduction to PYTHIA8.2, Comput. Phys. Commun. **191**, 159 (2015).
[68] ATLAS Collaboration, ATLAS PYTHIA8 tunes to 7 TeV data, Report No. ATL-PHYS-PUB-2014-021, 2014, https://cds.cern.ch/record/1966419.
[69] R. D. Ball *et al.*, Parton distributions for the LHC run II, J. High Energy Phys. 04 (2015) 040.
[70] S. Gieseke, C. Röhr, and A. Siodmok, Colour reconnections in HERWIG++, Eur. Phys. J. C **72**, 2225 (2012).
[71] K. Hamilton, P. Nason, and G. Zanderighi, MINLO: multi-scale improved NLO, J. High Energy Phys. 10 (2012) 155.
[72] J. M. Campbell, R. Keith Ellis, R. Frederix, P. Nason, C. Oleari, and C. Williams, NLO Higgs boson production plus one and two jets using the POWHEG BOX, MadGraph4 and MCFM, J. High Energy Phys. 07 (2012) 092.
[73] K. Hamilton, P. Nason, C. Oleari, and G. Zanderighi, Merging H/W/Z + 0 and 1 jet at NLO with no merging scale: a path to parton shower + NNLO matching, J. High Energy Phys. 05 (2013) 082.
[74] G. Bozzi, S. Catani, D. de Florian, and M. Grazzini, Transverse-momentum resummation and the spectrum of the Higgs boson at the LHC, Nucl. Phys. **B737**, 73 (2006).
[75] D. de Florian, G. Ferrera, M. Grazzini, and D. Tommasini, Transverse-momentum resummation: Higgs boson production at the Tevatron and the LHC, J. High Energy Phys. 11 (2011) 064.
[76] ATLAS Collaboration, Measurement of the Z/γ^* boson transverse momentum distribution in pp collisions at $\sqrt{s} = 7$ TeV with the ATLAS detector, J. High Energy Phys. 09 (2014) 145.
[77] K. Hamilton, P. Nason, E. Re, and G. Zanderighi, NNLOPS simulation of Higgs boson production, J. High Energy Phys. 10 (2013) 222.
[78] P. Nason, A new method for combining NLO QCD with shower Monte Carlo algorithms, J. High Energy Phys. 11 (2004) 040.
[79] S. Frixione, P. Nason, and C. Oleari, Matching NLO QCD computations with parton shower simulations: the POWHEG method, J. High Energy Phys. 11 (2007) 070.
[80] S. Alioli, P. Nason, C. Oleari, and E. Re, A general framework for implementing NLO calculations in shower Monte Carlo programs: The POWHEG BOX, J. High Energy Phys. 06 (2010) 043.
[81] K. Mimasu, V. Sanz, and C. Williams, Higher order QCD predictions for associated Higgs production with

anomalous couplings to gauge bosons, J. High Energy Phys. 08 (2016) 039.
[82] G. Luisoni, P. Nason, C. Oleari, and F. Tramontano, $HW^{\pm}/HZ + 0$ and 1 jet at NLO with the POWHEG BOX interfaced to GoSam and their merging within MiNLO, J. High Energy Phys. 10 (2013) 083.
[83] H. B. Hartanto, B. Jäger, L. Reina, and D. Wackeroth, Higgs boson production in association with top quarks in the POWHEG BOX, Phys. Rev. D **91**, 094003 (2015).
[84] S. Frixione, G. Ridolfi, and P. Nason, A positive-weight next-to-leading-order Monte Carlo for heavy flavour hadroproduction, J. High Energy Phys. 09 (2007) 126.
[85] ATLAS Collaboration, The PYTHIA8 A3 tune description of ATLAS minimum bias and inelastic measurements incorporating the Donnachie–Landshoff diffractive model, Report No. ATL-PHYS-PUB-2016-017, 2016, https://cds.cern.ch/record/2206965.
[86] ATLAS Collaboration, The ATLAS simulation infrastructure, Eur. Phys. J. C **70**, 823 (2010).
[87] S. Agostinelli *et al.* (GEANT4 Collaboration), GEANT 4—a simulation toolkit, Nucl. Instrum. Methods Phys. Res., Sect. A **506**, 250 (2003).
[88] ATLAS Collaboration, The simulation principle and performance of the ATLAS fast calorimeter simulation FastCaloSim, Report No. ATL-PHYS-PUB-2010-013, 2010, http://cdsweb.cern.ch/record/1300517.
[89] ATLAS Collaboration, Electron and photon reconstruction and performance in ATLAS using a dynamical, topological cell clustering-based approach, Report No. ATL-PHYS-PUB-2017-022, 2017, https://cds.cern.ch/record/2298955.
[90] ATLAS Collaboration, Electron and photon performance measurements with the ATLAS detector using the 2015–2017 LHC proton–proton collision data, J. Instrum. **14**, P12006 (2019).
[91] ATLAS Collaboration, Measurement of Higgs boson production in the diphoton decay channel in pp collisions at center-of-mass energies of 7 and 8 TeV with the ATLAS detector, Phys. Rev. D **90**, 112015 (2014).
[92] ATLAS Collaboration, Muon reconstruction performance of the ATLAS detector in proton–proton collision data at $\sqrt{s} = 13$ TeV, Eur. Phys. J. C **76**, 292 (2016).
[93] ATLAS Collaboration, Muon reconstruction and identification efficiency in ATLAS using the full Run $2pp$ collision data set at $\sqrt{s} = 13$ TeV, Eur. Phys. J. C **81**, 578 (2021).
[94] ATLAS Collaboration, Jet reconstruction and performance using particle flow with the ATLAS Detector, Eur. Phys. J. C **77**, 466 (2017).
[95] M. Cacciari, G. P. Salam, and G. Soyez, FastJet user manual, Eur. Phys. J. C **72**, 1896 (2012).
[96] M. Cacciari, G. P. Salam, and G. Soyez, The anti-k_t jet clustering algorithm, J. High Energy Phys. 04 (2008) 063.
[97] ATLAS Collaboration, Tagging and suppression of pileup jets with the ATLAS detector, Report No. ATLAS-CONF-2014-018, 2014, https://cds.cern.ch/record/1700870.
[98] ATLAS Collaboration, ATLAS b-jet identification performance and efficiency measurement with $t\bar{t}$, Eur. Phys. J. C **79**, 970 (2019).
[99] ATLAS Collaboration, Identification of jets containing b-hadrons with recurrent neural networks at the ATLAS experiment, Report No. ATL-PHYS-PUB-2017-003, 2017, https://cds.cern.ch/record/2255226.
[100] ATLAS Collaboration, Optimisation and performance studies of the ATLAS b-tagging algorithms for the 2017-18 LHC run, Report No. ATL-PHYS-PUB-2017-013, 2017, https://cds.cern.ch/record/2273281.
[101] ATLAS Collaboration, Performance of b-jet identification in the ATLAS experiment, J. Instrum. **11**, P04008 (2016).
[102] ATLAS Collaboration, Evidence for the $H \to b\bar{b}$ decay with the ATLAS detector, J. High Energy Phys. 12 (2017) 024.
[103] ATLAS Collaboration, Performance of missing transverse momentum reconstruction with the ATLAS detector using proton–proton collisions at $\sqrt{s} = 13$ TeV, Eur. Phys. J. C **78**, 903 (2018).
[104] ATLAS Collaboration, Performance of electron and photon triggers in ATLAS during LHC Run 2, Eur. Phys. J. C **80**, 47 (2020).
[105] ATLAS Collaboration, Search for pair production of Higgs bosons in the $b\bar{b}b\bar{b}$ final state using proton–proton collisions at $\sqrt{s} = 13$ TeV with the ATLAS detector, J. High Energy Phys. 01 (2019) 030.
[106] T. Chen and C. Guestrin, XGBoost: A scalable tree boosting system, *KDD'16: Proceedings of the 22nd ACM SIGKDD International Conference on Knowledge Discovery and Data Mining* (2016), pp. 785–794, arXiv:1603.02754.
[107] G. Cowan, K. Cranmer, E. Gross, and O. Vitells, Asymptotic formulae for likelihood-based tests of new physics, Eur. Phys. J. C **71**, 1554 (2011); Erratum, Eur. Phys. J. C **73**, 2501 (2013).
[108] A. Hoecker *et al.*, TMVA—Toolkit for multivariate data analysis, arXiv:physics/0703039.
[109] ATLAS Collaboration, Measurement of isolated-photon pair production in pp collisions at $\sqrt{s} = 7$ TeV with the ATLAS detector, J. High Energy Phys. 01 (2013) 086.
[110] M. Oreglia, A study of the reactions $\psi' \to \gamma\gamma\psi$, https://www.slac.stanford.edu/cgi-wrap/getdoc/slac-r-236.pdf.
[111] ATLAS Collaboration, Recommendations for the modeling of smooth backgrounds, Report No. ATL-PHYS-PUB-2020-028, 2020, https://cds.cern.ch/record/2743717.
[112] A. Wald, Sequential tests of statistical hypotheses, Ann. Math. Stat. **16**, 117 (1945).
[113] ATLAS Collaboration, Performance of electron and photon triggers in ATLAS during LHC Run 2, Eur. Phys. J. C **80**, 47 (2020).
[114] ATLAS Collaboration, Search for resonances in diphoton events at $\sqrt{s} = 13$ TeV with the ATLAS detector, J. High Energy Phys. 09 (2016) 001.
[115] ATLAS Collaboration, Jet energy scale and resolution measured in proton–proton collisions at $\sqrt{s} = 13$ TeV with the ATLAS detector, Eur. Phys. J. C **81**, 689 (2020).
[116] ATLAS Collaboration, Measurement of b-tagging efficiency of c-jets in $t\bar{t}$ events using a likelihood approach with the ATLAS detector, Report No. ATLAS-CONF-2018-001, 2018, https://cds.cern.ch/record/2306649.
[117] ATLAS Collaboration, Calibration of light-flavour b-jet mistagging rates using ATLAS proton–proton collision data at $\sqrt{s} = 13$ TeV, Report No. ATLAS-CONF-2018-006, 2018, https://cds.cern.ch/record/2314418.

[118] ATLAS Collaboration, Measurements of inclusive and differential fiducial cross-sections of $t\bar{t}$ production with additional heavy-flavour jets in proton–proton collisions at $\sqrt{s} = 13$ TeV with the ATLAS detector, J. High Energy Phys. 04 (2019) 046.

[119] ATLAS Collaboration, Study of heavy-flavor quarks produced in association with top quark pairs at $\sqrt{s} =$ 7 TeV using the ATLAS detector, Phys. Rev. D **89**, 072012 (2014).

[120] ATLAS Collaboration, Measurement of the cross-section for W boson production in association with b-jets in pp collisions at $\sqrt{s} = 7$ TeV with the ATLAS detector, J. High Energy Phys. 06 (**2013**) 084.

[121] A. L. Read, Presentation of search results: The CL_S technique, J. Phys. G **28**, 2693 (2002).

[122] ATLAS Collaboration, ATLAS computing acknowledgements, Report No. ATL-SOFT-PUB-2021-003, https://cds.cern.ch/record/2776662.

G. Aad,[99] B. Abbott,[124] D. C. Abbott,[100] A. Abed Abud,[34] K. Abeling,[51] D. K. Abhayasinghe,[91] S. H. Abidi,[27] H. Abramowicz,[157] H. Abreu,[156] Y. Abulaiti,[5] A. C. Abusleme Hoffman,[142a] B. S. Acharya,[64a,64b,b] B. Achkar,[51] L. Adam,[97] C. Adam Bourdarios,[4] L. Adamczyk,[81a] L. Adamek,[162] J. Adelman,[117] A. Adiguzel,[11c,c] S. Adorni,[52] T. Adye,[139] A. A. Affolder,[141] Y. Afik,[156] C. Agapopoulou,[62] M. N. Agaras,[12] J. Agarwala,[68a,68b] A. Aggarwal,[115] C. Agheorghiesei,[25c] J. A. Aguilar-Saavedra,[135f,135a,d] A. Ahmad,[34] F. Ahmadov,[77,e] W. S. Ahmed,[101] X. Ai,[44] G. Aielli,[71a,71b] S. Akatsuka,[83] M. Akbiyik,[97] T. P. A. Åkesson,[94] A. V. Akimov,[108] K. Al Khoury,[37] G. L. Alberghi,[21b] J. Albert,[171] M. J. Alconada Verzini,[86] S. Alderweireldt,[48] M. Aleksa,[34] I. N. Aleksandrov,[77] C. Alexa,[25b] T. Alexopoulos,[9] A. Alfonsi,[116] F. Alfonsi,[21b,21a] M. Alhroob,[124] B. Ali,[137] S. Ali,[154] M. Aliev,[161] G. Alimonti,[66a] C. Allaire,[34] B. M. M. Allbrooke,[152] P. P. Allport,[19] A. Aloisio,[67a,67b] F. Alonso,[86] C. Alpigiani,[144] E. Alunno Camelia,[71a,71b] M. Alvarez Estevez,[96] M. G. Alviggi,[67a,67b] Y. Amaral Coutinho,[78b] A. Ambler,[101] L. Ambroz,[130] C. Amelung,[34] D. Amidei,[103] S. P. Amor Dos Santos,[135a] S. Amoroso,[44] C. S. Amrouche,[52] C. Anastopoulos,[145] N. Andari,[140] T. Andeen,[10] J. K. Anders,[18] S. Y. Andrean,[43a,43b] A. Andreazza,[66a,66b] V. Andrei,[59a] S. Angelidakis,[8] A. Angerami,[37] A. V. Anisenkov,[118b,118a] A. Annovi,[69a] C. Antel,[52] M. T. Anthony,[145] E. Antipov,[125] M. Antonelli,[49] D. J. A. Antrim,[16] F. Anulli,[70a] M. Aoki,[79] J. A. Aparisi Pozo,[169] M. A. Aparo,[152] L. Aperio Bella,[44] N. Aranzabal,[34] V. Araujo Ferraz,[78a] C. Arcangeletti,[49] A. T. H. Arce,[47] E. Arena,[88] J-F. Arguin,[107] S. Argyropoulos,[50] J.-H. Arling,[44] A. J. Armbruster,[34] A. Armstrong,[166] O. Arnaez,[162] H. Arnold,[34] Z. P. Arrubarrena Tame,[111] G. Artoni,[130] H. Asada,[113] K. Asai,[122] S. Asai,[159] N. A. Asbah,[57] E. M. Asimakopoulou,[167] L. Asquith,[152] J. Assahsah,[33d] K. Assamagan,[27] R. Astalos,[26a] R. J. Atkin,[31a] M. Atkinson,[168] N. B. Atlay,[17] H. Atmani,[58b] P. A. Atmasiddha,[103] K. Augsten,[137] S. Auricchio,[67a,67b] V. A. Austrup,[177] G. Avner,[156] G. Avolio,[34] M. K. Ayoub,[13c] G. Azuelos,[107,f] D. Babal,[26a] H. Bachacou,[140] K. Bachas,[158] F. Backman,[43a,43b] A. Badea,[57] P. Bagnaia,[70a,70b] H. Bahrasemani,[148] A. J. Bailey,[169] V. R. Bailey,[168] J. T. Baines,[139] C. Bakalis,[9] O. K. Baker,[178] P. J. Bakker,[116] E. Bakos,[14] D. Bakshi Gupta,[7] S. Balaji,[153] R. Balasubramanian,[116] E. M. Baldin,[118b,118a] P. Balek,[138] E. Ballabene,[66a,66b] F. Balli,[140] W. K. Balunas,[130] J. Balz,[97] E. Banas,[82] M. Bandieramonte,[134] A. Bandyopadhyay,[17] L. Barak,[157] E. L. Barberio,[102] D. Barberis,[53b,53a] M. Barbero,[99] G. Barbour,[92] K. N. Barends,[31a] T. Barillari,[112] M-S. Barisits,[34] J. Barkeloo,[127] T. Barklow,[149] B. M. Barnett,[139] R. M. Barnett,[16] A. Baroncelli,[58a] G. Barone,[27] A. J. Barr,[130] L. Barranco Navarro,[43a,43b] F. Barreiro,[96] J. Barreiro Guimarães da Costa,[13a] U. Barron,[157] S. Barsov,[133] F. Bartels,[59a] R. Bartoldus,[149] G. Bartolini,[99] A. E. Barton,[87] P. Bartos,[26a] A. Basalaev,[44] A. Basan,[97] I. Bashta,[72a,72b] A. Bassalat,[62,g] M. J. Basso,[162] C. R. Basson,[98] R. L. Bates,[55] S. Batlamous,[33e] J. R. Batley,[30] B. Batool,[147] M. Battaglia,[141] M. Bauce,[70a,70b] F. Bauer,[140,a] P. Bauer,[22] H. S. Bawa,[29] A. Bayirli,[11c] J. B. Beacham,[47] T. Beau,[131] P. H. Beauchemin,[165] F. Becherer,[50] P. Bechtle,[22] H. P. Beck,[18,h] K. Becker,[173] C. Becot,[44] A. J. Beddall,[11a] V. A. Bednyakov,[77] C. P. Bee,[151] T. A. Beermann,[177] M. Begalli,[78b] M. Begel,[27] A. Behera,[151] J. K. Behr,[44] C. Beirao Da Cruz E Silva,[34] J. F. Beirer,[51,34] F. Beisiegel,[22] M. Belfkir,[4] G. Bella,[157] L. Bellagamba,[21b] A. Bellerive,[32] P. Bellos,[19] K. Beloborodov,[118b,118a] K. Belotskiy,[109] N. L. Belyaev,[109] D. Benchekroun,[33a] Y. Benhammou,[157] D. P. Benjamin,[27] M. Benoit,[27] J. R. Bensinger,[24] S. Bentvelsen,[116] L. Beresford,[34] M. Beretta,[49] D. Berge,[17] E. Bergeaas Kuutmann,[167] N. Berger,[4] B. Bergmann,[137] L. J. Bergsten,[24] J. Beringer,[16] S. Berlendis,[6] G. Bernardi,[131] C. Bernius,[149] F. U. Bernlochner,[22] T. Berry,[91] P. Berta,[44] A. Berthold,[46] I. A. Bertram,[87] O. Bessidskaia Bylund,[177] S. Bethke,[112] A. Betti,[40] A. J. Bevan,[90] S. Bhatta,[151] D. S. Bhattacharya,[172] P. Bhattarai,[24] V. S. Bhopatkar,[5] R. Bi,[134] R. M. Bianchi,[134] O. Biebel,[111] R. Bielski,[34] N. V. Biesuz,[69a,69b] M. Biglietti,[72a] T. R. V. Billoud,[137] M. Bindi,[51] A. Bingul,[11d] C. Bini,[70a,70b] S. Biondi,[21b,21a] C. J. Birch-sykes,[98] G. A. Bird,[19,139] M. Birman,[175] T. Bisanz,[34] J. P. Biswal,[2] D. Biswas,[176,i] A. Bitadze,[98] C. Bittrich,[46] K. Bjørke,[129] I. Bloch,[44] C. Blocker,[24]

A. Blue,[55] U. Blumenschein,[90] J. Blumenthal,[97] G. J. Bobbink,[116] V. S. Bobrovnikov,[118b,118a] D. Bogavac,[12] A. G. Bogdanchikov,[118b,118a] C. Bohm,[43a] V. Boisvert,[91] P. Bokan,[44] T. Bold,[81a] M. Bomben,[131] M. Bona,[90] M. Boonekamp,[140] C. D. Booth,[91] A. G. Borbély,[55] H. M. Borecka-Bielska,[107] L. S. Borgna,[92] G. Borissov,[87] D. Bortoletto,[130] D. Boscherini,[21b] M. Bosman,[12] J. D. Bossio Sola,[101] K. Bouaouda,[33a] J. Boudreau,[134] E. V. Bouhova-Thacker,[87] D. Boumediene,[36] R. Bouquet,[131] A. Boveia,[123] J. Boyd,[34] D. Boye,[27] I. R. Boyko,[77] A. J. Bozson,[91] J. Bracinik,[19] N. Brahimi,[58d,58c] G. Brandt,[177] O. Brandt,[30] F. Braren,[44] B. Brau,[100] J. E. Brau,[127] W. D. Breaden Madden,[55] K. Brendlinger,[44] R. Brener,[175] L. Brenner,[34] R. Brenner,[167] S. Bressler,[175] B. Brickwedde,[97] D. L. Briglin,[19] D. Britton,[55] D. Britzger,[112] I. Brock,[22] R. Brock,[104] G. Brooijmans,[37] W. K. Brooks,[142d] E. Brost,[27] P. A. Bruckman de Renstrom,[82] B. Brüers,[44] D. Bruncko,[26b] A. Bruni,[21b] G. Bruni,[21b] M. Bruschi,[21b] N. Bruscino,[70a,70b] L. Bryngemark,[149] T. Buanes,[15] Q. Buat,[151] P. Buchholz,[147] A. G. Buckley,[55] I. A. Budagov,[77] M. K. Bugge,[129] O. Bulekov,[109] B. A. Bullard,[57] T. J. Burch,[117] S. Burdin,[88] C. D. Burgard,[44] A. M. Burger,[125] B. Burghgrave,[7] J. T. P. Burr,[44] C. D. Burton,[10] J. C. Burzynski,[100] V. Büscher,[97] P. J. Bussey,[55] J. M. Butler,[23] C. M. Buttar,[55] J. M. Butterworth,[92] W. Buttinger,[139] C. J. Buxo Vazquez,[104] A. R. Buzykaev,[118b,118a] G. Cabras,[21b] S. Cabrera Urbán,[169] D. Caforio,[54] H. Cai,[134] V. M. M. Cairo,[149] O. Cakir,[3a] N. Calace,[34] P. Calafiura,[16] G. Calderini,[131] P. Calfayan,[63] G. Callea,[55] L. P. Caloba,[78b] A. Caltabiano,[71a,71b] S. Calvente Lopez,[96] D. Calvet,[36] S. Calvet,[36] T. P. Calvet,[99] M. Calvetti,[69a,69b] R. Camacho Toro,[131] S. Camarda,[34] D. Camarero Munoz,[96] P. Camarri,[71a,71b] M. T. Camerlingo,[72a,72b] D. Cameron,[129] C. Camincher,[171] M. Campanelli,[92] A. Camplani,[38] V. Canale,[67a,67b] A. Canesse,[101] M. Cano Bret,[75] J. Cantero,[125] Y. Cao,[168] M. Capua,[39b,39a] A. Carbone,[66a,66b] R. Cardarelli,[71a] F. Cardillo,[169] G. Carducci,[39b,39a] T. Carli,[34] G. Carlino,[67a] B. T. Carlson,[134] E. M. Carlson,[171,163a] L. Carminati,[66a,66b] M. Carnesale,[70a,70b] R. M. D. Carney,[149] S. Caron,[115] E. Carquin,[142d] S. Carrá,[44] G. Carratta,[21b,21a] J. W. S. Carter,[162] T. M. Carter,[48] D. Casadei,[31c] M. P. Casado,[12,j] A. F. Casha,[162] E. G. Castiglia,[178] F. L. Castillo,[59a] L. Castillo Garcia,[12] V. Castillo Gimenez,[169] N. F. Castro,[135a,135e] A. Catinaccio,[34] J. R. Catmore,[129] A. Cattai,[34] V. Cavaliere,[27] N. Cavalli,[21b,21a] V. Cavasinni,[69a,69b] E. Celebi,[11b] F. Celli,[130] K. Cerny,[126] A. S. Cerqueira,[78a] A. Cerri,[152] L. Cerrito,[71a,71b] F. Cerutti,[16] A. Cervelli,[21b] S. A. Cetin,[11b] Z. Chadi,[33a] D. Chakraborty,[117] M. Chala,[135f] J. Chan,[176] W. S. Chan,[116] W. Y. Chan,[88] J. D. Chapman,[30] B. Chargeishvili,[155b] D. G. Charlton,[19] T. P. Charman,[90] M. Chatterjee,[18] C. C. Chau,[32] S. Chekanov,[5] S. V. Chekulaev,[163a] G. A. Chelkov,[77,k] A. Chen,[103] B. Chen,[157] C. Chen,[58a] C. H. Chen,[76] H. Chen,[13c] H. Chen,[27] J. Chen,[58a] J. Chen,[37] J. Chen,[24] S. Chen,[132] S. J. Chen,[13c] X. Chen,[58c] X. Chen,[13b] Y. Chen,[58a] Y-H. Chen,[44] C. L. Cheng,[176] H. C. Cheng,[60a] H. J. Cheng,[13a] A. Cheplakov,[77] E. Cheremushkina,[44] R. Cherkaoui El Moursli,[33e] E. Cheu,[6] K. Cheung,[61] L. Chevalier,[140] V. Chiarella,[49] G. Chiarelli,[69a] G. Chiodini,[65a] A. S. Chisholm,[19] A. Chitan,[25b] I. Chiu,[159] Y. H. Chiu,[171] M. V. Chizhov,[77,l] K. Choi,[10] A. R. Chomont,[70a,70b] Y. Chou,[100] E. Y. S. Chow,[116] L. D. Christopher,[31f] M. C. Chu,[60a] X. Chu,[13a,13d] J. Chudoba,[136] J. J. Chwastowski,[82] D. Cieri,[112] K. M. Ciesla,[82] V. Cindro,[89] I. A. Cioară,[25b] A. Ciocio,[16] F. Cirotto,[67a,67b] Z. H. Citron,[175,m] M. Citterio,[66a] D. A. Ciubotaru,[25b] B. M. Ciungu,[162] A. Clark,[52] P. J. Clark,[48] J. M. Clavijo Columbie,[44] S. E. Clawson,[98] C. Clement,[43a,43b] L. Clissa,[21b,21a] Y. Coadou,[99] M. Cobal,[64a,64c] A. Coccaro,[53b] J. Cochran,[76] R. F. Coelho Barrue,[135a] R. Coelho Lopes De Sa,[100] S. Coelli,[66a] H. Cohen,[157] A. E. C. Coimbra,[34] B. Cole,[37] J. Collot,[56] P. Conde Muiño,[135a,135h] S. H. Connell,[31c] I. A. Connelly,[55] E. I. Conroy,[130] F. Conventi,[67a,n] H. G. Cooke,[19] A. M. Cooper-Sarkar,[130] F. Cormier,[170] L. D. Corpe,[34] M. Corradi,[70a,70b] E. E. Corrigan,[94] F. Corriveau,[101,o] M. J. Costa,[169] F. Costanza,[4] D. Costanzo,[145] B. M. Cote,[123] G. Cowan,[91] J. W. Cowley,[30] J. Crane,[98] K. Cranmer,[121] R. A. Creager,[132] S. Crépé-Renaudin,[56] F. Crescioli,[131] M. Cristinziani,[147] M. Cristoforetti,[73a,73b,p] V. Croft,[165] G. Crosetti,[39b,39a] A. Cueto,[4] T. Cuhadar Donszelmann,[166] H. Cui,[13a,13d] A. R. Cukierman,[149] W. R. Cunningham,[55] S. Czekierda,[82] P. Czodrowski,[34] M. M. Czurylo,[59b] M. J. Da Cunha Sargedas De Sousa,[58a] J. V. Da Fonseca Pinto,[78b] C. Da Via,[98] W. Dabrowski,[81a] T. Dado,[45] S. Dahbi,[31f] T. Dai,[103] C. Dallapiccola,[100] M. Dam,[38] G. D'amen,[27] V. D'Amico,[72a,72b] J. Damp,[97] J. R. Dandoy,[132] M. F. Daneri,[28] M. Danninger,[148] V. Dao,[34] G. Darbo,[53b] S. Darmora,[5] A. Dattagupta,[127] S. D'Auria,[66a,66b] C. David,[163b] T. Davidek,[138] D. R. Davis,[47] B. Davis-Purcell,[32] I. Dawson,[90] K. De,[7] R. De Asmundis,[67a] M. De Beurs,[116] S. De Castro,[21b,21a] N. De Groot,[115] P. de Jong,[116] H. De la Torre,[104] A. De Maria,[13c] D. De Pedis,[70a] A. De Salvo,[70a] U. De Sanctis,[71a,71b] M. De Santis,[71a,71b] A. De Santo,[152] J. B. De Vivie De Regie,[56] D. V. Dedovich,[77] J. Degens,[116] A. M. Deiana,[40] J. Del Peso,[96] Y. Delabat Diaz,[44] F. Deliot,[140] C. M. Delitzsch,[6] M. Della Pietra,[67a,67b] D. Della Volpe,[52] A. Dell'Acqua,[34] L. Dell'Asta,[66a,66b] M. Delmastro,[4] P. A. Delsart,[56] S. Demers,[178] M. Demichev,[77] S. P. Denisov,[119] L. D'Eramo,[117] D. Derendarz,[82] J. E. Derkaoui,[33d] F. Derue,[131] P. Dervan,[88] K. Desch,[22] K. Dette,[162] C. Deutsch,[22] P. O. Deviveiros,[34] F. A. Di Bello,[70a,70b] A. Di Ciaccio,[71a,71b] L. Di Ciaccio,[4] C. Di Donato,[67a,67b] A. Di Girolamo,[34]

G. Di Gregorio,[69a,69b] A. Di Luca,[73a,73b] B. Di Micco,[72a,72b] R. Di Nardo,[72a,72b] C. Diaconu,[99] F. A. Dias,[116] T. Dias Do Vale,[135a] M. A. Diaz,[142a] F. G. Diaz Capriles,[22] J. Dickinson,[16] M. Didenko,[169] E. B. Diehl,[103] J. Dietrich,[17] S. Díez Cornell,[44] C. Diez Pardos,[147] A. Dimitrievska,[16] W. Ding,[13b] J. Dingfelder,[22] I-M. Dinu,[25b] S. J. Dittmeier,[59b] F. Dittus,[34] F. Djama,[99] T. Djobava,[155b] J. I. Djuvsland,[15] M. A. B. Do Vale,[143] D. Dodsworth,[24] C. Doglioni,[94] J. Dolejsi,[138] Z. Dolezal,[138] M. Donadelli,[78c] B. Dong,[58c] J. Donini,[36] A. D'onofrio,[13c] M. D'Onofrio,[88] J. Dopke,[139] A. Doria,[67a] M. T. Dova,[86] A. T. Doyle,[55] E. Drechsler,[148] E. Dreyer,[148] T. Dreyer,[51] A. S. Drobac,[165] D. Du,[58b] T. A. du Pree,[116] F. Dubinin,[108] M. Dubovsky,[26a] A. Dubreuil,[52] E. Duchovni,[175] G. Duckeck,[111] O. A. Ducu,[34,25b] D. Duda,[112] A. Dudarev,[34] M. D'uffizi,[98] L. Duflot,[62] M. Dührssen,[34] C. Dülsen,[177] A. E. Dumitriu,[25b] M. Dunford,[59a] S. Dungs,[45] A. Duperrin,[99] H. Duran Yildiz,[3a] M. Düren,[54] A. Durglishvili,[155b] B. Dutta,[44] D. Duvnjak,[1] B. L. Dwyer,[117] G. I. Dyckes,[132] M. Dyndal,[81a] S. Dysch,[98] B. S. Dziedzic,[82] B. Eckerova,[26a] M. G. Eggleston,[47] E. Egidio Purcino De Souza,[78b] L. F. Ehrke,[52] T. Eifert,[7] G. Eigen,[15] K. Einsweiler,[16] T. Ekelof,[167] Y. El Ghazali,[33b] H. El Jarrari,[33e] A. El Moussaouy,[33a] V. Ellajosyula,[167] M. Ellert,[167] F. Ellinghaus,[177] A. A. Elliot,[90] N. Ellis,[34] J. Elmsheuser,[27] M. Elsing,[34] D. Emeliyanov,[139] A. Emerman,[37] Y. Enari,[159] J. Erdmann,[45] A. Ereditato,[18] P. A. Erland,[82] M. Errenst,[177] M. Escalier,[62] C. Escobar,[169] O. Estrada Pastor,[169] E. Etzion,[157] G. Evans,[135a] H. Evans,[63] M. O. Evans,[152] A. Ezhilov,[133] F. Fabbri,[55] L. Fabbri,[21b,21a] V. Fabiani,[115] G. Facini,[173] V. Fadeyev,[141] R. M. Fakhrutdinov,[119] S. Falciano,[70a] P. J. Falke,[22] S. Falke,[34] J. Faltova,[138] Y. Fan,[13a] Y. Fang,[13a] Y. Fang,[13a] G. Fanourakis,[42] M. Fanti,[66a,66b] M. Faraj,[58c] A. Farbin,[7] A. Farilla,[72a] E. M. Farina,[68a,68b] T. Farooque,[104] S. M. Farrington,[48] P. Farthouat,[34] F. Fassi,[33e] D. Fassouliotis,[8] M. Faucci Giannelli,[71a,71b] W. J. Fawcett,[30] L. Fayard,[62] O. L. Fedin,[133,q] M. Feickert,[168] L. Feligioni,[99] A. Fell,[145] C. Feng,[58b] M. Feng,[13b] M. J. Fenton,[166] A. B. Fenyuk,[119] S. W. Ferguson,[41] J. Ferrando,[44] A. Ferrari,[167] P. Ferrari,[116] R. Ferrari,[68a] D. Ferrere,[52] C. Ferretti,[103] F. Fiedler,[97] A. Filipčič,[89] F. Filthaut,[115] M. C. N. Fiolhais,[135a,135c,r] L. Fiorini,[169] F. Fischer,[147] W. C. Fisher,[104] T. Fitschen,[19] I. Fleck,[147] P. Fleischmann,[103] T. Flick,[177] B. M. Flierl,[111] L. Flores,[132] L. R. Flores Castillo,[60a] F. M. Follega,[73a,73b] N. Fomin,[15] J. H. Foo,[162] G. T. Forcolin,[73a,73b] B. C. Forland,[63] A. Formica,[140] F. A. Förster,[12] A. C. Forti,[98] E. Fortin,[99] M. G. Foti,[130] D. Fournier,[62] H. Fox,[87] P. Francavilla,[69a,69b] S. Francescato,[70a,70b] M. Franchini,[21b,21a] S. Franchino,[59a] D. Francis,[34] L. Franco,[4] L. Franconi,[18] M. Franklin,[57] G. Frattari,[70a,70b] A. C. Freegard,[90] P. M. Freeman,[19] B. Freund,[107] W. S. Freund,[78b] E. M. Freundlich,[45] D. Froidevaux,[34] J. A. Frost,[130] Y. Fu,[58a] M. Fujimoto,[122] E. Fullana Torregrosa,[169] J. Fuster,[169] A. Gabrielli,[21b,21a] A. Gabrielli,[34] P. Gadow,[44] G. Gagliardi,[53b,53a] L. G. Gagnon,[16] G. E. Gallardo,[130] E. J. Gallas,[130] B. J. Gallop,[139] R. Gamboa Goni,[90] K. K. Gan,[123] S. Ganguly,[175] J. Gao,[58a] Y. Gao,[48] Y. S. Gao,[29,s] F. M. Garay Walls,[142a] C. García,[169] J. E. García Navarro,[169] J. A. García Pascual,[13a] M. Garcia-Sciveres,[16] R. W. Gardner,[35] D. Garg,[75] S. Gargiulo,[50] C. A. Garner,[162] V. Garonne,[129] S. J. Gasiorowski,[144] P. Gaspar,[78b] G. Gaudio,[68a] P. Gauzzi,[70a,70b] I. L. Gavrilenko,[108] A. Gavrilyuk,[120] C. Gay,[170] G. Gaycken,[44] E. N. Gazis,[9] A. A. Geanta,[25b] C. M. Gee,[141] C. N. P. Gee,[139] J. Geisen,[94] M. Geisen,[97] C. Gemme,[53b] M. H. Genest,[56] S. Gentile,[70a,70b] S. George,[91] T. Geralis,[42] L. O. Gerlach,[51] P. Gessinger-Befurt,[97] M. Ghasemi Bostanabad,[171] M. Ghneimat,[147] A. Ghosh,[166] A. Ghosh,[75] B. Giacobbe,[21b] S. Giagu,[70a,70b] N. Giangiacomi,[162] P. Giannetti,[69a] A. Giannini,[67a,67b] S. M. Gibson,[91] M. Gignac,[141] D. T. Gil,[81b] B. J. Gilbert,[37] D. Gillberg,[32] G. Gilles,[116] N. E. K. Gillwald,[44] D. M. Gingrich,[2,f] M. P. Giordani,[64a,64c] P. F. Giraud,[140] G. Giugliarelli,[64a,64c] D. Giugni,[66a] F. Giuli,[71a,71b] I. Gkialas,[8,t] E. L. Gkougkousis,[12] P. Gkountoumis,[9] L. K. Gladilin,[110] C. Glasman,[96] G. R. Gledhill,[127] M. Glisic,[127] I. Gnesi,[39b,u] M. Goblirsch-Kolb,[24] D. Godin,[107] S. Goldfarb,[102] T. Golling,[52] D. Golubkov,[119] J. P. Gombas,[104] A. Gomes,[135a,135b] R. Goncalves Gama,[51] R. Gonçalo,[135a,135c] G. Gonella,[127] L. Gonella,[19] A. Gongadze,[77] F. Gonnella,[19] J. L. Gonski,[37] S. González de la Hoz,[169] S. Gonzalez Fernandez,[12] R. Gonzalez Lopez,[88] C. Gonzalez Renteria,[16] R. Gonzalez Suarez,[167] S. Gonzalez-Sevilla,[52] G. R. Gonzalvo Rodriguez,[169] R. Y. González Andana,[142a] L. Goossens,[34] N. A. Gorasia,[19] P. A. Gorbounov,[120] H. A. Gordon,[27] B. Gorini,[34] E. Gorini,[65a,65b] A. Gorišek,[89] A. T. Goshaw,[47] M. I. Gostkin,[77] C. A. Gottardo,[115] M. Gouighri,[33b] V. Goumarre,[44] A. G. Goussiou,[144] N. Govender,[31c] C. Goy,[4] I. Grabowska-Bold,[81a] K. Graham,[32] E. Gramstad,[129] S. Grancagnolo,[17] M. Grandi,[152] V. Gratchev,[133] P. M. Gravila,[25f] F. G. Gravili,[65a,65b] H. M. Gray,[16] C. Grefe,[22] I. M. Gregor,[44] P. Grenier,[149] K. Grevtsov,[44] C. Grieco,[12] N. A. Grieser,[124] A. A. Grillo,[141] K. Grimm,[29,v] S. Grinstein,[12,w] J.-F. Grivaz,[62] S. Groh,[97] E. Gross,[175] J. Grosse-Knetter,[51] Z. J. Grout,[92] C. Grud,[103] A. Grummer,[114] J. C. Grundy,[130] L. Guan,[103] W. Guan,[176] C. Gubbels,[170] J. Guenther,[34] J. G. R. Guerrero Rojas,[169] F. Guescini,[112] D. Guest,[17] R. Gugel,[97] A. Guida,[44] T. Guillemin,[4] S. Guindon,[34] J. Guo,[58c] L. Guo,[62] Y. Guo,[103] R. Gupta,[44] S. Gurbuz,[22] G. Gustavino,[124] M. Guth,[50] P. Gutierrez,[124] L. F. Gutierrez Zagazeta,[132] C. Gutschow,[92] C. Guyot,[140] C. Gwenlan,[130] C. B. Gwilliam,[88] E. S. Haaland,[129] A. Haas,[121] M. Habedank,[17] C. Haber,[16] H. K. Hadavand,[7] A. Hadef,[97] M. Haleem,[172] J. Haley,[125] J. J. Hall,[145] G. Halladjian,[104]

G. D. Hallewell,[99] L. Halser,[18] K. Hamano,[171] H. Hamdaoui,[33e] M. Hamer,[22] G. N. Hamity,[48] K. Han,[58a] L. Han,[13c] L. Han,[58a] S. Han,[16] Y. F. Han,[162] K. Hanagaki,[79,x] M. Hance,[141] M. D. Hank,[35] R. Hankache,[98] E. Hansen,[94] J. B. Hansen,[38] J. D. Hansen,[38] M. C. Hansen,[22] P. H. Hansen,[38] K. Hara,[164] T. Harenberg,[177] S. Harkusha,[105] Y. T. Harris,[130] P. F. Harrison,[173] N. M. Hartman,[149] N. M. Hartmann,[111] Y. Hasegawa,[146] A. Hasib,[48] S. Hassani,[140] S. Haug,[18] R. Hauser,[104] M. Havranek,[137] C. M. Hawkes,[19] R. J. Hawkings,[34] S. Hayashida,[113] D. Hayden,[104] C. Hayes,[103] R. L. Hayes,[170] C. P. Hays,[130] J. M. Hays,[90] H. S. Hayward,[88] S. J. Haywood,[139] F. He,[58a] Y. He,[160] Y. He,[131] M. P. Heath,[48] V. Hedberg,[94] A. L. Heggelund,[129] N. D. Hehir,[90] C. Heidegger,[50] K. K. Heidegger,[50] W. D. Heidorn,[76] J. Heilman,[32] S. Heim,[44] T. Heim,[16] B. Heinemann,[44,y] J. G. Heinlein,[132] J. J. Heinrich,[127] L. Heinrich,[34] J. Hejbal,[136] L. Helary,[44] A. Held,[121] S. Hellesund,[129] C. M. Helling,[141] S. Hellman,[43a,43b] C. Helsens,[34] R. C. W. Henderson,[87] L. Henkelmann,[30] A. M. Henriques Correia,[34] H. Herde,[149] Y. Hernández Jiménez,[151] H. Herr,[97] M. G. Herrmann,[111] T. Herrmann,[46] G. Herten,[50] R. Hertenberger,[111] L. Hervas,[34] N. P. Hessey,[163a] H. Hibi,[80] S. Higashino,[79] E. Higón-Rodriguez,[169] K. K. Hill,[27] K. H. Hiller,[44] S. J. Hillier,[19] M. Hils,[46] I. Hinchliffe,[16] F. Hinterkeuser,[22] M. Hirose,[128] S. Hirose,[164] D. Hirschbuehl,[177] B. Hiti,[89] O. Hladik,[136] J. Hobbs,[151] R. Hobincu,[25e] N. Hod,[175] M. C. Hodgkinson,[145] B. H. Hodkinson,[30] A. Hoecker,[34] J. Hofer,[44] D. Hohn,[50] T. Holm,[22] T. R. Holmes,[35] M. Holzbock,[112] L. B. A. H. Hommels,[30] B. P. Honan,[98] J. Hong,[58c] T. M. Hong,[134] J. C. Honig,[50] A. Hönle,[112] B. H. Hooberman,[168] W. H. Hopkins,[5] Y. Horii,[113] P. Horn,[46] L. A. Horyn,[35] S. Hou,[154] J. Howarth,[55] J. Hoya,[86] M. Hrabovsky,[126] A. Hrynevich,[106] T. Hryn'ova,[4] P. J. Hsu,[61] S.-C. Hsu,[144] Q. Hu,[37] S. Hu,[58c] Y. F. Hu,[13a,13d,z] D. P. Huang,[92] X. Huang,[13c] Y. Huang,[58a] Y. Huang,[13a] Z. Hubacek,[137] F. Hubaut,[99] M. Huebner,[22] F. Huegging,[22] T. B. Huffman,[130] M. Huhtinen,[34] R. Hulsken,[56] N. Huseynov,[77,e] J. Huston,[104] J. Huth,[57] R. Hyneman,[149] S. Hyrych,[26a] G. Iacobucci,[52] G. Iakovidis,[27] I. Ibragimov,[147] L. Iconomidou-Fayard,[62] P. Iengo,[34] R. Ignazzi,[38] R. Iguchi,[159] T. Iizawa,[52] Y. Ikegami,[79] A. Ilg,[18] N. Ilic,[162] H. Imam,[33a] T. Ingebretsen Carlson,[43a,43b] G. Introzzi,[68a,68b] M. Iodice,[72a] V. Ippolito,[70a,70b] M. Ishino,[159] W. Islam,[125] C. Issever,[17,44] S. Istin,[11c,aa] J. M. Iturbe Ponce,[60a] R. Iuppa,[73a,73b] A. Ivina,[175] J. M. Izen,[41] V. Izzo,[67a] P. Jacka,[136] P. Jackson,[1] R. M. Jacobs,[44] B. P. Jaeger,[148] C. S. Jagfeld,[111] G. Jäkel,[177] K. B. Jakobi,[97] K. Jakobs,[50] T. Jakoubek,[175] J. Jamieson,[55] K. W. Janas,[81a] G. Jarlskog,[94] A. E. Jaspan,[88] N. Javadov,[77,e] T. Javůrek,[34] M. Javurkova,[100] F. Jeanneau,[140] L. Jeanty,[127] J. Jejelava,[155a,bb] P. Jenni,[50,cc] S. Jézéquel,[4] J. Jia,[151] Z. Jia,[13c] Y. Jiang,[58a] S. Jiggins,[50] J. Jimenez Pena,[112] S. Jin,[13c] A. Jinaru,[25b] O. Jinnouchi,[160] H. Jivan,[31f] P. Johansson,[145] K. A. Johns,[6] C. A. Johnson,[63] D. M. Jones,[30] E. Jones,[173] R. W. L. Jones,[87] T. J. Jones,[88] J. Jovicevic,[51] X. Ju,[16] J. J. Junggeburth,[34] A. Juste Rozas,[12,w] A. Kaczmarska,[82] M. Kado,[70a,70b] H. Kagan,[123] M. Kagan,[149] A. Kahn,[37] C. Kahra,[97] T. Kaji,[174] E. Kajomovitz,[156] C. W. Kalderon,[27] A. Kaluza,[97] A. Kamenshchikov,[119] M. Kaneda,[159] N. J. Kang,[141] S. Kang,[76] Y. Kano,[113] J. Kanzaki,[79] D. Kar,[31f] K. Karava,[130] M. J. Kareem,[163b] I. Karkanias,[158] S. N. Karpov,[77] Z. M. Karpova,[77] V. Kartvelishvili,[87] A. N. Karyukhin,[119] E. Kasimi,[158] C. Kato,[58d] J. Katzy,[44] K. Kawade,[146] K. Kawagoe,[85] T. Kawaguchi,[113] T. Kawamoto,[140] G. Kawamura,[51] E. F. Kay,[171] F. I. Kaya,[165] S. Kazakos,[12] V. F. Kazanin,[118b,118a] Y. Ke,[151] J. M. Keaveney,[31a] R. Keeler,[171] J. S. Keller,[32] D. Kelsey,[152] J. J. Kempster,[19] J. Kendrick,[19] K. E. Kennedy,[37] O. Kepka,[136] S. Kersten,[177] B. P. Kerševan,[89] S. Ketabchi Haghighat,[162] M. Khandoga,[131] A. Khanov,[125] A. G. Kharlamov,[118b,118a] T. Kharlamova,[118b,118a] E. E. Khoda,[170] T. J. Khoo,[17] G. Khoriauli,[172] E. Khramov,[77] J. Khubua,[155b] S. Kido,[80] M. Kiehn,[34] A. Kilgallon,[127] E. Kim,[160] Y. K. Kim,[35] N. Kimura,[92] A. Kirchhoff,[51] D. Kirchmeier,[46] J. Kirk,[139] A. E. Kiryunin,[112] T. Kishimoto,[159] D. P. Kisliuk,[162] V. Kitali,[44] C. Kitsaki,[9] O. Kivernyk,[22] T. Klapdor-Kleingrothaus,[50] M. Klassen,[59a] C. Klein,[32] L. Klein,[172] M. H. Klein,[103] M. Klein,[88] U. Klein,[88] P. Klimek,[34] A. Klimentov,[27] F. Klimpel,[34] T. Klingl,[22] T. Klioutchnikova,[34] F. F. Klitzner,[111] P. Kluit,[116] S. Kluth,[112] E. Kneringer,[74] T. M. Knight,[162] A. Knue,[50] D. Kobayashi,[85] M. Kobel,[46] M. Kocian,[149] T. Kodama,[159] P. Kodys,[138] D. M. Koeck,[152] P. T. Koenig,[22] T. Koffas,[32] N. M. Köhler,[34] M. Kolb,[140] I. Koletsou,[4] T. Komarek,[126] K. Köneke,[50] A. X. Y. Kong,[1] T. Kono,[122] V. Konstantinides,[92] N. Konstantinidis,[92] B. Konya,[94] R. Kopeliansky,[63] S. Koperny,[81a] K. Korcyl,[82] K. Kordas,[158] G. Koren,[157] A. Korn,[92] S. Korn,[51] I. Korolkov,[12] E. V. Korolkova,[145] N. Korotkova,[110] B. Kortman,[116] O. Kortner,[112] S. Kortner,[112] V. V. Kostyukhin,[145,161] A. Kotsokechagia,[62] A. Kotwal,[47] A. Koulouris,[34] A. Kourkoumeli-Charalampidi,[68a,68b] C. Kourkoumelis,[8] E. Kourlitis,[5] O. Kovanda,[152] R. Kowalewski,[171] W. Kozanecki,[140] A. S. Kozhin,[119] V. A. Kramarenko,[110] G. Kramberger,[89] D. Krasnopevtsev,[58a] M. W. Krasny,[131] A. Krasznahorkay,[34] J. A. Kremer,[97] J. Kretzschmar,[88] K. Kreul,[17] P. Krieger,[162] F. Krieter,[111] S. Krishnamurthy,[100] A. Krishnan,[59b] M. Krivos,[138] K. Krizka,[16] K. Kroeninger,[45] H. Kroha,[112] J. Kroll,[136] J. Kroll,[132] K. S. Krowpman,[104] U. Kruchonak,[77] H. Krüger,[22] N. Krumnack,[76] M. C. Kruse,[47] J. A. Krzysiak,[82] A. Kubota,[160] O. Kuchinskaia,[161] S. Kuday,[3b] D. Kuechler,[44] J. T. Kuechler,[44] S. Kuehn,[34] T. Kuhl,[44] V. Kukhtin,[77] Y. Kulchitsky,[105,dd] S. Kuleshov,[142b] M. Kumar,[31f] N. Kumari,[99] M. Kuna,[56] A. Kupco,[136] T. Kupfer,[45] O. Kuprash,[50] H. Kurashige,[80] L. L. Kurchaninov,[163a]

Y. A. Kurochkin,[105] A. Kurova,[109] M. G. Kurth,[13a,13d] E. S. Kuwertz,[34] M. Kuze,[160] A. K. Kvam,[144] J. Kvita,[126] T. Kwan,[101] C. Lacasta,[169] F. Lacava,[70a,70b] H. Lacker,[17] D. Lacour,[131] N. N. Lad,[92] E. Ladygin,[77] R. Lafaye,[4] B. Laforge,[131] T. Lagouri,[142c] S. Lai,[51] I. K. Lakomiec,[81a] N. Lalloue,[56] J. E. Lambert,[124] S. Lammers,[63] W. Lampl,[6] C. Lampoudis,[158] E. Lançon,[27] U. Landgraf,[50] M. P. J. Landon,[90] V. S. Lang,[50] J. C. Lange,[51] R. J. Langenberg,[100] A. J. Lankford,[166] F. Lanni,[27] K. Lantzsch,[22] A. Lanza,[68a] A. Lapertosa,[53b,53a] J. F. Laporte,[140] T. Lari,[66a] F. Lasagni Manghi,[21b] M. Lassnig,[34] V. Latonova,[136] T. S. Lau,[60a] A. Laudrain,[97] A. Laurier,[32] M. Lavorgna,[67a,67b] S. D. Lawlor,[91] M. Lazzaroni,[66a,66b] B. Le,[98] B. Leban,[89] A. Lebedev,[76] M. LeBlanc,[34] T. LeCompte,[5] F. Ledroit-Guillon,[56] A. C. A. Lee,[92] C. A. Lee,[27] G. R. Lee,[15] L. Lee,[57] S. C. Lee,[154] S. Lee,[76] L. L. Leeuw,[31c] B. Lefebvre,[163a] H. P. Lefebvre,[91] M. Lefebvre,[171] C. Leggett,[16] K. Lehmann,[148] N. Lehmann,[18] G. Lehmann Miotto,[34] W. A. Leight,[44] A. Leisos,[158,ee] M. A. L. Leite,[78c] C. E. Leitgeb,[44] R. Leitner,[138] K. J. C. Leney,[40] T. Lenz,[22] S. Leone,[69a] C. Leonidopoulos,[48] A. Leopold,[131] C. Leroy,[107] R. Les,[104] C. G. Lester,[30] M. Levchenko,[133] J. Levêque,[4] D. Levin,[103] L. J. Levinson,[175] D. J. Lewis,[19] A. Li,[131] B. Li,[13b] B. Li,[58b] C. Li,[58a] C-Q. Li,[58c,58d] H. Li,[58a] H. Li,[58b] J. Li,[58c] K. Li,[144] L. Li,[58c] M. Li,[13a,13d] Q. Y. Li,[58a] S. Li,[58d,58c,ff] X. Li,[44] Y. Li,[44] Z. Li,[58b] Z. Li,[130] Z. Li,[101] Z. Li,[88] Z. Liang,[13a] M. Liberatore,[44] B. Liberti,[71a] K. Lie,[60c] K. Lin,[104] R. A. Linck,[63] R. E. Lindley,[6] J. H. Lindon,[2] A. Linss,[44] A. L. Lionti,[52] E. Lipeles,[132] A. Lipniacka,[15] T. M. Liss,[168,gg] A. Lister,[170] J. D. Little,[7] B. Liu,[13a] B. X. Liu,[148] J. B. Liu,[58a] J. K. K. Liu,[35] K. Liu,[58d,58c] M. Liu,[58a] M. Y. Liu,[58a] P. Liu,[13a] X. Liu,[58a] Y. Liu,[44] Y. Liu,[13c,13d] Y. L. Liu,[103] Y. W. Liu,[58a] M. Livan,[68a,68b] A. Lleres,[56] J. Llorente Merino,[148] S. L. Lloyd,[90] E. M. Lobodzinska,[44] P. Loch,[6] S. Loffredo,[71a,71b] T. Lohse,[17] K. Lohwasser,[145] M. Lokajicek,[136] J. D. Long,[168] R. E. Long,[87] I. Longarini,[70a,70b] L. Longo,[34] R. Longo,[168] I. Lopez Paz,[12] A. Lopez Solis,[44] J. Lorenz,[111] N. Lorenzo Martinez,[4] A. M. Lory,[111] A. Lösle,[50] X. Lou,[43a,43b] X. Lou,[13a] A. Lounis,[62] J. Love,[5] P. A. Love,[87] J. J. Lozano Bahilo,[169] G. Lu,[13a,13d] M. Lu,[58a] S. Lu,[132] Y. J. Lu,[61] H. J. Lubatti,[144] C. Luci,[70a,70b] F. L. Lucio Alves,[13c] A. Lucotte,[56] F. Luehring,[63] I. Luise,[151] L. Luminari,[70a] B. Lund-Jensen,[150] N. A. Luongo,[127] M. S. Lutz,[157] D. Lynn,[27] H. Lyons,[88] R. Lysak,[136] E. Lytken,[94] F. Lyu,[13a] V. Lyubushkin,[77] T. Lyubushkina,[77] H. Ma,[27] L. L. Ma,[58b] Y. Ma,[92] D. M. Mac Donell,[171] G. Maccarrone,[49] C. M. Macdonald,[145] J. C. MacDonald,[145] R. Madar,[36] W. F. Mader,[46] M. Madugoda Ralalage Don,[125] N. Madysa,[46] J. Maeda,[80] T. Maeno,[27] M. Maerker,[46] V. Magerl,[50] J. Magro,[64a,64c] D. J. Mahon,[37] C. Maidantchik,[78b] A. Maio,[135a,135b,135d] K. Maj,[81a] O. Majersky,[26a] S. Majewski,[127] N. Makovec,[62] B. Malaescu,[131] Pa. Malecki,[82] V. P. Maleev,[133] F. Malek,[56] D. Malito,[39b,39a] U. Mallik,[75] C. Malone,[30] S. Maltezos,[9] S. Malyukov,[77] J. Mamuzic,[169] G. Mancini,[49] J. P. Mandalia,[90] I. Mandić,[89] L. Manhaes de Andrade Filho,[78a] I. M. Maniatis,[158] M. Manisha,[140] J. Manjarres Ramos,[46] K. H. Mankinen,[94] A. Mann,[111] A. Manousos,[74] B. Mansoulie,[140] I. Manthos,[158] S. Manzoni,[116] A. Marantis,[158,ee] L. Marchese,[130] G. Marchiori,[131] M. Marcisovsky,[136] L. Marcoccia,[71a,71b] C. Marcon,[94] M. Marjanovic,[124] Z. Marshall,[16] S. Marti-Garcia,[169] T. A. Martin,[173] V. J. Martin,[48] B. Martin dit Latour,[15] L. Martinelli,[70a,70b] M. Martinez,[12,w] P. Martinez Agullo,[169] V. I. Martinez Outschoorn,[100] S. Martin-Haugh,[139] V. S. Martoiu,[25b] A. C. Martyniuk,[92] A. Marzin,[34] S. R. Maschek,[112] L. Masetti,[97] T. Mashimo,[159] J. Masik,[98] A. L. Maslennikov,[118b,118a] L. Massa,[21b] P. Massarotti,[67a,67b] P. Mastrandrea,[69a,69b] A. Mastroberardino,[39b,39a] T. Masubuchi,[159] D. Matakias,[27] T. Mathisen,[167] A. Matic,[111] N. Matsuzawa,[159] J. Maurer,[25b] B. Maček,[89] D. A. Maximov,[118b,118a] R. Mazini,[154] I. Maznas,[158] S. M. Mazza,[141] C. Mc Ginn,[27] J. P. Mc Gowan,[101] S. P. Mc Kee,[103] T. G. McCarthy,[112] W. P. McCormack,[16] E. F. McDonald,[102] A. E. McDougall,[116] J. A. Mcfayden,[152] G. Mchedlidze,[155b] M. A. McKay,[40] K. D. McLean,[171] S. J. McMahon,[139] P. C. McNamara,[102] R. A. McPherson,[171,o] J. E. Mdhluli,[31f] Z. A. Meadows,[100] S. Meehan,[34] T. Megy,[36] S. Mehlhase,[111] A. Mehta,[88] B. Meirose,[41] D. Melini,[156] B. R. Mellado Garcia,[31f] F. Meloni,[44] A. Melzer,[22] E. D. Mendes Gouveia,[135a] A. M. Mendes Jacques Da Costa,[19] H. Y. Meng,[162] L. Meng,[34] S. Menke,[112] M. Mentink,[34] E. Meoni,[39b,39a] S. A. M. Merkt,[134] C. Merlassino,[130] P. Mermod,[52,a] L. Merola,[67a,67b] C. Meroni,[66a] G. Merz,[103] O. Meshkov,[110,108] J. K. R. Meshreki,[147] J. Metcalfe,[5] A. S. Mete,[5] C. Meyer,[63] J-P. Meyer,[140] M. Michetti,[17] R. P. Middleton,[139] L. Mijović,[48] G. Mikenberg,[175] M. Mikestikova,[136] M. Mikuž,[89] H. Mildner,[145] A. Milic,[162] C. D. Milke,[40] D. W. Miller,[35] L. S. Miller,[32] A. Milov,[175] D. A. Milstead,[43a,43b] A. A. Minaenko,[119] I. A. Minashvili,[155b] L. Mince,[55] A. I. Mincer,[121] B. Mindur,[81a] M. Mineev,[77] Y. Minegishi,[159] Y. Mino,[83] L. M. Mir,[12] M. Miralles Lopez,[169] M. Mironova,[130] T. Mitani,[174] V. A. Mitsou,[169] M. Mittal,[58c] O. Miu,[162] P. S. Miyagawa,[90] Y. Miyazaki,[85] A. Mizukami,[79] J. U. Mjörnmark,[94] T. Mkrtchyan,[59a] M. Mlynarikova,[117] T. Moa,[43a,43b] S. Mobius,[51] K. Mochizuki,[107] P. Moder,[44] P. Mogg,[111] A. F. Mohammed,[13a] S. Mohapatra,[37] G. Mokgatitswane,[31f] B. Mondal,[147] S. Mondal,[137] K. Mönig,[44] E. Monnier,[99] A. Montalbano,[148] J. Montejo Berlingen,[34] M. Montella,[123] F. Monticelli,[86] N. Morange,[62] A. L. Moreira De Carvalho,[135a] M. Moreno Llácer,[169] C. Moreno Martinez,[12] P. Morettini,[53b] M. Morgenstern,[156] S. Morgenstern,[173] D. Mori,[148] M. Morii,[57] M. Morinaga,[159] V. Morisbak,[129] A. K. Morley,[34]

A. P. Morris,[92] L. Morvaj,[34] P. Moschovakos,[34] B. Moser,[116] M. Mosidze,[155b] T. Moskalets,[50] P. Moskvitina,[115] J. Moss,[29,hh] E. J. W. Moyse,[100] S. Muanza,[99] J. Mueller,[134] R. Mueller,[18] D. Muenstermann,[87] G. A. Mullier,[94] J. J. Mullin,[132] D. P. Mungo,[66a,66b] J. L. Munoz Martinez,[12] F. J. Munoz Sanchez,[98] M. Murin,[98] P. Murin,[26b] W. J. Murray,[173,139] A. Murrone,[66a,66b] J. M. Muse,[124] M. Muškinja,[16] C. Mwewa,[27] A. G. Myagkov,[119,k] A. A. Myers,[134] G. Myers,[63] M. Myska,[137] B. P. Nachman,[16] O. Nackenhorst,[45] A. Nag Nag,[46] K. Nagai,[130] K. Nagano,[79] J. L. Nagle,[27] E. Nagy,[99] A. M. Nairz,[34] Y. Nakahama,[113] K. Nakamura,[79] H. Nanjo,[128] F. Napolitano,[59a] R. Narayan,[40] I. Naryshkin,[133] M. Naseri,[32] C. Nass,[22] T. Naumann,[44] G. Navarro,[20a] J. Navarro-Gonzalez,[169] P. Y. Nechaeva,[108] F. Nechansky,[44] T. J. Neep,[19] A. Negri,[68a,68b] M. Negrini,[21b] C. Nellist,[115] C. Nelson,[101] K. Nelson,[103] M. E. Nelson,[43a,43b] S. Nemecek,[136] M. Nessi,[34,ii] M. S. Neubauer,[168] F. Neuhaus,[97] J. Neundorf,[44] R. Newhouse,[170] P. R. Newman,[19] C. W. Ng,[134] Y. S. Ng,[17] Y. W. Y. Ng,[166] B. Ngair,[33e] H. D. N. Nguyen,[99] T. Nguyen Manh,[107] R. B. Nickerson,[130] R. Nicolaidou,[140] D. S. Nielsen,[38] J. Nielsen,[141] M. Niemeyer,[51] N. Nikiforou,[10] V. Nikolaenko,[119,k] I. Nikolic-Audit,[131] K. Nikolopoulos,[19] P. Nilsson,[27] H. R. Nindhito,[52] A. Nisati,[70a] N. Nishu,[2] R. Nisius,[112] T. Nitta,[174] T. Nobe,[159] D. L. Noel,[30] Y. Noguchi,[83] I. Nomidis,[131] M. A. Nomura,[27] M. B. Norfolk,[145] R. R. B. Norisam,[92] J. Novak,[89] T. Novak,[44] O. Novgorodova,[46] L. Novotny,[137] R. Novotny,[114] L. Nozka,[126] K. Ntekas,[166] E. Nurse,[92] F. G. Oakham,[32,f] J. Ocariz,[131] A. Ochi,[80] I. Ochoa,[135a] J. P. Ochoa-Ricoux,[142a] K. O'Connor,[24] S. Oda,[85] S. Odaka,[79] S. Oerdek,[167] A. Ogrodnik,[81a] A. Oh,[98] C. C. Ohm,[150] H. Oide,[160] R. Oishi,[159] M. L. Ojeda,[162] Y. Okazaki,[83] M. W. O'Keefe,[88] Y. Okumura,[159] A. Olariu,[25b] L. F. Oleiro Seabra,[135a] S. A. Olivares Pino,[142c] D. Oliveira Damazio,[27] D. Oliveira Goncalves,[78a] J. L. Oliver,[166] M. J. R. Olsson,[166] A. Olszewski,[82] J. Olszowska,[82] Ö. O. Öncel,[22] D. C. O'Neil,[148] A. P. O'neill,[130] A. Onofre,[135a,135e] P. U. E. Onyisi,[10] H. Oppen,[129] R. G. Oreamuno Madriz,[117] M. J. Oreglia,[35] G. E. Orellana,[86] D. Orestano,[72a,72b] N. Orlando,[12] R. S. Orr,[162] V. O'Shea,[55] R. Ospanov,[58a] G. Otero y Garzon,[28] H. Otono,[85] P. S. Ott,[59a] G. J. Ottino,[16] M. Ouchrif,[33d] J. Ouellette,[27] F. Ould-Saada,[129] A. Ouraou,[140,a] Q. Ouyang,[13a] M. Owen,[55] R. E. Owen,[139] V. E. Ozcan,[11c] N. Ozturk,[7] S. Ozturk,[11c] J. Pacalt,[126] H. A. Pacey,[30] K. Pachal,[47] A. Pacheco Pages,[12] C. Padilla Aranda,[12] S. Pagan Griso,[16] G. Palacino,[63] S. Palazzo,[48] S. Palestini,[34] M. Palka,[81b] P. Palni,[81a] D. K. Panchal,[10] C. E. Pandini,[52] J. G. Panduro Vazquez,[91] P. Pani,[44] G. Panizzo,[64a,64c] L. Paolozzi,[52] C. Papadatos,[107] S. Parajuli,[40] A. Paramonov,[5] C. Paraskevopoulos,[9] D. Paredes Hernandez,[60b] S. R. Paredes Saenz,[130] B. Parida,[175] T. H. Park,[162] A. J. Parker,[29] M. A. Parker,[30] F. Parodi,[53b,53a] E. W. Parrish,[117] J. A. Parsons,[37] U. Parzefall,[50] L. Pascual Dominguez,[157] V. R. Pascuzzi,[16] F. Pasquali,[116] E. Pasqualucci,[70a] S. Passaggio,[53b] F. Pastore,[91] P. Pasuwan,[43a,43b] J. R. Pater,[98] A. Pathak,[176] J. Patton,[88] T. Pauly,[34] J. Pearkes,[149] M. Pedersen,[129] L. Pedraza Diaz,[115] R. Pedro,[135a] T. Peiffer,[51] S. V. Peleganchuk,[118b,118a] O. Penc,[136] C. Peng,[60b] H. Peng,[58a] M. Penzin,[161] B. S. Peralva,[78a] M. M. Perego,[62] A. P. Pereira Peixoto,[135a] L. Pereira Sanchez,[43a,43b] D. V. Perepelitsa,[27] E. Perez Codina,[163a] M. Perganti,[9] L. Perini,[66a,66b] H. Pernegger,[34] S. Perrella,[34] A. Perrevoort,[116] K. Peters,[44] R. F. Y. Peters,[98] B. A. Petersen,[34] T. C. Petersen,[38] E. Petit,[99] V. Petousis,[137] C. Petridou,[158] P. Petroff,[62] F. Petrucci,[72a,72b] M. Pettee,[178] N. E. Pettersson,[34] K. Petukhova,[138] A. Peyaud,[140] R. Pezoa,[142d] L. Pezzotti,[68a,68b] G. Pezzullo,[178] T. Pham,[102] P. W. Phillips,[139] M. W. Phipps,[168] G. Piacquadio,[151] E. Pianori,[16] F. Piazza,[66a,66b] A. Picazio,[100] R. Piegaia,[28] D. Pietreanu,[25b] J. E. Pilcher,[35] A. D. Pilkington,[98] M. Pinamonti,[64a,64c] J. L. Pinfold,[2] C. Pitman Donaldson,[92] D. A. Pizzi,[32] L. Pizzimento,[71a,71b] A. Pizzini,[116] M.-A. Pleier,[27] V. Plesanovs,[50] V. Pleskot,[138] E. Plotnikova,[77] P. Podberezko,[118b,118a] R. Poettgen,[94] R. Poggi,[52] L. Poggioli,[131] I. Pogrebnyak,[104] D. Pohl,[22] I. Pokharel,[51] G. Polesello,[68a] A. Poley,[148,163a] A. Policicchio,[70a,70b] R. Polifka,[138] A. Polini,[21b] C. S. Pollard,[44] Z. B. Pollock,[123] V. Polychronakos,[27] D. Ponomarenko,[109] L. Pontecorvo,[34] S. Popa,[25a] G. A. Popeneciu,[25d] L. Portales,[4] D. M. Portillo Quintero,[56] S. Pospisil,[137] P. Postolache,[25c] K. Potamianos,[130] I. N. Potrap,[77] C. J. Potter,[30] H. Potti,[1] T. Poulsen,[44] J. Poveda,[169] T. D. Powell,[145] G. Pownall,[44] M. E. Pozo Astigarraga,[34] A. Prades Ibanez,[169] P. Pralavorio,[99] M. M. Prapa,[42] S. Prell,[76] D. Price,[98] M. Primavera,[65a] M. A. Principe Martin,[96] M. L. Proffitt,[144] N. Proklova,[109] K. Prokofiev,[60c] F. Prokoshin,[77] S. Protopopescu,[27] J. Proudfoot,[5] M. Przybycien,[81a] D. Pudzha,[133] P. Puzo,[62] D. Pyatiizbyantseva,[109] J. Qian,[103] Y. Qin,[98] A. Quadt,[51] M. Queitsch-Maitland,[34] G. Rabanal Bolanos,[57] F. Ragusa,[66a,66b] G. Rahal,[95] J. A. Raine,[52] S. Rajagopalan,[27] K. Ran,[13a,13d] D. F. Rassloff,[59a] D. M. Rauch,[44] S. Rave,[97] B. Ravina,[55] I. Ravinovich,[175] M. Raymond,[34] A. L. Read,[129] N. P. Readioff,[145] D. M. Rebuzzi,[68a,68b] G. Redlinger,[27] K. Reeves,[41] D. Reikher,[157] A. Reiss,[97] A. Rej,[147] C. Rembser,[34] A. Renardi,[44] M. Renda,[25b] M. B. Rendel,[112] A. G. Rennie,[55] S. Resconi,[66a] E. D. Resseguie,[16] S. Rettie,[92] B. Reynolds,[123] E. Reynolds,[19] M. Rezaei Estabragh,[177] O. L. Rezanova,[118b,118a] P. Reznicek,[138] E. Ricci,[73a,73b] R. Richter,[112] S. Richter,[44] E. Richter-Was,[81b] M. Ridel,[131] P. Rieck,[112] P. Riedler,[34] O. Rifki,[44] M. Rijssenbeek,[151] A. Rimoldi,[68a,68b] M. Rimoldi,[44] L. Rinaldi,[21b,21a] T. T. Rinn,[168] M. P. Rinnagel,[111] G. Ripellino,[150] I. Riu,[12] P. Rivadeneira,[44] J. C. Rivera Vergara,[171]

F. Rizatdinova,[125] E. Rizvi,[90] C. Rizzi,[52] B. A. Roberts,[173] S. H. Robertson,[101,o] M. Robin,[44] D. Robinson,[30] C. M. Robles Gajardo,[142d] M. Robles Manzano,[97] A. Robson,[55] A. Rocchi,[71a,71b] C. Roda,[69a,69b] S. Rodriguez Bosca,[59a] A. Rodriguez Rodriguez,[50] A. M. Rodríguez Vera,[163b] S. Roe,[34] J. Roggel,[177] O. Røhne,[129] R. A. Rojas,[142d] B. Roland,[50] C. P. A. Roland,[63] J. Roloff,[27] A. Romaniouk,[109] M. Romano,[21b] A. C. Romero Hernandez,[168] N. Rompotis,[88] M. Ronzani,[121] L. Roos,[131] S. Rosati,[70a] G. Rosin,[100] B. J. Rosser,[132] E. Rossi,[162] E. Rossi,[4] E. Rossi,[67a,67b] L. P. Rossi,[53b] L. Rossini,[44] R. Rosten,[123] M. Rotaru,[25b] B. Rottler,[50] D. Rousseau,[62] D. Rousso,[30] G. Rovelli,[68a,68b] A. Roy,[10] A. Rozanov,[99] Y. Rozen,[156] X. Ruan,[31f] A. J. Ruby,[88] T. A. Ruggeri,[1] F. Rühr,[50] A. Ruiz-Martinez,[169] A. Rummler,[34] Z. Rurikova,[50] N. A. Rusakovich,[77] H. L. Russell,[34] L. Rustige,[36] J. P. Rutherfoord,[6] E. M. Rüttinger,[145] M. Rybar,[138] E. B. Rye,[129] A. Ryzhov,[119] J. A. Sabater Iglesias,[44] P. Sabatini,[169] L. Sabetta,[70a,70b] H. F-W. Sadrozinski,[141] R. Sadykov,[77] F. Safai Tehrani,[70a] B. Safarzadeh Samani,[152] M. Safdari,[149] P. Saha,[117] S. Saha,[101] M. Sahinsoy,[112] A. Sahu,[177] M. Saimpert,[140] M. Saito,[159] T. Saito,[159] D. Salamani,[52] G. Salamanna,[72a,72b] A. Salnikov,[149] J. Salt,[169] A. Salvador Salas,[12] D. Salvatore,[39b,39a] F. Salvatore,[152] A. Salzburger,[34] D. Sammel,[50] D. Sampsonidis,[158] D. Sampsonidou,[58d,58c] J. Sánchez,[169] A. Sanchez Pineda,[4] V. Sanchez Sebastian,[169] H. Sandaker,[129] C. O. Sander,[44] I. G. Sanderswood,[87] J. A. Sandesara,[100] M. Sandhoff,[177] C. Sandoval,[20b] D. P. C. Sankey,[139] M. Sannino,[53b,53a] Y. Sano,[113] A. Sansoni,[49] C. Santoni,[36] H. Santos,[135a,135b] S. N. Santpur,[16] A. Santra,[175] K. A. Saoucha,[145] A. Sapronov,[77] J. G. Saraiva,[135a,135d] J. Sardain,[99] O. Sasaki,[79] K. Sato,[164] C. Sauer,[59b] F. Sauerburger,[50] E. Sauvan,[4] P. Savard,[162,f] R. Sawada,[159] C. Sawyer,[139] L. Sawyer,[93] I. Sayago Galvan,[169] C. Sbarra,[21b] A. Sbrizzi,[64a,64c] T. Scanlon,[92] J. Schaarschmidt,[144] P. Schacht,[112] D. Schaefer,[35] L. Schaefer,[132] U. Schäfer,[97] A. C. Schaffer,[62] D. Schaile,[111] R. D. Schamberger,[151] E. Schanet,[111] C. Scharf,[17] N. Scharmberg,[98] V. A. Schegelsky,[133] D. Scheirich,[138] F. Schenck,[17] M. Schernau,[166] C. Schiavi,[53b,53a] L. K. Schildgen,[22] Z. M. Schillaci,[24] E. J. Schioppa,[65a,65b] M. Schioppa,[39b,39a] B. Schlag,[97] K. E. Schleicher,[50] S. Schlenker,[34] K. Schmieden,[97] C. Schmitt,[97] S. Schmitt,[44] L. Schoeffel,[140] A. Schoening,[59b] P. G. Scholer,[50] E. Schopf,[130] M. Schott,[97] J. Schovancova,[34] S. Schramm,[52] F. Schroeder,[177] H-C. Schultz-Coulon,[59a] M. Schumacher,[50] B. A. Schumm,[141] Ph. Schune,[140] A. Schwartzman,[149] T. A. Schwarz,[103] Ph. Schwemling,[140] R. Schwienhorst,[104] A. Sciandra,[141] G. Sciolla,[24] F. Scuri,[69a] F. Scutti,[102] C. D. Sebastiani,[88] K. Sedlaczek,[45] P. Seema,[17] S. C. Seidel,[114] A. Seiden,[141] B. D. Seidlitz,[27] T. Seiss,[35] C. Seitz,[44] J. M. Seixas,[78b] G. Sekhniaidze,[67a] S. J. Sekula,[40] L. Selem,[4] N. Semprini-Cesari,[21b,21a] S. Sen,[47] C. Serfon,[27] L. Serin,[62] L. Serkin,[64a,64b] M. Sessa,[58a] H. Severini,[124] S. Sevova,[149] F. Sforza,[53b,53a] A. Sfyrla,[52] E. Shabalina,[51] R. Shaheen,[150] J. D. Shahinian,[132] N. W. Shaikh,[43a,43b] D. Shaked Renous,[175] L. Y. Shan,[13a] M. Shapiro,[16] A. Sharma,[34] A. S. Sharma,[1] S. Sharma,[44] P. B. Shatalov,[120] K. Shaw,[152] S. M. Shaw,[98] P. Sherwood,[92] L. Shi,[92] C. O. Shimmin,[178] Y. Shimogama,[174] J. D. Shinner,[91] I. P. J. Shipsey,[130] S. Shirabe,[52] M. Shiyakova,[77] J. Shlomi,[175] M. J. Shochet,[35] J. Shojaii,[102] D. R. Shope,[150] S. Shrestha,[123] E. M. Shrif,[31f] M. J. Shroff,[171] E. Shulga,[175] P. Sicho,[136] A. M. Sickles,[168] E. Sideras Haddad,[31f] O. Sidiropoulou,[34] A. Sidoti,[21b] F. Siegert,[46] Dj. Sijacki,[14] M. V. Silva Oliveira,[34] S. B. Silverstein,[43a] S. Simion,[62] R. Simoniello,[34] S. Simsek,[11b] P. Sinervo,[162] V. Sinetckii,[110] S. Singh,[148] S. Sinha,[44] S. Sinha,[31f] M. Sioli,[21b,21a] I. Siral,[127] S. Yu. Sivoklokov,[110] J. Sjölin,[43a,43b] A. Skaf,[51] E. Skorda,[94] P. Skubic,[124] M. Slawinska,[82] K. Sliwa,[165] V. Smakhtin,[175] B. H. Smart,[139] J. Smiesko,[138] S. Yu. Smirnov,[109] Y. Smirnov,[109] L. N. Smirnova,[110,jj] O. Smirnova,[94] E. A. Smith,[35] H. A. Smith,[130] M. Smizanska,[87] K. Smolek,[137] A. Smykiewicz,[82] A. A. Snesarev,[108] H. L. Snoek,[116] S. Snyder,[27] R. Sobie,[171,o] A. Soffer,[157] F. Sohns,[51] C. A. Solans Sanchez,[34] E. Yu. Soldatov,[109] U. Soldevila,[169] A. A. Solodkov,[119] S. Solomon,[50] A. Soloshenko,[77] O. V. Solovyanov,[119] V. Solovyev,[133] P. Sommer,[145] H. Son,[165] A. Sonay,[12] W. Y. Song,[163b] A. Sopczak,[137] A. L. Sopio,[92] F. Sopkova,[26b] S. Sottocornola,[68a,68b] R. Soualah,[64a,64c] A. M. Soukharev,[118b,118a] Z. Soumaimi,[33e] D. South,[44] S. Spagnolo,[65a,65b] M. Spalla,[112] M. Spangenberg,[173] F. Spanò,[91] D. Sperlich,[50] T. M. Spieker,[59a] G. Spigo,[34] M. Spina,[152] D. P. Spiteri,[55] M. Spousta,[138] A. Stabile,[66a,66b] R. Stamen,[59a] M. Stamenkovic,[116] A. Stampekis,[19] M. Standke,[22] E. Stanecka,[82] B. Stanislaus,[34] M. M. Stanitzki,[44] M. Stankaityte,[130] B. Stapf,[44] E. A. Starchenko,[119] G. H. Stark,[141] J. Stark,[99] D. M. Starko,[163b] P. Staroba,[136] P. Starovoitov,[59a] S. Stärz,[101] R. Staszewski,[82] G. Stavropoulos,[42] P. Steinberg,[27] A. L. Steinhebel,[127] B. Stelzer,[148,163a] H. J. Stelzer,[134] O. Stelzer-Chilton,[163a] H. Stenzel,[54] T. J. Stevenson,[152] G. A. Stewart,[34] M. C. Stockton,[34] G. Stoicea,[25b] M. Stolarski,[135a] S. Stonjek,[112] A. Straessner,[46] J. Strandberg,[150] S. Strandberg,[43a,43b] M. Strauss,[124] T. Strebler,[99] P. Strizenec,[26b] R. Ströhmer,[172] D. M. Strom,[127] L. R. Strom,[44] R. Stroynowski,[40] A. Strubig,[43a,43b] S. A. Stucci,[27] B. Stugu,[15] J. Stupak,[124] N. A. Styles,[44] D. Su,[149] S. Su,[58a] W. Su,[58d,144,58c] X. Su,[58a] N. B. Suarez,[134] K. Sugizaki,[159] V. V. Sulin,[108] M. J. Sullivan,[88] D. M. S. Sultan,[52] S. Sultansoy,[3c] T. Sumida,[83] S. Sun,[103] S. Sun,[176] X. Sun,[98] O. Sunneborn Gudnadottir,[167] C. J. E. Suster,[153] M. R. Sutton,[152] M. Svatos,[136] M. Swiatlowski,[163a] T. Swirski,[172] I. Sykora,[26a] M. Sykora,[138] T. Sykora,[138]

D. Ta,[97] K. Tackmann,[44,kk] A. Taffard,[166] R. Tafirout,[163a] E. Tagiev,[119] R. H. M. Taibah,[131] R. Takashima,[84] K. Takeda,[80] T. Takeshita,[146] E. P. Takeva,[48] Y. Takubo,[79] M. Talby,[99] A. A. Talyshev,[118b,118a] K. C. Tam,[60b] N. M. Tamir,[157] A. Tanaka,[159] J. Tanaka,[159] R. Tanaka,[62] Z. Tao,[170] S. Tapia Araya,[76] S. Tapprogge,[97] A. Tarek Abouelfadl Mohamed,[104] S. Tarem,[156] K. Tariq,[58b] G. Tarna,[25b,ll] G. F. Tartarelli,[66a] P. Tas,[138] M. Tasevsky,[136] E. Tassi,[39b,39a] G. Tateno,[159] Y. Tayalati,[33e] G. N. Taylor,[102] W. Taylor,[163b] H. Teagle,[88] A. S. Tee,[176] R. Teixeira De Lima,[149] P. Teixeira-Dias,[91] H. Ten Kate,[34] J. J. Teoh,[116] K. Terashi,[159] J. Terron,[96] S. Terzo,[12] M. Testa,[49] R. J. Teuscher,[162,o] N. Themistokleous,[48] T. Theveneaux-Pelzer,[17] O. Thielmann,[177] D. W. Thomas,[91] J. P. Thomas,[19] E. A. Thompson,[44] P. D. Thompson,[19] E. Thomson,[132] E. J. Thorpe,[90] Y. Tian,[51] V. Tikhomirov,[108,mm] Yu. A. Tikhonov,[118b,118a] S. Timoshenko,[109] P. Tipton,[178] S. Tisserant,[99] S. H. Tlou,[31f] A. Tnourji,[36] K. Todome,[21b,21a] S. Todorova-Nova,[138] S. Todt,[46] M. Togawa,[79] J. Tojo,[85] S. Tokár,[26a] K. Tokushuku,[79] E. Tolley,[123] R. Tombs,[30] M. Tomoto,[79,113] L. Tompkins,[149] P. Tornambe,[100] E. Torrence,[127] H. Torres,[46] E. Torró Pastor,[169] M. Toscani,[28] C. Tosciri,[35] J. Toth,[99,nn] D. R. Tovey,[145] A. Traeet,[15] C. J. Treado,[121] T. Trefzger,[172] A. Tricoli,[27] I. M. Trigger,[163a] S. Trincaz-Duvoid,[131] D. A. Trischuk,[170] W. Trischuk,[162] B. Trocmé,[56] A. Trofymov,[62] C. Troncon,[66a] F. Trovato,[152] L. Truong,[31c] M. Trzebinski,[82] A. Trzupek,[82] F. Tsai,[151] A. Tsiamis,[158] P. V. Tsiareshka,[105,dd] A. Tsirigotis,[158,ee] V. Tsiskaridze,[151] E. G. Tskhadadze,[155a] M. Tsopoulou,[158] I. I. Tsukerman,[120] V. Tsulaia,[16] S. Tsuno,[79] O. Tsur,[156] D. Tsybychev,[151] Y. Tu,[60b] A. Tudorache,[25b] V. Tudorache,[25b] A. N. Tuna,[34] S. Turchikhin,[77] D. Turgeman,[175] I. Turk Cakir,[3b,oo] R. J. Turner,[19] R. Turra,[66a] P. M. Tuts,[37] S. Tzamarias,[158] P. Tzanis,[9] E. Tzovara,[97] K. Uchida,[159] F. Ukegawa,[164] G. Unal,[34] M. Unal,[10] A. Undrus,[27] G. Unel,[166] F. C. Ungaro,[102] K. Uno,[159] J. Urban,[26b] P. Urquijo,[102] G. Usai,[7] R. Ushioda,[160] M. Usman,[107] Z. Uysal,[11d] V. Vacek,[137] B. Vachon,[101] K. O. H. Vadla,[129] T. Vafeiadis,[34] C. Valderanis,[111] E. Valdes Santurio,[43a,43b] M. Valente,[163a] S. Valentinetti,[21b,21a] A. Valero,[169] L. Valéry,[44] R. A. Vallance,[19] A. Vallier,[99] J. A. Valls Ferrer,[169] T. R. Van Daalen,[12] P. Van Gemmeren,[5] S. Van Stroud,[92] I. Van Vulpen,[116] M. Vanadia,[71a,71b] W. Vandelli,[34] M. Vandenbroucke,[140] E. R. Vandewall,[125] D. Vannicola,[70a,70b] L. Vannoli,[53b,53a] R. Vari,[70a] E. W. Varnes,[6] C. Varni,[53b,53a] T. Varol,[154] D. Varouchas,[62] K. E. Varvell,[153] M. E. Vasile,[25b] L. Vaslin,[36] G. A. Vasquez,[171] F. Vazeille,[36] D. Vazquez Furelos,[12] T. Vazquez Schroeder,[34] J. Veatch,[51] V. Vecchio,[98] M. J. Veen,[116] I. Veliscek,[130] L. M. Veloce,[162] F. Veloso,[135a,135c] S. Veneziano,[70a] A. Ventura,[65a,65b] A. Verbytskyi,[112] M. Verducci,[69a,69b] C. Vergis,[22] M. Verissimo De Araujo,[78b] W. Verkerke,[116] A. T. Vermeulen,[116] J. C. Vermeulen,[116] C. Vernieri,[149] P. J. Verschuuren,[91] M. L. Vesterbacka,[121] M. C. Vetterli,[148,f] N. Viaux Maira,[142d] T. Vickey,[145] O. E. Vickey Boeriu,[145] G. H. A. Viehhauser,[130] L. Vigani,[59b] M. Villa,[21b,21a] M. Villaplana Perez,[169] E. M. Villhauer,[48] E. Vilucchi,[49] M. G. Vincter,[32] G. S. Virdee,[19] A. Vishwakarma,[48] C. Vittori,[21b,21a] I. Vivarelli,[152] V. Vladimirov,[173] E. Voevodina,[112] M. Vogel,[177] P. Vokac,[137] J. Von Ahnen,[44] S. E. von Buddenbrock,[31f] E. Von Toerne,[22] V. Vorobel,[138] K. Vorobev,[109] M. Vos,[169] J. H. Vossebeld,[88] M. Vozak,[98] L. Vozdecky,[90] N. Vranjes,[14] M. Vranjes Milosavljevic,[14] V. Vrba,[137,a] M. Vreeswijk,[116] N. K. Vu,[99] R. Vuillermet,[34] I. Vukotic,[35] S. Wada,[164] C. Wagner,[100] P. Wagner,[22] W. Wagner,[177] S. Wahdan,[177] H. Wahlberg,[86] R. Wakasa,[164] M. Wakida,[113] V. M. Walbrecht,[112] J. Walder,[139] R. Walker,[111] S. D. Walker,[91] W. Walkowiak,[147] A. M. Wang,[57] A. Z. Wang,[176] C. Wang,[58a] C. Wang,[58c] H. Wang,[16] J. Wang,[60a] P. Wang,[40] R.-J. Wang,[97] R. Wang,[57] R. Wang,[117] S. M. Wang,[154] S. Wang,[58b] T. Wang,[58a] W. T. Wang,[58a] W. X. Wang,[58a] X. Wang,[13c] X. Wang,[168] Y. Wang,[58a] Z. Wang,[103] C. Wanotayaroj,[34] A. Warburton,[101] C. P. Ward,[30] R. J. Ward,[19] N. Warrack,[55] A. T. Watson,[19] M. F. Watson,[19] G. Watts,[144] B. M. Waugh,[92] A. F. Webb,[10] C. Weber,[27] M. S. Weber,[18] S. A. Weber,[32] S. M. Weber,[59a] C. Wei,[58a] Y. Wei,[130] A. R. Weidberg,[130] J. Weingarten,[45] M. Weirich,[97] C. Weiser,[50] T. Wenaus,[27] B. Wendland,[45] T. Wengler,[34] S. Wenig,[34] N. Wermes,[22] M. Wessels,[59a] K. Whalen,[127] A. M. Wharton,[87] A. S. White,[57] A. White,[7] M. J. White,[1] D. Whiteson,[166] W. Wiedenmann,[176] C. Wiel,[46] M. Wielers,[139] N. Wieseotte,[97] C. Wiglesworth,[38] L. A. M. Wiik-Fuchs,[50] D. J. Wilbern,[124] H. G. Wilkens,[34] L. J. Wilkins,[91] D. M. Williams,[37] H. H. Williams,[132] S. Williams,[30] S. Willocq,[100] P. J. Windischhofer,[130] I. Wingerter-Seez,[4] F. Winklmeier,[127] B. T. Winter,[50] M. Wittgen,[149] M. Wobisch,[93] A. Wolf,[97] R. Wölker,[130] J. Wollrath,[166] M. W. Wolter,[82] H. Wolters,[135a,135c] V. W. S. Wong,[170] A. F. Wongel,[44] S. D. Worm,[44] B. K. Wosiek,[82] K. W. Woźniak,[82] K. Wraight,[55] J. Wu,[13a,13d] S. L. Wu,[176] X. Wu,[52] Y. Wu,[58a] Z. Wu,[140,58a] J. Wuerzinger,[130] T. R. Wyatt,[98] B. M. Wynne,[48] S. Xella,[38] J. Xiang,[60c] X. Xiao,[103] X. Xie,[58a] I. Xiotidis,[152] D. Xu,[13a] H. Xu,[58a] H. Xu,[58a] L. Xu,[58a] R. Xu,[132] T. Xu,[58a] W. Xu,[103] Y. Xu,[13b] Z. Xu,[58b] Z. Xu,[149] B. Yabsley,[153] S. Yacoob,[31a] N. Yamaguchi,[85] Y. Yamaguchi,[160] M. Yamatani,[159] H. Yamauchi,[164] T. Yamazaki,[16] Y. Yamazaki,[80] J. Yan,[58c] S. Yan,[130] Z. Yan,[23] H. J. Yang,[58c,58d] H. T. Yang,[16] S. Yang,[58a] T. Yang,[60c] X. Yang,[58a] X. Yang,[13a] Y. Yang,[159] Z. Yang,[103,58a] W-M. Yao,[16] Y. C. Yap,[44] H. Ye,[13c] J. Ye,[40] S. Ye,[27] I. Yeletskikh,[77] M. R. Yexley,[87] P. Yin,[37] K. Yorita,[174] K. Yoshihara,[76] C. J. S. Young,[34] C. Young,[149] R. Yuan,[58b,pp] X. Yue,[59a] M. Zaazoua,[33e] B. Zabinski,[82] G. Zacharis,[9] E. Zaffaroni,[52]

A. M. Zaitsev,[119,k] T. Zakareishvili,[155b] N. Zakharchuk,[32] S. Zambito,[34] D. Zanzi,[50] S. V. Zeißner,[45] C. Zeitnitz,[177] G. Zemaityte,[130] J. C. Zeng,[168] O. Zenin,[119] T. Ženiš,[26a] S. Zenz,[90] S. Zerradi,[33a] D. Zerwas,[62] M. Zgubič,[130] B. Zhang,[13c] D. F. Zhang,[13b] G. Zhang,[13b] J. Zhang,[5] K. Zhang,[13a] L. Zhang,[13c] M. Zhang,[168] R. Zhang,[176] S. Zhang,[103] X. Zhang,[58c] X. Zhang,[58b] Z. Zhang,[62] P. Zhao,[47] Y. Zhao,[141] Z. Zhao,[58a] A. Zhemchugov,[77] Z. Zheng,[149] D. Zhong,[168] B. Zhou,[103] C. Zhou,[176] H. Zhou,[6] N. Zhou,[58c] Y. Zhou,[6] C. G. Zhu,[58b] C. Zhu,[13a,13d] H. L. Zhu,[58a] H. Zhu,[13a] J. Zhu,[103] Y. Zhu,[58a] X. Zhuang,[13a] K. Zhukov,[108] V. Zhulanov,[118b,118a] D. Zieminska,[63] N. I. Zimine,[77] S. Zimmermann,[50,a] M. Ziolkowski,[147] L. Živković,[14] A. Zoccoli,[21b,21a] K. Zoch,[52] T. G. Zorbas,[145] O. Zormpa,[42] W. Zou,[37] and L. Zwalinski[34]

(ATLAS Collaboration)

[1]*Department of Physics, University of Adelaide, Adelaide, Australia*
[2]*Department of Physics, University of Alberta, Edmonton, Alberta, Canada*
[3a]*Department of Physics, Ankara University, Ankara, Turkey*
[3b]*Istanbul Aydin University, Application and Research Center for Advanced Studies, Istanbul, Turkey*
[3c]*Division of Physics, TOBB University of Economics and Technology, Ankara, Turkey*
[4]*LAPP, Univ. Savoie Mont Blanc, CNRS/IN2P3, Annecy, France*
[5]*High Energy Physics Division, Argonne National Laboratory, Argonne, Illinois, USA*
[6]*Department of Physics, University of Arizona, Tucson, Arizona, USA*
[7]*Department of Physics, University of Texas at Arlington, Arlington, Texas, USA*
[8]*Physics Department, National and Kapodistrian University of Athens, Athens, Greece*
[9]*Physics Department, National Technical University of Athens, Zografou, Greece*
[10]*Department of Physics, University of Texas at Austin, Austin, Texas, USA*
[11a]*Bahcesehir University, Faculty of Engineering and Natural Sciences, Istanbul, Turkey*
[11b]*Istanbul Bilgi University, Faculty of Engineering and Natural Sciences, Istanbul, Turkey*
[11c]*Department of Physics, Bogazici University, Istanbul, Turkey*
[11d]*Department of Physics Engineering, Gaziantep University, Gaziantep, Turkey*
[12]*Institut de Física d'Altes Energies (IFAE), Barcelona Institute of Science and Technology, Barcelona, Spain*
[13a]*Institute of High Energy Physics, Chinese Academy of Sciences, Beijing, China*
[13b]*Physics Department, Tsinghua University, Beijing, China*
[13c]*Department of Physics, Nanjing University, Nanjing, China*
[13d]*University of Chinese Academy of Science (UCAS), Beijing, China*
[14]*Institute of Physics, University of Belgrade, Belgrade, Serbia*
[15]*Department for Physics and Technology, University of Bergen, Bergen, Norway*
[16]*Physics Division, Lawrence Berkeley National Laboratory and University of California, Berkeley, California, USA*
[17]*Institut für Physik, Humboldt Universität zu Berlin, Berlin, Germany*
[18]*Albert Einstein Center for Fundamental Physics and Laboratory for High Energy Physics, University of Bern, Bern, Switzerland*
[19]*School of Physics and Astronomy, University of Birmingham, Birmingham, United Kingdom*
[20a]*Facultad de Ciencias y Centro de Investigaciónes, Universidad Antonio Nariño, Bogotá, Colombia*
[20b]*Departamento de Física, Universidad Nacional de Colombia, Bogotá, Colombia*
[21a]*Dipartimento di Fisica e Astronomia A. Righi, Università di Bologna, Bologna, Italy*
[21b]*INFN Sezione di Bologna, Italy*
[22]*Physikalisches Institut, Universität Bonn, Bonn, Germany*
[23]*Department of Physics, Boston University, Boston, Massachusetts, USA*
[24]*Department of Physics, Brandeis University, Waltham, Massachusetts, USA*
[25a]*Transilvania University of Brasov, Brasov, Romania*
[25b]*Horia Hulubei National Institute of Physics and Nuclear Engineering, Bucharest, Romania*
[25c]*Department of Physics, Alexandru Ioan Cuza University of Iasi, Iasi, Romania*
[25d]*National Institute for Research and Development of Isotopic and Molecular Technologies, Physics Department, Cluj-Napoca, Romania*
[25e]*University Politehnica Bucharest, Bucharest, Romania*
[25f]*West University in Timisoara, Timisoara, Romania*
[26a]*Faculty of Mathematics, Physics and Informatics, Comenius University, Bratislava, Slovak Republic*
[26b]*Department of Subnuclear Physics, Institute of Experimental Physics of the Slovak Academy of Sciences, Kosice, Slovak Republic*
[27]*Physics Department, Brookhaven National Laboratory, Upton, New York, USA*

[28]Universidad de Buenos Aires, Facultad de Ciencias Exactas y Naturales, Departamento de Física, y CONICET, Instituto de Física de Buenos Aires (IFIBA), Buenos Aires, Argentina
[29]California State University, California, USA
[30]Cavendish Laboratory, University of Cambridge, Cambridge, United Kingdom
[31a]Department of Physics, University of Cape Town, Cape Town, South Africa
[31b]iThemba Labs, Western Cape, South Africa
[31c]Department of Mechanical Engineering Science, University of Johannesburg, Johannesburg, South Africa
[31d]National Institute of Physics, University of the Philippines Diliman (Philippines), Philippines
[31e]University of South Africa, Department of Physics, Pretoria, South Africa
[31f]School of Physics, University of the Witwatersrand, Johannesburg, South Africa
[32]Department of Physics, Carleton University, Ottawa, Ontario, Canada
[33a]Faculté des Sciences Ain Chock, Réseau Universitaire de Physique des Hautes Energies—Université Hassan II, Casablanca, Morocco
[33b]Faculté des Sciences, Université Ibn-Tofail, Kénitra, Morocco
[33c]Faculté des Sciences Semlalia, Université Cadi Ayyad, LPHEA-Marrakech, Morocco
[33d]LPMR, Faculté des Sciences, Université Mohamed Premier, Oujda, Morocco
[33e]Faculté des sciences, Université Mohammed V, Rabat, Morocco
[34]CERN, Geneva, Switzerland
[35]Enrico Fermi Institute, University of Chicago, Chicago, Illinois, USA
[36]LPC, Université Clermont Auvergne, CNRS/IN2P3, Clermont-Ferrand, France
[37]Nevis Laboratory, Columbia University, Irvington, New York, USA
[38]Niels Bohr Institute, University of Copenhagen, Copenhagen, Denmark
[39a]Dipartimento di Fisica, Università della Calabria, Rende, Italy
[39b]INFN Gruppo Collegato di Cosenza, Laboratori Nazionali di Frascati, Italy
[40]Physics Department, Southern Methodist University, Dallas, Texas, USA
[41]Physics Department, University of Texas at Dallas, Richardson, Texas, USA
[42]National Centre for Scientific Research "Demokritos", Agia Paraskevi, Greece
[43a]Department of Physics, Stockholm University, Sweden
[43b]Oskar Klein Centre, Stockholm, Sweden
[44]Deutsches Elektronen-Synchrotron DESY, Hamburg and Zeuthen, Germany
[45]Fakultät Physik, Technische Universität Dortmund, Dortmund, Germany
[46]Institut für Kern- und Teilchenphysik, Technische Universität Dresden, Dresden, Germany
[47]Department of Physics, Duke University, Durham, North Carolina, USA
[48]SUPA—School of Physics and Astronomy, University of Edinburgh, Edinburgh, United Kingdom
[49]INFN e Laboratori Nazionali di Frascati, Frascati, Italy
[50]Physikalisches Institut, Albert-Ludwigs-Universität Freiburg, Freiburg, Germany
[51]II. Physikalisches Institut, Georg-August-Universität Göttingen, Göttingen, Germany
[52]Département de Physique Nucléaire et Corpusculaire, Université de Genève, Genève, Switzerland
[53a]Dipartimento di Fisica, Università di Genova, Genova, Italy
[53b]INFN Sezione di Genova, Italy
[54]II. Physikalisches Institut, Justus-Liebig-Universität Giessen, Giessen, Germany
[55]SUPA—School of Physics and Astronomy, University of Glasgow, Glasgow, United Kingdom
[56]LPSC, Université Grenoble Alpes, CNRS/IN2P3, Grenoble INP, Grenoble, France
[57]Laboratory for Particle Physics and Cosmology, Harvard University, Cambridge, Massachusetts, USA
[58a]Department of Modern Physics and State Key Laboratory of Particle Detection and Electronics, University of Science and Technology of China, Hefei, China
[58b]Institute of Frontier and Interdisciplinary Science and Key Laboratory of Particle Physics and Particle Irradiation (MOE), Shandong University, Qingdao, China
[58c]School of Physics and Astronomy, Shanghai Jiao Tong University, Key Laboratory for Particle Astrophysics and Cosmology (MOE), SKLPPC, Shanghai, China
[58d]Tsung-Dao Lee Institute, Shanghai, China
[59a]Kirchhoff-Institut für Physik, Ruprecht-Karls-Universität Heidelberg, Heidelberg, Germany
[59b]Physikalisches Institut, Ruprecht-Karls-Universität Heidelberg, Heidelberg, Germany
[60a]Department of Physics, Chinese University of Hong Kong, Shatin, N.T., Hong Kong, China
[60b]Department of Physics, University of Hong Kong, Hong Kong, China
[60c]Department of Physics and Institute for Advanced Study, Hong Kong University of Science and Technology, Clear Water Bay, Kowloon, Hong Kong, China
[61]Department of Physics, National Tsing Hua University, Hsinchu, Taiwan
[62]IJCLab, Université Paris-Saclay, CNRS/IN2P3, 91405, Orsay, France

[63]*Department of Physics, Indiana University, Bloomington, Indiana, USA*
[64a]*INFN Gruppo Collegato di Udine, Sezione di Trieste, Udine, Italy*
[64b]*ICTP, Trieste, Italy*
[64c]*Dipartimento Politecnico di Ingegneria e Architettura, Università di Udine, Udine, Italy*
[65a]*INFN Sezione di Lecce, Italy*
[65b]*Dipartimento di Matematica e Fisica, Università del Salento, Lecce, Italy*
[66a]*INFN Sezione di Milano, Italy*
[66b]*Dipartimento di Fisica, Università di Milano, Milano, Italy*
[67a]*INFN Sezione di Napoli, Italy*
[67b]*Dipartimento di Fisica, Università di Napoli, Napoli, Italy*
[68a]*INFN Sezione di Pavia, Italy*
[68b]*Dipartimento di Fisica, Università di Pavia, Pavia, Italy*
[69a]*INFN Sezione di Pisa, Italy*
[69b]*Dipartimento di Fisica E. Fermi, Università di Pisa, Pisa, Italy*
[70a]*INFN Sezione di Roma, Italy*
[70b]*Dipartimento di Fisica, Sapienza Università di Roma, Roma, Italy*
[71a]*INFN Sezione di Roma Tor Vergata, Italy*
[71b]*Dipartimento di Fisica, Università di Roma Tor Vergata, Roma, Italy*
[72a]*INFN Sezione di Roma Tre, Italy*
[72b]*Dipartimento di Matematica e Fisica, Università Roma Tre, Roma, Italy*
[73a]*INFN-TIFPA, Italy*
[73b]*Università degli Studi di Trento, Trento, Italy*
[74]*Institut für Astro- und Teilchenphysik, Leopold-Franzens-Universität, Innsbruck, Austria*
[75]*University of Iowa, Iowa City, Iowa, USA*
[76]*Department of Physics and Astronomy, Iowa State University, Ames, Iowa, USA*
[77]*Joint Institute for Nuclear Research, Dubna, Russia*
[78a]*Departamento de Engenharia Elétrica, Universidade Federal de Juiz de Fora (UFJF), Juiz de Fora, Brazil*
[78b]*Universidade Federal do Rio De Janeiro COPPE/EE/IF, Rio de Janeiro, Brazil*
[78c]*Instituto de Física, Universidade de São Paulo, São Paulo, Brazil*
[79]*KEK, High Energy Accelerator Research Organization, Tsukuba, Japan*
[80]*Graduate School of Science, Kobe University, Kobe, Japan*
[81a]*AGH University of Science and Technology, Faculty of Physics and Applied Computer Science, Krakow, Poland*
[81b]*Marian Smoluchowski Institute of Physics, Jagiellonian University, Krakow, Poland*
[82]*Institute of Nuclear Physics Polish Academy of Sciences, Krakow, Poland*
[83]*Faculty of Science, Kyoto University, Kyoto, Japan*
[84]*Kyoto University of Education, Kyoto, Japan*
[85]*Research Center for Advanced Particle Physics and Department of Physics, Kyushu University, Fukuoka, Japan*
[86]*Instituto de Física La Plata, Universidad Nacional de La Plata and CONICET, La Plata, Argentina*
[87]*Physics Department, Lancaster University, Lancaster, United Kingdom*
[88]*Oliver Lodge Laboratory, University of Liverpool, Liverpool, United Kingdom*
[89]*Department of Experimental Particle Physics, Jožef Stefan Institute and Department of Physics, University of Ljubljana, Ljubljana, Slovenia*
[90]*School of Physics and Astronomy, Queen Mary University of London, London, United Kingdom*
[91]*Department of Physics, Royal Holloway University of London, Egham, United Kingdom*
[92]*Department of Physics and Astronomy, University College London, London, United Kingdom*
[93]*Louisiana Tech University, Ruston, Louisiana, USA*
[94]*Fysiska institutionen, Lunds universitet, Lund, Sweden*
[95]*Centre de Calcul de l'Institut National de Physique Nucléaire et de Physique des Particules (IN2P3), Villeurbanne, France*
[96]*Departamento de Física Teorica C-15 and CIAFF, Universidad Autónoma de Madrid, Madrid, Spain*
[97]*Institut für Physik, Universität Mainz, Mainz, Germany*
[98]*School of Physics and Astronomy, University of Manchester, Manchester, United Kingdom*
[99]*CPPM, Aix-Marseille Université, CNRS/IN2P3, Marseille, France*
[100]*Department of Physics, University of Massachusetts, Amherst, Massachusetts, USA*
[101]*Department of Physics, McGill University, Montreal, Québec, Canada*
[102]*School of Physics, University of Melbourne, Victoria, Australia*
[103]*Department of Physics, University of Michigan, Ann Arbor, Michigan, USA*

[104]Department of Physics and Astronomy, Michigan State University, East Lansing, Michigan, USA
[105]B.I. Stepanov Institute of Physics, National Academy of Sciences of Belarus, Minsk, Belarus
[106]Research Institute for Nuclear Problems of Byelorussian State University, Minsk, Belarus
[107]Group of Particle Physics, University of Montreal, Montreal, Québec, Canada
[108]P.N. Lebedev Physical Institute of the Russian Academy of Sciences, Moscow, Russia
[109]National Research Nuclear University MEPhI, Moscow, Russia
[110]D.V. Skobeltsyn Institute of Nuclear Physics, M.V. Lomonosov Moscow State University, Moscow, Russia
[111]Fakultät für Physik, Ludwig-Maximilians-Universität München, München, Germany
[112]Max-Planck-Institut für Physik (Werner-Heisenberg-Institut), München, Germany
[113]Graduate School of Science and Kobayashi-Maskawa Institute, Nagoya University, Nagoya, Japan
[114]Department of Physics and Astronomy, University of New Mexico, Albuquerque, New Mexico, USA
[115]Institute for Mathematics, Astrophysics and Particle Physics, Radboud University/Nikhef, Nijmegen, Netherlands
[116]Nikhef National Institute for Subatomic Physics and University of Amsterdam, Amsterdam, Netherlands
[117]Department of Physics, Northern Illinois University, DeKalb, Illinois, USA
[118a]Budker Institute of Nuclear Physics and NSU, SB RAS, Novosibirsk, Russia
[118b]Novosibirsk State University Novosibirsk, Russia
[119]Institute for High Energy Physics of the National Research Centre Kurchatov Institute, Protvino, Russia
[120]Institute for Theoretical and Experimental Physics named by A.I. Alikhanov of National Research Centre "Kurchatov Institute", Moscow, Russia
[121]Department of Physics, New York University, New York, New York, USA
[122]Ochanomizu University, Otsuka, Bunkyo-ku, Tokyo, Japan
[123]Ohio State University, Columbus, Ohio, USA
[124]Homer L. Dodge Department of Physics and Astronomy, University of Oklahoma, Norman, Oklahoma, USA
[125]Department of Physics, Oklahoma State University, Stillwater, Oklahoma, USA
[126]Palacký University, Joint Laboratory of Optics, Olomouc, Czech Republic
[127]Institute for Fundamental Science, University of Oregon, Eugene, Oregon, USA
[128]Graduate School of Science, Osaka University, Osaka, Japan
[129]Department of Physics, University of Oslo, Oslo, Norway
[130]Department of Physics, Oxford University, Oxford, United Kingdom
[131]LPNHE, Sorbonne Université, Université Paris Cité, CNRS/IN2P3, Paris, France
[132]Department of Physics, University of Pennsylvania, Philadelphia, Pennsylvania, USA
[133]Konstantinov Nuclear Physics Institute of National Research Centre "Kurchatov Institute", PNPI, St. Petersburg, Russia
[134]Department of Physics and Astronomy, University of Pittsburgh, Pittsburgh, Pennsylvania, USA
[135a]Laboratório de Instrumentação e Física Experimental de Partículas—LIP, Lisboa, Portugal
[135b]Departamento de Física, Faculdade de Ciências, Universidade de Lisboa, Lisboa, Portugal
[135c]Departamento de Física, Universidade de Coimbra, Coimbra, Portugal
[135d]Centro de Física Nuclear da Universidade de Lisboa, Lisboa, Portugal
[135e]Departamento de Física, Universidade do Minho, Braga, Portugal
[135f]Departamento de Física Teórica y del Cosmos, Universidad de Granada, Granada (Spain), Spain
[135g]Dep Física and CEFITEC of Faculdade de Ciências e Tecnologia, Universidade Nova de Lisboa, Caparica, Portugal
[135h]Instituto Superior Técnico, Universidade de Lisboa, Lisboa, Portugal
[136]Institute of Physics of the Czech Academy of Sciences, Prague, Czech Republic
[137]Czech Technical University in Prague, Prague, Czech Republic
[138]Charles University, Faculty of Mathematics and Physics, Prague, Czech Republic
[139]Particle Physics Department, Rutherford Appleton Laboratory, Didcot, United Kingdom
[140]IRFU, CEA, Université Paris-Saclay, Gif-sur-Yvette, France
[141]Santa Cruz Institute for Particle Physics, University of California Santa Cruz, Santa Cruz, California, USA
[142a]Departamento de Física, Pontificia Universidad Católica de Chile, Santiago, Chile
[142b]Universidad Andres Bello, Department of Physics, Santiago, Chile
[142c]Instituto de Alta Investigación, Universidad de Tarapacá, Arica, Chile
[142d]Departamento de Física, Universidad Técnica Federico Santa María, Valparaíso, Chile
[143]Universidade Federal de São João del Rei (UFSJ), São João del Rei, Brazil
[144]Department of Physics, University of Washington, Seattle, Washington, USA
[145]Department of Physics and Astronomy, University of Sheffield, Sheffield, United Kingdom

[146]*Department of Physics, Shinshu University, Nagano, Japan*
[147]*Department Physik, Universität Siegen, Siegen, Germany*
[148]*Department of Physics, Simon Fraser University, Burnaby, British Columbia, Canada*
[149]*SLAC National Accelerator Laboratory, Stanford, California, USA*
[150]*Department of Physics, Royal Institute of Technology, Stockholm, Sweden*
[151]*Departments of Physics and Astronomy, Stony Brook University, Stony Brook, New York, USA*
[152]*Department of Physics and Astronomy, University of Sussex, Brighton, United Kingdom*
[153]*School of Physics, University of Sydney, Sydney, Australia*
[154]*Institute of Physics, Academia Sinica, Taipei, Taiwan*
[155a]*E. Andronikashvili Institute of Physics, Iv. Javakhishvili Tbilisi State University, Tbilisi, Georgia*
[155b]*High Energy Physics Institute, Tbilisi State University, Tbilisi, Georgia*
[156]*Department of Physics, Technion, Israel Institute of Technology, Haifa, Israel*
[157]*Raymond and Beverly Sackler School of Physics and Astronomy, Tel Aviv University, Tel Aviv, Israel*
[158]*Department of Physics, Aristotle University of Thessaloniki, Thessaloniki, Greece*
[159]*International Center for Elementary Particle Physics and Department of Physics, University of Tokyo, Tokyo, Japan*
[160]*Department of Physics, Tokyo Institute of Technology, Tokyo, Japan*
[161]*Tomsk State University, Tomsk, Russia*
[162]*Department of Physics, University of Toronto, Toronto, Ontario, Canada*
[163a]*TRIUMF, Vancouver, British Columbia, Canada*
[163b]*Department of Physics and Astronomy, York University, Toronto, Ontario, Canada*
[164]*Division of Physics and Tomonaga Center for the History of the Universe, Faculty of Pure and Applied Sciences, University of Tsukuba, Tsukuba, Japan*
[165]*Department of Physics and Astronomy, Tufts University, Medford, Massachusetts, USA*
[166]*Department of Physics and Astronomy, University of California Irvine, Irvine, California, USA*
[167]*Department of Physics and Astronomy, University of Uppsala, Uppsala, Sweden*
[168]*Department of Physics, University of Illinois, Urbana, Illinois, USA*
[169]*Instituto de Física Corpuscular (IFIC), Centro Mixto Universidad de Valencia—CSIC, Valencia, Spain*
[170]*Department of Physics, University of British Columbia, Vancouver, British Columbia, Canada*
[171]*Department of Physics and Astronomy, University of Victoria, Victoria, British Columbia, Canada*
[172]*Fakultät für Physik und Astronomie, Julius-Maximilians-Universität Würzburg, Würzburg, Germany*
[173]*Department of Physics, University of Warwick, Coventry, United Kingdom*
[174]*Waseda University, Tokyo, Japan*
[175]*Department of Particle Physics and Astrophysics, Weizmann Institute of Science, Rehovot, Israel*
[176]*Department of Physics, University of Wisconsin, Madison, Wisconsin, USA*
[177]*Fakultät für Mathematik und Naturwissenschaften, Fachgruppe Physik, Bergische Universität Wuppertal, Wuppertal, Germany*
[178]*Department of Physics, Yale University, New Haven, Connecticut, USA*

[a]Deceased.
[b]Also at Department of Physics, King's College London, London, United Kingdom.
[c]Also at Istanbul University, Department of Physics, Istanbul, Turkey.
[d]Also at Instituto de Fisica Teorica, IFT-UAM/CSIC, Madrid, Spain.
[e]Also at Institute of Physics, Azerbaijan Academy of Sciences, Baku, Azerbaijan.
[f]Also at TRIUMF, Vancouver, British Columbia, Canada.
[g]Also at Physics Department, An-Najah National University, Nablus, Palestine.
[h]Also at Department of Physics, University of Fribourg, Fribourg, Switzerland.
[i]Also at Department of Physics and Astronomy, University of Louisville, Louisville, Kentucky, USA.
[j]Also at Departament de Fisica de la Universitat Autonoma de Barcelona, Barcelona, Spain.
[k]Also at Moscow Institute of Physics and Technology State University, Dolgoprudny, Russia.
[l]Also at Faculty of Physics, Sofia University, 'St. Kliment Ohridski', Sofia, Bulgaria.
[m]Also at Department of Physics, Ben Gurion University of the Negev, Beer Sheva, Israel.
[n]Also at Università di Napoli Parthenope, Napoli, Italy.
[o]Also at Institute of Particle Physics (IPP), Canada.
[p]Also at Bruno Kessler Foundation, Trento, Italy.
[q]Also at Department of Physics, St. Petersburg State Polytechnical University, St. Petersburg, Russia.
[r]Also at Borough of Manhattan Community College, City University of New York, New York, New York, USA.
[s]Also at Department of Physics, California State University, Fresno, USA.
[t]Also at Department of Financial and Management Engineering, University of the Aegean, Chios, Greece.
[u]Also at Centro Studi e Ricerche Enrico Fermi, Italy.

[v]Also at Department of Physics, California State University, East Bay, USA.
[w]Also at Institucio Catalana de Recerca i Estudis Avancats, ICREA, Barcelona, Spain.
[x]Also at Graduate School of Science, Osaka University, Osaka, Japan.
[y]Also at Physikalisches Institut, Albert-Ludwigs-Universität Freiburg, Freiburg, Germany.
[z]Also at University of Chinese Academy of Sciences (UCAS), Beijing, China.
[aa]Also at Yeditepe University, Physics Department, Istanbul, Turkey.
[bb]Also at Institute of Theoretical Physics, Ilia State University, Tbilisi, Georgia.
[cc]Also at CERN, Geneva, Switzerland.
[dd]Also at Joint Institute for Nuclear Research, Dubna, Russia.
[ee]Also at Hellenic Open University, Patras, Greece.
[ff]Also at Center for High Energy Physics, Peking University, China.
[gg]Also at The City College of New York, New York, New York, USA.
[hh]Also at Department of Physics, California State University, Sacramento, USA.
[ii]Also at Département de Physique Nucléaire et Corpusculaire, Université de Genève, Genève, Switzerland.
[jj]Also at Faculty of Physics, M.V. Lomonosov Moscow State University, Moscow, Russia.
[kk]Also at Institut für Experimentalphysik, Universität Hamburg, Hamburg, Germany.
[ll]Also at CPPM, Aix-Marseille Université, CNRS/IN2P3, Marseille, France.
[mm]Also at National Research Nuclear University MEPhI, Moscow, Russia.
[nn]Also at Institute for Particle and Nuclear Physics, Wigner Research Centre for Physics, Budapest, Hungary.
[oo]Also at Giresun University, Faculty of Engineering, Giresun, Turkey.
[pp]Also at Department of Physics and Astronomy, Michigan State University, East Lansing, Michigan, USA.